Induction of site-specific methylation in induced pluripotent stem cells of a patient with Angelman syndrome

Inaugural Dissertation

to obtain the degree of

Dr. rer. nat.

of the Department Biology

at the University Duisburg-Essen

presented by

Jana Staňurová

from Prague

June 2017

Die der vorliegenden Arbeit zugrunde liegenden Experimente wurden am Institut für Humangenetik an der Universität Duisburg-Essen durchgeführt.

1. Gutachter: Prof. Dr. Bernhard Horsthemke

2. Gutachter: Prof. Dr. Hemmo Meyer

Vorsitzender des Prüfungsausschusses: Prof. Dr. George Iliakis

Tag der mündlichen Prüfung: 9.10.2017

Parts of this work have been published in:

Stanurova J.*, Neureiter A.*, Hiber M., de Oliveira Kessler H., Stolp K., Goetzke R., Klein D., Bankfalvi A., Klump H., Steenpass L. (2016) Angelman syndrome-derived neurons display late onset of paternal *UBE3A* silencing. *Sci Rep, 6,* 30792. doi:10.1038/srep30792
* shared first authorship

Table of Contents

Abbreviations and Units

Abbreviations

A	Adenine
AS	Angelman Syndrome
C	Cytosine
cDNA	Complementary DNA
CO_2	Carbon dioxide
CpG	Dinucleotide with the sequence CG in 5´-3´ orientation
DMEM	Dulbecco´s Modified Eagle´s Medium
DMR	Differentially Methylated Region
DMSO	Dimethylsulfoxide
DNA	Deoxyribonucleic Acid
DNase	Deoxyribonuclease
DNMT	DNA Methyltransferase
dNTP	Deoxyribonucleotidetriphosphate
EB	Embryoid Body
EDTA	Ethylenediaminetetraacetic Acid
EtBr	Ethidium bromide
FACS	Fluorescence-Activated Cell Sorting
FBS	Foetal Bovine Serum
Fig	Figure
G	Guanine
GAPDH	Glyceraldehyde-3-phosphate Dehydrogenase
gDNA	Genomic DNA
GFP	Green Fluorescent Protein
H_2O	Water
hESCs	Human Embryonic Stem Cells
ICR	Imprinting Control Region
iPSCs	Induced Pluripotent Stem Cells
MgCl	Magnesium Chloride
mRNA	Messenger RNA

NaCl	Sodium Chloride
NaOH	Sodium Hydroxide
ORF	Open Reading Frame
p	*petit*; short arm of a chromosome
PBS	Phosphate Buffered Saline
PCR	Polymerase Chain Reaction
PFA	Paraformaldehyde
PWS	Prader-Willi Syndrome
q	*queue*; long arm of a chromosome
qRT-PCR	Quantitative Real-Time PCR
RNA	Ribonucleic Acid
RNase	Ribonuclease
RT	Room Temperature
SAM	S-adenosylmethionine
SDS	Sodium Dodecyl Sulfate
SNaPshot	Single-Nucleotide Primer Extension Assay
SNP	Single Nucleotide Polymorphism
SRO	Shortest Region of Overlap
SV40	Simian Virus 40
T	Thymine
TAE	Tris-acetate-EDTA Buffer
TE	Tris-EDTA Buffer
Tris	Tris(hydroxymethyl)aminomethane
U	Uracil
UV	Ultraviolet
YFP	Yellow Fluorescent Protein
ZTL	*Zentrales Tierlaboratorium*; Central Animal Facility

Units

°C	degrees Celsius
aa	amino acid(s)
bp	base pair(s)

g	gram
g	earth´s acceleration
h	hour
kb	kilobase(s)
l	litre
M	molar (mol/l)
µ	micro (10^{-6})
m	milli (10^{-3})
Mb	megabase
min	minute
ml	millilitre
n	nano (10^{-9})
rpm	rotations per minute
s	second(s)
U	unit(s)
V	Volt
v/v	volume per volume
w/v	weight per volume

1. Introduction

1.1 DNA Methylation

There are three major mechanisms of epigenetic regulation in mammals: DNA methylation, histone modification and chromatin remodelling, among which DNA methylation is the most stable. It is crucial for X-chromosome inactivation, retrotransposon repression, chromosome structure and gene silencing (Dean *et al.*, 2005; Brockdorff, 2011; Probst & Almouzni, 2011). Also, it plays a key role in genomic imprinting (Li *et al.*, 1993; Peters, 2014), which is a widely-studied function of DNA methylation due to its heritability (Reik & Walter, 2001). Methylation of cytosines on C5 in the context of CpG dinucleotides is typically associated with transcriptional silencing and chromosome stability.

Methylated cytosines tend to undergo deamination, which results in their conversion into thymines. Thus, CpG dinucleotides are underrepresented in the genome. In contrast, their abundance is high in the so-called CpG islands. CpGs in these clusters are mostly unmethylated (Deaton & Bird, 2011). Originally, CpG islands were defined by a length of at least 200 bp, a CG content exceeding 50 % and a ratio of observed CpGs to expected CpGs above 0.6 (Gardiner-Garden & Frommer, 1987). To exclude repetitive sequences, the definition was adjusted to at least 500 bp in length, 55 % CG content or greater and the observed CpGs to expected CpGs ratio of 0.65 (Takai & Jones, 2002).

DNA methylation is mostly symmetrical on both DNA strands. Its maintenance and establishment relies on DNA methyltransferases, which are conserved in plant and animal kingdoms (Bestor, 2000). S-adenosyl-methionine (SAM) serves as a donor of the methyl group (Goll & Bestor, 2005). DNMT1 was the first methyltransferase to be identified in mammals (Yen *et al.*, 1992). It maintains DNA methylation during replication (Leonhardt *et al.*, 1992; Lyko *et al.*, 1999; Goll & Bestor, 2005), since it recognises hemi-methylated DNA as its substrate and methylates the newly synthesised DNA strand (Yoder *et al.*, 1997). It is essential for the maintenance of DNA methylation at imprinting centres and repetitive sequences during embryonic development (Li *et al.*, 1992; Howell *et al.*, 2001; Gaudet *et al.*,

2004; Kurihara *et al.*, 2008). A possible de novo methylation activity has been suggested for DNMT1, too (Arand *et al.*, 2012; Feltus *et al.*, 2003).
DNMT3A and DNMT3B are de novo methyltransferases necessary for the establishment of DNA methylation. They require the co-factor DNMT3L to function (Bourc'his *et al.*, 2001; Hata *et al.*, 2002) and are also indispensable for embryonic development (Okano *et al.*, 1999). Maintenance activity during replication has been observed in both DNMT3A and DNMT3B (Arand *et al.*, 2012; MacDonald & Mann, 2014).

1.1.1 Genomic Imprinting

Presence of both the maternal and the paternal genome copy is mandatory for a normal embryonic development. Maternal or paternal uniparental murine embryos exhibited fatal developmental failures (Barton *et al.*, 1984; McGrath & Solter, 1984; Surani *et al.*, 1984). Maternally diploid embryos contained embryonic structures but no trophoblast. Paternally diploid embryos only developed extra-embryonic tissue. Similar phenotypes to those described in mice were observed in humans. The absence of the paternal genome resulted in the development of ovarian teratoma containing embryonic tissue of all three germ layers but without trophoblast. The absence of the maternal genome led to the formation of hydatidiform mole consisting of extra-embryonic tissue (Hall, 1990; Williams *et al.*, 2010 Fallahian *et al.*, 2013).
The necessity of both parental genomes stems from the asymmetrical DNA methylation resulting in parent-of-origin gene expression at specific loci known as genomic imprinting (Li *et al.*, 1993). Approximately 100 imprinted genes have been identified in humans including protein-coding genes as well as ncRNA (non-coding RNA) genes (Dindot *et al.*, 2009; Bartolomei & Ferguson-Smith, 2011; Horsthemke, 2014). Some of them are only expressed in certain tissues or at a particular time point during embryonic development, for instance in placenta (Prickett & Oakey, 2012). One of the possible hypotheses for the evolution of genomic imprinting is the kinship hypothesis, originally formulated as the conflict hypothesis (Moore & Haig, 1991; Haig, 1997; Wilkins & Haig, 2003 Trivers & Burt, 1999). According to the original hypothesis, paternally expressed genes stimulate growth of the embryo at the expense of the mother, whereas the maternally expressed genes restrict the growth of the embryo in order to preserve the mother’s resources. The supposed reason for this behaviour is

that while males may pass their genes on to offspring through several females, females may only do so through consecutive pregnancies. The kinship hypothesis is an expansion of the conflict hypothesis operating with the influence of all maternally related kin versus the influence of all paternally related kin (Wilkins & Haig, 2003). Among all hypotheses, this is the most accepted and empirically supported one. The growth factor IGF2 (insulin-like growth factor II) and its receptor IGF2R represent an example supporting the hypothesis. IGF2 supporting growth is paternally expressed. The maternally expressed IGF2R binds IGF2 and mediates its degradation, thereby restricting growth (Chao & D'Amore, 2008). Another piece of evidence supporting the hypothesis is that imprinting only occurs in placentals and marsupials as well as in some plants, but not in monotremes that lay eggs, so the investment of the mother is a priori limited. It is assumed that genomic imprinting co-evolved with the placenta of the mammals and the endosperm of the plants (Feil & Berger, 2007; Renfree *et al.*, 2013; Horsthemke, 2010). However, the hypothesis does not apply to all imprinted genes. Among them, retrotransposed genes seem to be over-represented. It has been hypothesised that the host-defence system neutralising potentially deleterious DNA elements erroneously silenced other genes, whose inactivity proved to be beneficial (Barlow, 2011).

Most imprinted genes are organised in clusters of several kb to several Mb in length, encompassing a differentially methylated CpG-rich imprinting control region (ICR). The ICR regulates the gene expression *in cis* (Barlow, 2011). Transcriptional interference plays an important role in imprinting, especially in the form of long non-coding RNAs (lncRNAs), whose presence has been detected at various imprinted loci (Latos *et al.*, 2012; Meng *et al.*, 2013; Barlow & Bartolomei, 2014). Differential DNA methylation is established already in the parental germline. It is maintained after fertilisation during the global wave of demethylation (Messerschmidt, 2012; Proudhon *et al.*, 2012; Smallwood *et al.*, 2014; Hanna & Kelsey, 2014) and further on throughout development, and preserved in mature tissues (Reik & Walter, 2001; Lucifero *et al.*, 2004; Ideraabdullah *et al.*, 2008; Messerschmidt, 2012; Kelsey & Feil, 2013).

In the female germline, the establishment of DNA methylation relies on DNMT3A and its co-factor DNMT3L. The mechanism targeting DNMT3A and DNMT3L to specific regions has yet to be elucidated. However, in the oocyte, transcription overlapping an ICR seems to be critical for the specificity of de novo DNA methylation (Chotalia *et al.*, 2009; Horsthemke, 2010; Lewis *et al.*, 2015). The phenomenon is apparently not restricted to the establishment of DNA methylation at imprinted loci (Veselovska *et al.*, 2015). Transcription might indirectly

facilitate methylation by inducing histone modifications promoting interactions with DNMT3A and DNMT3L (Baubec *et al.*, 2015). Since maternally methylated ICRs localise to promoter regions, it is feasible that overlapping transcription does support the establishment of the methylation mark. On the other hand, some regions might be protected from being methylated. For instance, proteins containing the CXXC domain bind specifically to unmethylated CpG dinucleotides in somatic cells. Such a process might also occur in the oocyte and prevent methylation of the bound sequences (Kelsey & Feil, 2013; Lewis *et al.*, 2015). The PWS/AS (Prader-Willi syndrome / Angelman syndrome) locus represents an example of a cluster containing a maternally methylated ICR. Methylation on the maternal chromosome inhibits the expression of *MKRN3*, *MAGEL2*, *NDN*, *NPAP1*, *SNURF-SNRPN*, *SNORD116*, *SNORD115* and *SNHG14* that are expressed from the unmethylated paternal allele. The only gene expressed from the maternal allele is *UBE3A* (Greally *et al.*, 1999; Nicholls & Knepper, 2001).

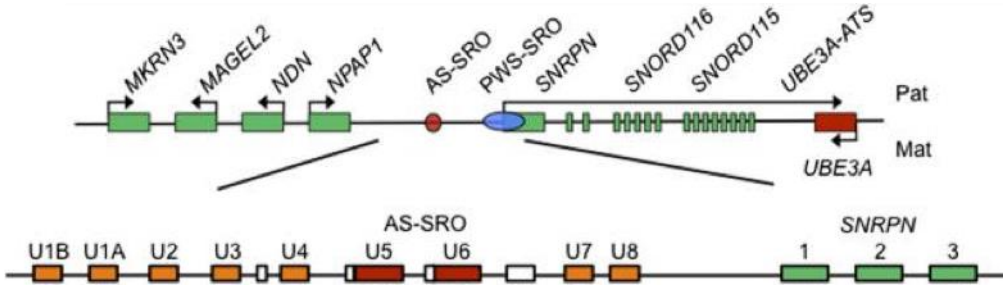

Figure 1. Expression at the PWS/AS locus in the brain. Genes expressed from the paternal (pat) allele, *MKRN3*, *MAGEL2*, *NDN*, *NPAP1*, *SNURF-SNRPN*, *SNORD116*, *SNORD115* and *SNHG14* (here *UBE3A-ATS*), are depicted in green. *UBE3A* is expressed from the maternal allele (mat), displayed in red. The imprinting centre regulating the expression of the locus is indicated by a red circle for AS-SRO and a blue oval for PWS-SRO. Detailed structure of the imprinting centre containing upstream exons is shown in a blow-up. The figure was adapted from Lewis *et al.*, 2015.

In the male germline, the processes leading to DNA methylation are even less understood. High transcriptional activity was detected at the differentially methylated regions ICR1 and IG-DMR in gametes. It mainly occurred on one DNA strand simultaneously with the establishment of DNA methylation. Also in these cases, transcription overlapped the ICR. However, it is not known if and how transcription contributes to de novo methylation in the paternal germline (Henckel *et al.*, 2012; Barlow & Bartolomei, 2014). ICRs methylated on the paternal allele are usually intergenic, as in the case of the *IGF2/H19* locus (Bartolomei *et al.*, 1993; Peters, 2014). This locus illustrates the insulator model of imprinted gene expression

regulation (Bell & Felsenfeld, 2000; Hark *et al.*, 2000; Nordin *et al.*, 2014). The ICR situated between the two genes encompasses a binding site for the zinc-finger CCCTC-binding factor (CTCF). The maternal allele is unmethylated, which allows for the binding of CTCF. Its presence prevents methylation of the maternal ICR facilitating *H19* expression. Moreover, it results in the formation of chromatin structures of higher order. Therefore, *IGF2* promoters lying upstream of the ICR cannot be activated by downstream enhancers and *IGF2* transcription is inhibited on the maternal allele. Methylation on the paternal allele hinders the binding of CTCF, thus restricting the insulator function of the ICR, and *IGF2* is expressed (Bell & Felsenfeld, 2000; Hark *et al.*, 2000).

Disturbances of imprinted gene expression are caused by various defects including deletions, uniparental disomies or discrepancies in methylation of the ICRs. Such conditions result in imprinting disorders in humans, since imprinted genes are expressed monoallelically and the only active allele is lost. In case of Beckwith-Wiedemann and Silver-Russell syndromes, disturbances of the *IGF2/H19* locus are involved, although the situation is not straightforward. Angelman and Prader-Willi syndromes represent examples of imprinting disorders in humans with a single affected locus.

1.1.2 Angelman Syndrome

Angelman syndrome is a rare neurodevelopmental imprinting disorder characterised by a happy demeanour, ataxic gait, absence of speech and developmental impairment, and often also abnormal EEG readings, microcephaly and seizures (Dagli *et al.*, 2012; Buiting, 2010). It was first described by Dr. Harry Angelman in 1965 and occurs with a frequency of 1:12 000 to 1:20 000. The underlying molecular cause is the lack of a functional E3 ubiquitin protein ligase UBE3A in the brain (Kishino *et al.*, 1997; Yu *et al.*, 2007; Rougeulle *et al.*, 1997). UBE3A catalyses ubiquitination of lysine residues in proteins targeting such marked proteins for degradation by the proteasome. Three different isoforms of UBE3A have been identified resulting from alternative splicing of the *UBE3A* transcript (Scheffner *et al.*, 1993; Yamamoto *et al.*, 1997; Martinez-Noel *et al.*, 2012). The *UBE3A* gene is part of the PWS/AS cluster on chromosome 15q11q13. While it is only expressed from the maternal allele in the brain (Dagli *et al.*, 2012; Rougeulle *et al.*, 1998; Landers *et al.*, 2004; Meng *et al.*, 2012; Meng *et al.*, 2013; Meng *et al.*, 2015; Chamberlain & Brannan, 2001; Horsthemke & Wagstaff, 2008; Fink *et al.*, 2017), its expression is biallelic in all other tissues (Albrecht *et al.*, 1997; Rougeulle *et*

al., 1997; Vu & Hoffman, 1997; Chamberlain & Lalande, 2010). In the human brain, *SNHG14* (small nucleolar RNA host gene 14) of 900 kb is transcribed in antisense direction to *UBE3A* and overlaps the whole gene and its promoter (Landers *et al.*, 2004; Numata *et al.*, 2011; Rougeulle *et al.*, 1997; Runte *et al.*, 2001). Therefore, *UBE3A* is susceptible to mutations occurring on the maternal chromosome because there is no compensation available from the paternal allele in the brain.

The most frequent cause of Angelman syndrome responsible for approximately 70 % of the cases is a 5 Mb to 7 Mb large de novo deletion occurring on the maternal chromosome 15 (Knoll *et al.*, 1989; Buiting, 2010). In about 5-10 % of the cases, it is a mutation in the maternal *UBE3A* gene. Such a mutation led to the identification of this gene as the Angelman syndrome gene (Kishino *et al.*, 1997; Loh *et al.*, 2006; Buiting, 2010). An imprinting defect causes 2-4 % of the cases. In such cases, the maternal chromosome carries a paternal imprint (Buiting *et al.*, 1998; Buiting, 2010). Paternal uniparental disomy was reported to be the cause of 1-2 % of the cases (Malcolm *et al.*, 1991; Buiting, 2010; Buiting *et al.*, 2015). In 10 to 15 % of clinically diagnosed cases of Angelman syndrome, the molecular cause could not be determined (Kishino *et al.*, 1997; Matsuura *et al.*, 1997; Buiting, 2010). The different nature of the underlying mutation corresponds with the severity of the phenotype. Patients harbouring a point mutation in the *UBE3A* gene present with a less pronounced phenotype than those with a large deletion on chromosome 15 (Mertz *et al.*, 2014; Lossie *et al.*, 2001; Sahoo *et al.*, 2007; Varela *et al.*, 2004; Gentile *et al.*, 2010; Tan *et al.*, 2011; Margolis *et al.*, 2015).

The ICR of the locus encompasses exon 1 of *SNURF-SNRPN*, its promoter, and a region upstream of it. In humans, it is composed of AS-SRO and PWS-SRO (Angelman syndrome / Prader-Willi syndrome shortest region of overlap) (Buiting *et al.*, 1999; Ohta *et al.*, 1999a; Ohta *et al.*, 1999b; Buiting *et al.*, 2003; Horsthemke & Wagstaff, 2008). An oocyte-specific promoter is localised at AS-SRO. Between AS-SRO and PWS-SRO, upstream exons of the *SNURF-SNRPN* gene are localised that are only included in the oocyte-specific transcripts and *SNHG14* (Fig. 1). Transcription initiated from the oocyte-specific promoter transits PWS-SRO probably causing its inactivation by inducing DNA methylation. Thus, PWS-SRO remains unmethylated and therefore active on the paternal allele only (Dittrich *et al.*, 1996; Lewis *et al.*, 2015). Two clusters of small nucleolar RNA (snoRNA) genes, *SNORD116* and *SNORD115*, lie downstream of the ICR. They are processed from the intronic regions of lncRNA *SNHG14*. Further downstream, the *UBE3A* gene is situated in antisense orientation to

SNURF-SNRPN, the *SNORD* clusters and *SNHG14* (Runte *et al.*, 2001; Wawrzik *et al.*, 2009; Lewis *et al.*, 2015). Expression of *SNORD115* and silencing of *UBE3A* on the paternal allele occurs only in neurons, as the lncRNA *SNHG14* is significantly longer than in other cell types. It has been proposed that a boundary element between the two *SNORD* clusters prevents *SNHG14* synthesis beyond this point in non-neural cells (Runte *et al.*, 2001; Runte *et al.*, 2004; Martins-Taylor *et al.*, 2014).

Mouse studies have shown that *Snhg14* transcription overlapping the *Ube3a* gene results in monoallelic *Ube3a* expression (Chamberlain & Brannan, 2001; Landers *et al.*, 2004; Numata *et al.*, 2011; Meng *et al.*, 2012). Integration of a stop cassette upstream of the *Ube3a* gene led to a truncation of the *Snhg14* transcript and activation of the paternal *Ube3a* allele. The expression pattern of the paternally expressed *Ube3a* was similar to the maternally expressed *Ube3a*. The paternal Ube3a protein was detected in neocortex, hippocampus and cerebellum of the transgenic mice (Meng *et al.*, 2012; Meng *et al.*, 2013).

Unlike other imprinted genes silenced by antisense transcriptional interference (Sleutels *et al.*, 2002; Williamson *et al.*, 2011), the paternal *Ube3a* promoter does not acquire methylation (Lossie *et al.*, 2001). Moreover, H3K4me3 can be found in the region, which is a hallmark of transcriptionally active promoters (Xie *et al.*, 2012; Meng *et al.*, 2013). Indeed, transcription of the paternal *Ube3a* gene on the 5'-end was shown to occur at a rate comparable to that of the maternal *Ube3a* gene. However, the paternal transcripts undergo premature termination in intron 4 excluding the synthesis of mature mRNA and subsequent translation to proteins (Numata *et al.*, 2011; Meng *et al.*, 2013). A model was proposed suggesting collision of convergent polymerase complexes transcribing *Ube3a* and *Snhg14* in intron 4 of the paternal *Ube3a*. Translocation of the polymerase complex elongating the *Ube3a* transcript could explain the premature termination of *Ube3a* transcription (Meng *et al.*, 2013).

Since *UBE3A* silencing on the paternal chromosome is a condition restricted to the brain, neurons are essential to study Angelman syndrome and the function of UBE3A at the molecular level. The only two means of obtaining them is the generation of induced pluripotent stem cells (iPSCs) from an Angelman syndrome patient by reprogramming and CRISPR/Cas engineering of human embryonic stem cells, coupled with their consecutive neuronal differentiation. Up to date, no therapy has been developed for Angelman syndrome. The antibiotic minocycline has been reported to alleviate the symptoms of the syndrome (Grieco *et al.*, 2014). Alternatively, topoisomerase I inhibitor topotecan can be applied to

activate the paternal *UBE3A* allele but it can hardly be used in therapy due to its heavy side effects (Armstrong, 2004; Markman, 2005; Penson & Seiden, 2005). A very promising approach utilising antisense oligonucleotides (ASO) specifically targeting *SNHG14* has been developed. The method relies on the formation of ASO-RNA heteroduplexes and the subsequent cleavage of the RNA strand within them by RNAse H leading to its degradation. So far, the technique has successfully been applied in mice, both in vitro and in vivo, resulting in the activation of the paternal *Ube3a* allele (Meng *et al.*, 2015). Concerning clinical therapy, delivery of the ASOs into the neurons of Angelman syndrome patients poses a considerable problem. Therefore, research on potential novel approaches to treat Angelman syndrome is necessary.

1.1.3 Epigenetic Reprogramming

Two major waves of epigenetic reprogramming take place during mammalian development (Dean *et al.*, 2003). The first one occurs in primordial germ cells. DNA methylation at imprinted loci undergoes erasure in order to be reset as germ cells develop (Hajkova *et al.*, 2002; Lee *et al.*, 2002). Imprint reestablishment is dependent on the activity of DNMT3A with its co-factor DNMT3L (Bourc'his *et al.*, 2001; Hata *et al.*, 2002; Kaneda *et al.*, 2004). In males, imprints are acquired during late foetal development (Davis *et al.*, 2000; Ueda *et al.*, 2000). In females, imprint establishment occurs postnatally in the growing oocyte before ovulation (Obata & Kono, 2002; Lucifero *et al.*, 2004) (Fig. 2).

The second wave of reprogramming occurs during embryonic development as genome activation is required at the 2-cell stage. The paternal genome exhibits a high level of methylation prior to fertilisation (Monk *et al.*, 1987; Kobayashi *et al.*, 2012). It undergoes demethylation first, before the maternal genome does. The process is realised actively with the contribution of TET (ten-eleven translocation family protein) enzymes. The maternal genome displays a lower level of methylation in comparison with the paternal one (Monk *et al.*, 1987; Kobayashi *et al.*, 2012). Its demethylation was supposed to be passive, mediated merely by the exclusion of DNMT1 from the nucleus during replication. This would explain why the process of demethylation is finished later than that of the paternal genome (Santos *et al.*, 2002; Dean *et al.*, 2003). However, active demethylation of the maternal genome has been

reported as well (Peat *et al.*, 2014; Wang *et al.*, 2004). Once demethylation is completed, de novo methylation occurs in the inner cell mass (Santos *et al.*, 2002) (Fig. 2).

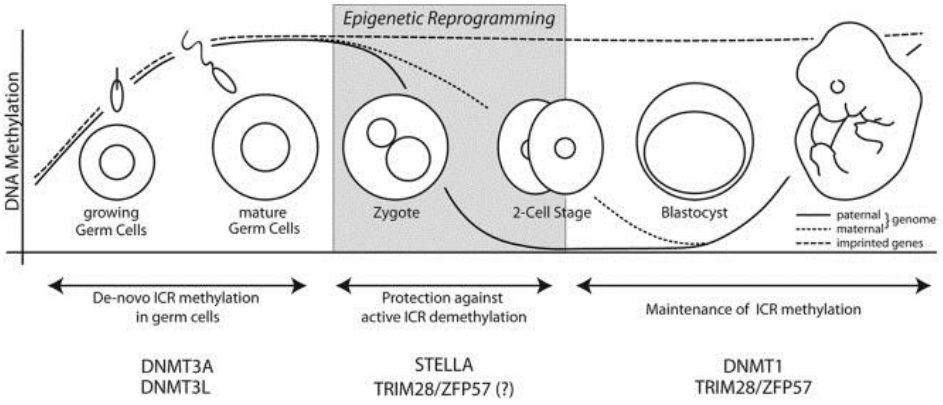

Figure 2. Protection of imprinted loci during development. In the growing germ cells, genomic imprints are set by de novo methyltransferases DNMT3A and DNMT3L. Major demethylation occurs first in the paternal, then also in the maternal genome during early development up to the 2-cell stage. In the blastocyst, the genome of the embryo undergoes de novo methylation. ICRs remain protected throughout the latter two phases by DPPA3 (here STELLA), TRIM28, ZFP57 and DNMT1. Factors playing important roles in the imprint protection are indicated below each stage. The figure was taken from Messerschmidt, 2012.

Imprinted genes are protected throughout the process of DNA demethylation (Messerschmidt, 2012). There are several proteins known to be involved in imprint maintenance, for instance DPPA3 (developmental pluripotency associated 3) encoded by one of the maternal effect genes. Maternal effect genes are crucial in the early development. While some are expressed only by the oocyte and exert their function during the transition from the oocyte to the embryo, others are required later in development and are expressed by the oocyte as well as by the embryo (Li *et al.*, 2010). DPPA3 plays a role in distinguishing the parental alleles and prevents active demethylation of certain loci (Nakamura *et al.*, 2007). Another maternal effect gene essential for imprint maintenance during the preimplantation phase is *TRIM28* (tripartite motif containing 28). TRIM28 is a key scaffold component of a heterochromatin inducing complex. Among other factors, it binds the H3K9me3-catalysing histone methyltransferase SETDB1 (SET domain bifurcated 1, SET = Su(var)3-9, Enhancer-of-zeste and Trithorax), nucleosome remodelling deacetylase complex (NuRD), and heterochromatin protein 1 (HP1) (Schultz, 2002). Binding specificity of the complex to DNA is provided by the interaction of TRIM28 with KRAB-ZFPs (Krüppel-associated box-containing zinc-finger proteins), for example ZFP57 (Li *et al.*, 2008). ZFP57 is another protein encoded by a maternal effect gene.

It recognises DNA methylation at ICRs via a specific hexanucleotide motif (Quenneville *et al.*, 2011). Both TRIM28 and ZFP57 are essential for imprint maintenance in embryonic stem cells (Messerschmidt, 2012). In human embryonic stem cells, DNMT1, DNMT3A and DNMT3B have been reported to be part of the complex as well (Quenneville *et al.*, 2011; Zuo *et al.*, 2012). Apart from this observation, it has been proposed that DNMT1, also a product of a maternal effect gene, may contribute to the protection of imprints by selectively binding to them despite its general exclusion from the nucleus required to allow passive demethylation (Borowczyk *et al.*, 2009).

Upon reprogramming, somatic cells need to undergo a number of molecular changes including epigenetic reprogramming partly similar to that of early embryonic development to reach a state of true pluripotency. The process requires a long time, it is ineffective and often yields partly reprogrammed cells or cells carrying epigenetic memory instead of fully reprogrammed induced pluripotent stem cells (Chan *et al.*, 2009; Deng *et al.*, 2009; Lister *et al.*, 2009; Kim *et al.*, 2010; Kim *et al.*, 2014). This indicates the presence of epigenetic barriers difficult to overcome. In addition, disturbances of methylation at imprinted loci occur frequently, suggesting their unfaithful protection throughout reprogramming (Johannesson *et al.*, 2014; Ma *et al.*, 2014b). Deeper understanding of processes involved in epigenetic reprogramming occurring in the early embryo and the protection of DNA methylation at imprinted loci during development could contribute to improving the efficiency of reprogramming.

1.2 Stem Cells

The hallmark of stem cells is their ability of self-renewal and their capacity of differentiation into cells with a distinct identity and function (Jaenisch & Young, 2008). Based on their differentiation potential, stem cells are divided as follows. Pluripotent stem cells are able to differentiate into cells of all three germ layers, ectoderm, mesoderm and endoderm. In vivo, they occur exclusively in the inner cell mass of the blastocyst. In vitro, their stable cultivation as embryonic stem cells is well-established, while pluripotency is retained. Multipotent and oligopotent stem cells are involved in the regeneration of mature tissues. Their differentiation

potential is restricted to a few specific cell types within their germ layer (Hochedlinger & Plath, 2009).

1.2.1 Pluripotent Stem Cells

Embryonic stem cells are pluripotent giving rise to all embryonic tissues but for placenta. They may only be isolated from the inner cell mass of the blastocyst, a stage of embryonic development before implantation. Their removal leads to the destruction of the embryo, naturally raising ethical issues regarding their use in research. Human embryonic stem cells were first established in cell culture in 1998 by James Thomson (Thomson *et al.*, 1998).

Pluripotent stem cells are characterised by the presence of various features. They exhibit enhanced activity of alkaline phosphatase (Wobus *et al.*, 1984; Thomson *et al.*, 1998) and express typical markers. Transcription factors OCT4, NANOG and SOX2 represent nuclear markers of pluripotency, while SSEA3, SSEA4, TRA-1-60, TRA-1-81 and GCTM-2 exemplify typical surface pluripotency markers (Thomson *et al.*, 1998; Reubinoff *et al.*, 2000; Xu *et al.*, 2001; Henderson *et al.*, 2002; Boyer *et al.*, 2005). Furthermore, stem cells may be characterised by their potential to differentiate into derivatives of all three germ layers in vitro (Doetschman *et al.*, 1985; Itskovitz-Eldor *et al.*, 2000). In vivo, this ability may be verified by teratoma assay. Embryonic stem cells are injected subcutaneously into immunodeficient mice and the teratomas they form over time are analysed for the presence of derivatives of all three germ layers (Wobus *et al.*, 1984; Thomson *et al.*, 1998).

The aforementioned transcription factors OCT4, NANOG and SOX2 are crucial for the maintenance of pluripotency. They form a regulatory network controlling their own expression in a positive feedback loop and the expression of other genes essential for retaining pluripotency. Other genes are repressed and maintained in a poised status until their expression is required upon differentiation (Boyer *et al.*, 2005; Loh *et al.*, 2006). Apart from OCT4, NANOG and SOX2, many more transcription factors have been identified that are part of the regulatory network maintaining pluripotency. For instance, KLF4, MYC, LIN28, DNMT3B as well as ZFP42 belong to these factors (Li *et al.*, 2005; Wang *et al.*, 2006; Zhou *et al.*, 2007).

As described above, DNA methylation is generally associated with gene repression. Therefore, it is not surprising that the overall level of methylation is lower in transcriptionally very active embryonic stem cells needing to maintain their pluripotency than in differentiated

somatic cells, as shown by a comparison of the respective global methylomes (Collas, 2009). Accordingly, chromatin of embryonic stem cells is in a less compact state than that of differentiated cells. This finding also corresponds with the observed high chromatin plasticity of embryonic stem cells (Strickfaden *et al.*, 2010). Upon differentiation, promoters of genes associated with pluripotency such as *POU5F1* (encoding OCT4) or *NANOG* undergo extensive methylation, histone modification and alteration of chromatin structure leading to their repression (Fisher & Fisher, 2011).

Signalling involved in retaining pluripotency and promoting self-renewal is a complex, finely balanced network of intertwined pathways. PI3K/AKT, MAPK/ERK, TGFβ/SMAD2/3 and Wnt pathways play an important role in pluripotency maintenance. This explains the dependence of embryonic stem cells on bFGF2 (basic fibroblast growth factor 2) in cell culture because bFGF2 activates the PI3K/AKT cascade (Amit *et al.*, 2000; Dalton, 2013). The cascade contributes to maintaining pluripotency in several ways. It suppresses MAPK/ERK signalling keeping it at a rather low level of activity. High activity of this pathway results in destabilisation of c-myc by GSK3 and the induction of differentiation (Singh *et al.*, 2012a; Singh *et al.*, 2012b). Furthermore, PI3K/AKT activates mTOR. Although the mechanism is not clear, specific mTOR inhibition has a similar effect on embryonic stem cells as does the inhibition of PI3K itself, both causing a loss of pluripotency and triggering differentiation (McLean *et al.*, 2007; Zhou *et al.*, 2009b). Moreover, PI3K/AKT cross-talks with the TGFβ/SMAD2/3 pathway that exhibits dual function in embryonic stem cells similar to that of the MAPK/ERK cascade (McLean *et al.*, 2007; Brown *et al.*, 2011; Teng *et al.*, 2011; Singh *et al.*, 2012b). High levels of SMAD2/3 induce differentiation, whereas at low levels, SMAD2/3 activates transcription of *NANOG*, for instance (Xu *et al.*, 2008; Yu *et al.*, 2011). Even though the exact way of modulating SMAD2/3 has not yet been understood, PI3K/AKT maintains pluripotency by restricting the activity of SMAD2/3 (Dalton, 2013). In addition, PI3K/AKT indirectly inhibits Wnt signalling by suppressing MAPK/ERK, thereby further supporting pluripotency. While a role in self-renewal has been suggested for the Wnt pathway by some studies, there is growing evidence that its activation leads to differentiation instead (Davidson *et al.*, 2012; Sumi *et al.*, 2008). Apart from conventional signal transduction, its transcriptional effector β-catenin alters the specificity of SMAD2/3 to promote differentiation (Singh *et al.*, 2012b). Therefore, suppression of the pathway seems to be significant for pluripotency maintenance. It has been reported that also OCT4 functionally represses the Wnt pathway, thereby additionally

contributing to self-renewal and pluripotency maintenance, and underlining the opposing roles of Wnt signalling and pluripotency-associated networks (Davidson *et al.*, 2012).

1.2.2 Induced Pluripotent Stem Cells

The first experiments on somatic cell nuclear transfer, also known as therapeutic cloning, were performed with *Xenopus laevis* (Gurdon, 1962). The breakthrough in this field was the successful cloning of the sheep Dolly (Wilmut *et al.*, 1997). Soon after, cloning of other species followed (Wakayama *et al.*, 1998; Polejaeva *et al.*, 2000; Chesne *et al.*, 2002; Byrne *et al.*, 2007). Alternatively, pluripotent stem cells may be generated by fusing an embryonic and a somatic cell, giving rise to hybrid cells. Pluripotency of murine as well as human hybrid cells induced by this method was verified (Tada *et al.*, 2001; Terada *et al.*, 2002; Ying *et al.*, 2002; Cowan *et al.*, 2005; Yu *et al.*, 2006). A great drawback of cells created this way is their tetraploidy excluding therapeutic application.

To generate iPSCs, transcription factors OCT4, KLF4, SOX2 and MYC, the so-called Yamanaka factors, are overexpressed in somatic cells (Takahashi & Yamanaka, 2006; Takahashi *et al.*, 2007). MYC was reported to be dispensable (Nakagawa *et al.*, 2008). The combination of OCT4, SOX2, NANOG and LIN28 also leads to reprogramming and induction of pluripotency in human fibroblasts (Yu *et al.*, 2007). In general, single Yamanaka factors may be substituted by other proteins provided that the pluripotency network comprising OCT4, NANOG and SOX2 is activated (Buganim *et al.*, 2012).

Delivery of the factors into the cells usually relies on a self-inactivating retroviral vector, although other methods have been developed. Since retroviral delivery invariably results in the vector integrating into the host genome, insertion mutations are likely to occur (Woods *et al.*, 2003). Furthermore, activation of the vector during differentiation may take place preventing successful completion of the process (Okita *et al.*, 2007; Ramos-Mejia *et al.*, 2012). Therefore, lentiviral vectors have been engineered to allow for virus excision via Flp recombinase after reprogramming (Sommer *et al.*, 2010; Voelkel *et al.*, 2010). Systems using transposon vectors have also been adjusted to facilitate their removal. Thus, both PiggyBac (Kaji *et al.*, 2009; Woltjen *et al.*, 2009; Yusa *et al.*, 2009) and Sleeping Beauty (Muenthaisong *et al.*, 2012; Davis *et al.*, 2013; Kues *et al.*, 2013) support the possibility of excision as well. Only a very small portion of the exogenic DNA sequence remains in the genome after removal. Non-integrating adenoviral or Sendai virus vectors represent a good

alternative (Stadtfeld *et al.*, 2008; Zhou & Freed, 2009; Fusaki *et al.*, 2009) and so does transient expression of the reprogramming factors from episomal plasmids or non-viral minicircles (Gonzalez *et al.*, 2009; Jia *et al.*, 2010; Montserrat *et al.*, 2011). For successful reprogramming, it is also sufficient to deliver the required transcription factors in the form of their mRNA (Warren *et al.*, 2010) or even as recombinant proteins (Kim *et al.*, 2009; Zhou *et al.*, 2009a).
Reprogramming efficiency ranges from 0.01 % to 0.2 % (Okita *et al.*, 2007; Wernig *et al.*, 2008) but may be increased by targeted activation of certain transcription factors, chromatin remodelling or manipulation of selected signalling pathways (Silva *et al.*, 2008; Mikkelsen *et al.*, 2008; Kim *et al.*, 2010; Onder *et al.*, 2012; Huangfu *et al.*, 2008a; Huangfu *et al.*, 2008b; Chen *et al.*, 2013).

Derivation of patient-specific induced pluripotent stem cells (iPSCs) was a very important and promising step for regenerative medicine. This success partly solved the problem of restricted access to human embryonic stem cells due to ethical issues regarding their use and the need of cells with the ability to differentiate into cells of tissues inaccessible in patients. Not only may iPSCs be cultured over a long period of time facilitating research on the pathogenesis of various diseases and drug screening in vitro but they could also be applied in therapy, once genetically corrected. As autologous transplants, they would not cause any immune defence reaction. It has been shown in a mouse model of sickle-cell anaemia that transplantation of corrected iPSCs rescued the phenotype (Hanna *et al.*, 2007). However, concerns regarding their utilisation in human therapy due to the risk of oncogenesis are certainly justified and need to be resolved first.

1.2.3 Epigenetic Stability during Reprogramming

Demethylation of many loci associated with pluripotency is required during reprogramming to facilitate the transition from a fully differentiated state to a pluripotent mode. Loosening of dense chromatin structure and modification of histone marks are equally important to enable their transcription (Cedar & Bergman, 2009). Even after a successful reprogramming process, methylomes of human embryonic stem cells (hESCs) and iPSCs are not identical (Deng *et al.*, 2009; Lister *et al.*, 2009; Tesarova *et al.*, 2016). iPSCs display signs of epigenetic memory

influencing their differentiation potential (Kim *et al.*, 2010; Ma *et al.*, 2014b). Interestingly though, incomplete deactivation of certain genes may increase reprogramming efficiency (Ohi *et al.*, 2011). According to some studies, the methylome profile of iPSCs undergoes changes upon prolonged cultivation eventually resembling that of hESCs (Nishino *et al.*, 2011; Tesarova *et al.*, 2016). However, aberrant methylation at imprinted loci after reprogramming or long-term culture has been observed (Nazor *et al.*, 2012; Johannesson *et al.*, 2014; Ma *et al.*, 2014b; Pick *et al.*, 2009). Alteration of imprinting at a certain locus in a clone does not predispose other imprinted loci in that clone to a change in methylation, neither to one in the same direction, nor in the opposing one. This finding indicates stochastic incidence of such abnormalities. Also, specific genes exhibit different frequencies of perturbation, which argues in favour of the stochastic occurrence theory as well (Johannesson *et al.*, 2014). Some loci such as PWS-SRO have been reported to display exceptional stability but for very rare cases (Chamberlain *et al.*, 2010; Ma *et al.*, 2014b). At ICR1 of the *IGF2/H19* locus and ICR2 of the *KCNQ1* cluster, aberrant methylation was detected (Nazor *et al.*, 2012; Johannesson *et al.*, 2014; Ma *et al.*, 2014b). Similar observations of instability have been described for NESPAS of the *GNAS* cluster (Grybek *et al.*, 2014). CpG85 of the *RB1* gene repeatedly showed varying methylation between tissues as well (Kanber, unpublished data). Susceptibility of IG-DMR of the *DLK1/MEG3* cluster to a loss of differential methylation has also been documented (Nazor *et al.*, 2012; Stadtfeld *et al.*, 2012; Johannesson *et al.*, 2014; Ma *et al.*, 2014b; Xu *et al.*, 2015). Abnormalities may be present in somatic cells to a certain extent and be clonally expanded, or they may be introduced during reprogramming. Since methylation at imprinted loci is fairly stable in hESCs (International Stem Cell Initiative, 2007; Rugg-Gunn *et al.*, 2007), it is feasible that the anomalies in reprogrammed cells are a result of their somatic origin occurring independently of the method used for reprogramming (Johannesson *et al.*, 2014).

In a study comparing hESCs, iPSCs and pluripotent cells generated by somatic nuclear transfer (NT-ESCs), significant differences were detected between hESCs clustering together with NT-ESCs, and iPSCs clearly forming a separate group in a genome-wide DNA methylation microarray analysis (Ma *et al.*, 2014b). An explanation for a more efficient reprogramming in NT-ESCs than in iPSCs might be the role of ooplasm. For instance, demethylation commences immediately after somatic nuclear transfer (Santos *et al.*, 2002), while with factor-induced reprogramming, the process takes days to weeks, likely being passive (Mikkelsen *et al.*, 2008). As described earlier, maternal effect genes play an important

role in the transition from the oocyte to the embryo as well as in imprint maintenance during embryonic development. Obviously, these genes are not present in an active state in adult differentiated cells prior to their reprogramming. Taken that into account together with the absence of further essential components in somatic cells, it becomes evident that the ooplasm contains specific reprogramming factors functioning upstream of pluripotency (Ma *et al.*, 2014b). Studies focusing on their identification could improve the existing reprogramming methods with regard to methylation maintenance as well as removal.

1.3 Site-Specific Induction of DNA Methylation

Aberrant expression of imprinted genes resulting from disturbances of methylation at the corresponding ICRs is responsible for the development of imprinting disorders in humans, such as Angelman and Prader-Willi syndromes or Beckwith-Wiedemann syndrome. Among other features, the latter syndrome is characterised by overgrowth and a high predisposition for childhood cancer due to the loss of imprinting of *IGF2*. Particularly Wilms' tumour (nephroblastoma), pancreatoblastoma and hepatoblastoma are likely to develop in children with Beckwith-Wiedemann syndrome (DeBaun & Tucker, 1998). However, the loss of imprinting of *IGF2* has also been described in other types of cancer (Ulaner *et al.*, 2003; Sakatani *et al.*, 2005). Similarly, the overexpression of other oncogenes often confers growth and proliferation advantage and results in cancer. Targeted silencing to suppress transcription may represent an effective and useful tool in therapy, at least supporting conventional treatment. Since DNA methylation represses transcription efficiently, various methods have been established to exploit that property of this epigenetic modification by inducing methylation at a selected locus.

1.3.1 Induction of DNA Methylation by Artificial Methylated Oligonucleotides

DNA methylation induction at promoter regions targeted by methylated oligonucleotides has been described (Yao *et al.*, 2003; Zhu *et al.*, 2004; Hoffman & Hu, 2006; Ma *et al.*, 2010). Oligonucleotides utilised in this method are 21 to 25 nucleotides long. Within their sequence, at least two methylated cytosines are present. The oligonucleotides are protected from

degradation by cellular nucleases by phosphorothioate backbones. In theory, upon replication or transcription initiation when the DNA helix is transiently molten, methylated oligonucleotides anneal to the complementary genomic DNA strand forming a hemi-methylated double-stranded stretch of DNA. DNMT1 recognises the hemi-methylated portion of DNA and methylates the endogenous DNA strand. As the endogenous DNA strands reanneal, hemi-methylated template is formed again and is targeted by DNMT1 producing a fully methylated segment of DNA.

In an in vitro model of hepatocellular carcinoma, the application of methylated oligonucleotides resulted in a rapid significant decrease in RNA expression of the selected gene. Methylation induction at the targeted region could already be observed eight hours after delivery of the methylated oligonucleotides into the cells (Yao *et al.*, 2003). More importantly, the approach employed in vivo led to a markedly prolonged survival of treated animals as compared with negative controls. Interestingly, when stability of the effect was assayed in vitro, the inhibiting effect was present after one cell passage but lost in the following one (Yao *et al.*, 2003). The process leading to demethylation was not examined further in detail. In a different study, not only was methylation induced by methylated oligonucleotides stable but it also promoted histone modifications associated with chromatin silencing (Ma *et al.*, 2010). Also, induced methylation was reported to spread to adjacent sites (Zhu *et al.*, 2004).

1.3.2 Induction of DNA Methylation by In Vitro-Methylated Fragments

An alternative to the aforementioned method relies on longer single-stranded DNA fragments targeting the selected region (Hsiao *et al.*, 2010; Hsu *et al.*, 2011; Teng *et al.*, 2011). The principle of functioning is basically identical to the one described above for methylated oligonucleotides, requiring replication or transcription. This approach has the advantage that it targets both endogenous DNA strands simultaneously, providing higher efficiency.

There are two ways to achieve methylation of a fragment in vitro. The first one employs methyltransferase *Sss*I and a donor of the methyl group, S-adenosylmethionine. *Sss*I methylates cytosines in the context of CpG dinucleotides on both strands, which results in methylation of the fragment equivalent to physiological conditions. The other possibility utilises direct incorporation of methylated cytosines into the fragment during PCR

amplification. As a result, the fragments contain methylated cytosines in the physiological context as well as outside of CpG dinucleotides, which occurs rarely in the human genome.
It has been shown that methylation of the *TRIP10* promoter in human mesenchymal stem cells mediated by the application of in vitro-methylated fragments accelerates their differentiation. Methylation induced by this technique was maintained over several passages but could be reversed by methyltransferase inhibitors (Hsiao *et al.*, 2010). Induced methylation of two tumour suppressor genes in mesenchymal stem cells was sufficient to cause their transformation into malignant cells (Teng *et al.*, 2011). Using in vitro-methylated fragments, it is possible to silence even strong viral promoters such as CMV (Hsu *et al.*, 2011).

1.3.3 Induction of DNA Methylation by a Modified CRISPR/Cas System

1.3.3.1 CRISPR/Cas

Bacteria and archaea developed adaptive immune defence systems termed clustered regularly interspaced short palindromic repeats (CRISPR)/CRISPR-associated (Cas) as a protection against viruses or plasmids (Bhaya *et al.*, 2011; Terns & Terns, 2011; Wiedenheft *et al.*, 2012). Nearly all archaea and about half of bacteria are equipped with CRISPR/Cas systems (Grissa *et al.*, 2007; Rousseau *et al.*, 2009). CRISPR loci contain short repeat sequences of 30 to 40 nucleotides separating variable sequences of comparable size (Kunin *et al.*, 2007). The variable sequences (also named spacers or guides) are derived from invaders (Bolotin *et al.*, 2005; Lillestol *et al.*, 2006). Transcripts of the CRISPR locus are cleaved into small crRNAs (CRISPR RNAs) that target foreign nucleic acids and induce their degradation (Brouns *et al.*, 2008; Hale *et al.*, 2009). *Cas* genes are organised in operons situated near CRISPR loci in the genome and represent the effector nucleases in the defence systems (Jansen *et al.*, 2002; Terns & Terns, 2011; Wiedenheft *et al.*, 2012). Together with crRNAs, Cas proteins form ribonucleoprotein complexes (Wang *et al.*, 2011; Gasiunas *et al.*, 2012). tracrRNA (transactivating RNA) pairs with a repeat sequence found in crRNA and is essential for activating DNA cleavage by Cas. Reaction to invaders occurs in three phases. In the acquisition step, foreign fragments are integrated into the host genome at the proximal end of a CRISPR locus (Bhaya *et al.*, 2011; Terns & Terns, 2011; Wiedenheft *et al.*, 2012). In the expression stage, CRISPR transcripts are generated, processed to produce crRNAs and assembled with Cas into ribonucleoprotein complexes (Haurwitz *et al.*, 2010; Deltcheva *et al.*,

2011; Wang *et al.*, 2011). In the interference phase, base-pairing of crRNAs mediates target recognition and the foreign sequence is eliminated by the nuclease activity of the complex (Brouns *et al.*, 2008; Lintner *et al.*, 2011; Hale *et al.*, 2012).

Out of the three described types of CRISPR/Cas systems (Makarova *et al.*, 2011), especially type II relying on Cas9 has been widely adopted as a tool for genetic engineering (Terns & Terns, 2014). The only requirement restricting target selection is the presence of a sequence motif known as PAM (protospacer adjacent motif) directly neighbouring the target site (Terns & Terns, 2014). For Cas9 from *Streptococcus pyogenes*, this motif is minimal, a 5'-NGG-3' trinucleotide (Fonfara *et al.*, 2014; Jinek *et al.*, 2012; Cong *et al.*, 2013). This system was adjusted to a more straightforward variant requiring a single-guide RNA (sgRNA or gRNA) molecule instead of the original two, the targeting crRNA and the activating tracrRNA (Jinek *et al.*, 2012). Furthermore, diverse variants of Cas9 were developed to better suit research purposes (Gasiunas & Siksnys, 2013; Jinek *et al.*, 2013). Wildtype Cas9 utilises different nuclease active sites in RuvC and HNH nuclease domains to cut each DNA strand. The induced DNA double-strand breaks are repaired by the cellular error-prone non-homologous end joining pathway (Terns & Terns, 2014). Inactivation of one of the domains yields a nicking enzyme favouring homologous recombination as a repair mechanism with a more predictable outcome (Cong *et al.*, 2013; Mali *et al.*, 2013). This system may well be employed to introduce insertions or deletions in a reliable manner. Modification of both nuclease domains at a time produces a potent, targetable and site-specific DNA-binding complex capable of impairing or silencing gene expression by interfering with transcription initiation or elongation, respectively (Qi *et al.*, 2013). However, steric hindrance may contribute to gene expression activation as well when directed to transcriptional repressor binding sites (Qi *et al.*, 2013). Fusion constructs of the Cas9 complex with transcription modulators, for instance VP16 for activation, conveys even higher precision in transcription control than mere DNA-binding complexes (Bikard *et al.*, 2013; Cheng *et al.*, 2013). In general, targeting specificity has extensively been studied and the system has undergone substantial engineering to minimise off-target effects (Kleinstiver *et al.*, 2016; Slaymaker *et al.*, 2016). It can be tailored to facilitate effective genome editing of virtually any kind.

The CRISPR/Cas9 technology offers several advantages over the established ZFNs (zinc finger nucleases) and TALENs (transcription activator-like effector nucleases) gene-editing methods. Performance efficiency is comparable or higher relative to both approaches (Jinek *et al.*, 2013; Mali *et al.*, 2013). More importantly, targeting a new site only requires designing

a gRNA complementary to the selected sequence, which is faster, easier and more cost-effective than creating a new ZNF or TALEN protein. In addition, more than one site may be targeted at a time (Cong *et al.*, 2013; Mali *et al.*, 2013). Also, combining Cas9 proteins with different PAM sequence specifications provides further targeting possibilities (Cong *et al.*, 2013; Esvelt *et al.*, 2013; Fonfara *et al.*, 2014). The flexibility and the straightforward implementation of CRISPR/Cas9 outperform both ZFNs and TALENs in more ways than one.

1.3.3.2 Induction of DNA Methylation by CRISPR/Cas9

Up to now, most targeted epigenetic tools utilised ZNFs or TALENs. As described above, there are certain disadvantages to the systems and CRISPR/Cas9 is gradually replacing them. Fusion proteins of the inactivated Cas9 nucleases with histone acetyltransferases or histone demethylases targeting regulatory elements represent only some of the possible options the technology offers regarding epigenetic modifications (Hilton *et al.*, 2015; Kearns *et al.*, 2015; Thakore *et al.*, 2015). Constructs with the C-terminal domain of DNA methyltransferase Dnmt3a alone or with Dnmt3L in addition can be utilised to successfully introduce methylation at CpG islands free of methylation within gene promoters (Siddique *et al.*, 2013; McDonald *et al.*, 2016; Vojta *et al.*, 2016) (Fig. 3). It has been shown that the presence of the co-factor Dnmt3L increases the efficiency of methylation induction (Stepper *et al.*, 2017). Methylation was most prominent at the sites adjacent to the gRNA binding site, 25 bp upstream and 40 bp downstream of it. Spreading of methylation has been observed preferentially to regions approximately 200 bp apart from the gRNA binding site, both downstream and upstream, suggesting probable blocking by nucleosomes. Such observations have also been made previously in studies inducing targeted methylation using ZNFs or TALENs. Upon methylation induction, gene repression has been detected (Li *et al.*, 2007; Bernstein *et al.*, 2015; Stolzenburg *et al.*, 2015). As described above, modified Cas9 binds to DNA and causes impairment of gene expression on its own. Indeed, this effect did contribute to the decrease in expression, as shown by a negative control experiment with an inactive mutant protein incapable of inducing methylation that also partly reduced expression. However, the difference in repression caused by the active and the inactive variant was significant (Stepper *et al.*, 2017). Constructs capable of multimerisation due to favourable interactions between the interfaces of adjacent proteins facilitate DNA methylation as far as 1

kb away from the target site. Fibres formed by the components are likely oligomers but methylation of distant regions could be accomplished by DNA looping and subsequent assembly of new filaments at these sites (Jurkowska *et al.*, 2008; Rajavelu *et al.*, 2012; Emperle *et al.*, 2014).

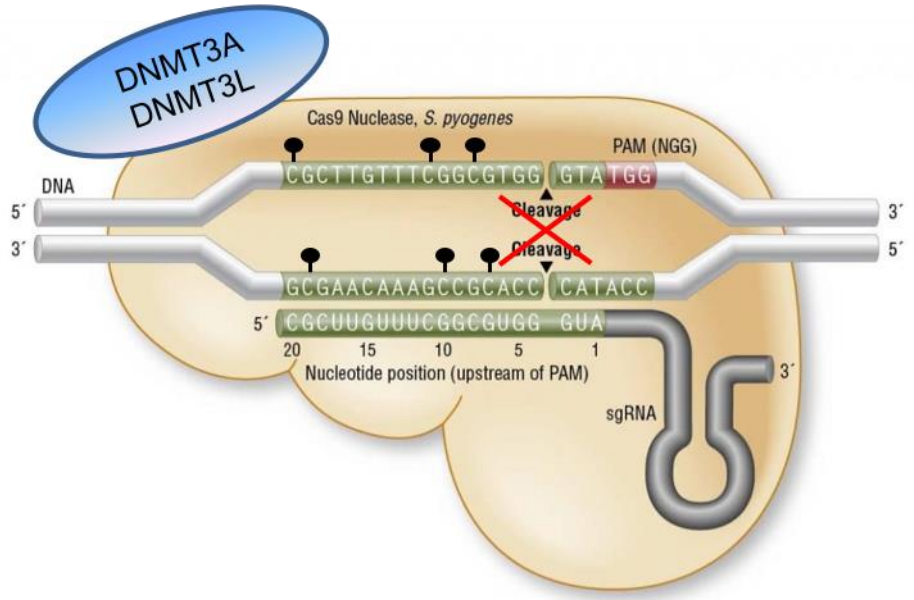

Figure 3. Schematic depiction of a methylating CRISPR/Cas9 system. A fusion protein of Cas9 from *Streptococcus pyogenes* with catalytic domains of DNMT3A and DNMT3L (blue) is engineered to induce methylation (black lollipops) instead of double-strand DNA breaks. Guide RNA (here sgRNA) targeting the complex to the selected sequence is indicated. The figure was adapted from www.neb.com.

Implementation of the CRISPR/Cas9 system functionally coupled to methyltransferases has a great potential not only in gene expression regulation. Its accuracy and efficiency, yet combined with exceptional adaptability, allows for many possible applications with the capacity of causing durable effects. Another advantage over the two other methods utilising methylated oligonucleotides or in vitro-methylated fragments to induce methylation is the independence of the approach from mitosis or transcription.

Up to date, none of the mentioned techniques has been used to target imprinted loci. Successful implementation of any of them at an imprinted locus would represent a proof of concept in epigenetic therapy and, in the long term, could perhaps contribute to the development of a new means of treatment.

1.4 Aim

In the first part of this study, the aim was to establish a functional iPSC model of Angelman syndrome. The molecular cause of Angelman syndrome is the absence of a functional E3 ubiquitin protein ligase UBE3A in the brain, whose expression occurs only on the maternal allele. The imprinting centre PWS-SRO that indirectly regulates the expression of *UBE3A* is not methylated on the paternal allele. This allows the expression of the long non-coding RNA *SNHG14* that silences the paternal *UBE3A* allele by transcriptional interference, thus excluding the possibility of allele compensation. Up to now, only a few direct targets of UBE3A have been identified. Very limited knowledge is available on the manifestation of UBE3A loss on the symptoms characteristic for the disorder. Since brain tissue from patients during the course of development cannot be obtained, the first milestone to facilitate the study was to successfully reprogram donor skin fibroblasts by a lentiviral vector into patient-specific and healthy control iPSCs. Their careful characterisation and the confirmation of their pluripotency was an essential prerequisite for further work. Standard methods of verifying pluripotency were employed, that is, AP staining, immunocytochemistry, FACS and qRT-PCR. In addition, EB formation assay, TaqMan array, Epi-Pluri-Score analysis, and teratoma formation assay as the most stringent pluripotency test were performed. Quality testing included Southern blot, Sanger sequencing, karyotyping and high-resolution HLA typing. Second, it was necessary to develop a reliable neuronal differentiation protocol in order to obtain mature neurons from the iPSCs. This part of the project was addressed in cooperation with Anika Neureiter. Silencing of the paternal *UBE3A* allele by *SNHG14* occurs during neuronal maturation. It is the mechanism preventing allele compensation in case the maternal allele is lost or damaged. To determine when exactly the silencing takes place, the expression dynamics of the respective parental alleles throughout the process of neuronal differentiation were investigated. In order to do this, the three-base pair deletion present in the maternal *UBE3A* allele of the patient-derived iPSCs was used as a SNP and single-nucleotide primer extension assay of cells at selected stages of neuronal differentiation was performed. In addition, I developed a quantitative assay to evaluate the expression levels of both parental *UBE3A* alleles during differentiation separately in more detail.

In the second part of the project, I aimed to induce methylation at the paternal PWS-SRO. Since the presence of methylation is usually associated with transcriptional silencing, my hypothesis was that introducing methylation at this region would lead to the abolishment of *SNHG14* expression. Successful interference with *SNHG14* expression would then activate the paternal *UBE3A* allele and allow compensation for the defective maternal allele. First, it was necessary to assess the level of methylation at the locus I planned to methylate and evaluate its stability, which was essential for the model to work. Apart from PWS-SRO, I analysed the methylation status at five other differentially methylated loci by next-generation bisulphite sequencing to investigate their stability during reprogramming. I performed the analyses not only in the patient-derived and healthy control iPSCs generated in this study but also in hESCs H1 and H9, and the previously published Angelman syndrome iPSC line AGI-0 and its healthy iPSC counterpart MCH2-10. For comparison, I assessed the methylation status in the parental fibroblasts used for reprogramming. To induce methylation at the paternal PWS-SRO, I utilised three different methods: 1) artificial methylated oligonucleotides, 2) in vitro-methylated fragments, and 3) a modified CRISPR/Cas9 system fused with DNMT3A and DNMT3L. I employed the iPSC line AGI-0 for the optimisation phase because it harbours a large deletion on chromosome 15 encompassing the whole maternal PWS-SRO and therefore exhibits only unmethylated reads in the next-generation bisulphite sequencing analysis. Thus, it was easier to evaluate the extent of methylation induced by the respective applied methods.

This study introduced a new iPSC model of Angelman syndrome. In comparison with the already existing Angelman syndrome iPSC lines, it has the advantage of both parental *UBE3A* alleles being present. This makes it possible to study their expression dynamics in detail and to identify potential interaction partners of UBE3A, thereby also the pathways affected by its physical or functional absence.

2. Materials and Methods

2.1 Materials

2.1.1 Chemicals, Enzymes and Solutions

Chemicals and enzymes were purchased from AppliChem (Darmstadt), BD (Heidelberg), Bio-Rad Laboratories (Munich), Biozym Scientific (Hessisch Oldendorf), Carl Roth (Karlsruhe), Merck (Darmstadt), New England Biolabs (Ipswich, MA, USA), PeproTech (Hamburg), Peqlab (Erlangen), Promega (Mannheim), Qiagen (Hilden), Roche (Mannheim), Sellekchem (Munich), Sigma-Aldrich (Hamburg), STEMCELL Technologies (Cologne), tebu-bio (Offenbach), Thermo Fisher Scientific (Braunschweig) and VWR International (Langenfeld).

2.1.1.1 DNA Markers

FastRuler™ DNA Ladder, Ultra Low Range, Thermo Fisher Scientific
FastRuler™ DNA Ladder, Low Range, Thermo Fisher Scientific
FastRuler™ DNA Ladder, Middle Range, Thermo Fisher Scientific
MassRuler™ DNA Ladder, Low Range, Thermo Fisher Scientific

2.1.1.2 Oligonucleotides

All primers and oligonucleotides including the synthetically methylated ones were created with the Geneious and Primer3 software (geneious.com; bioinfo.ut.ee/primer3-0.4.0/primer3/), and synthesised by Biomers (Ulm), Metabion (Planegg) or Gene Tools (Philomath, OR, USA) with the exception of qRT-PCR probes, which were designed with the Primer Express software and purchased from Eurogentec (Cologne).

2.1.1.3 Enzymes

Restriction and methylation enzymes and their co-factors were purchased from New England Biolabs (Ipswich, MA, USA), GoTaq Green 2 Hot Start Polymerase and GoTaq G2 Flexi from Promega (Mannheim), Q5 Hot Start High-Fidelity DNA Polymerase from New England Biolabs (Ipswich, MA, USA), HotStarTaq from Qiagen (Hilden), DNase I from Promega (Mannheim), qRT-PCR master mixes from Qiagen (Hilden) and Roche (Mannheim).

2.1.1.4 Antibodies

Primary antibodies for the determination of pluripotency of iPSCs by immunohistochemical staining as well as secondary antibodies were bought from Cell Signaling Technology (Leiden, The Netherlands) as part of the StemLight™ Pluripotency Antibody Kit.

Primary antibodies

StemLight™ Pluripotency Antibody Kit #9656 including:
Oct-4A (C30A3) Rabbit mAb
Nanog (D73G4) XP® Rabbit mAb
Sox2 (D6D9) Rabbit mAb
SSEA4 (MC813) Mouse mAb
TRA-1-60(S) (TRA-1-60(S)) Mouse mAb
TRA-1-81 (TRA-1-81) Mouse mAb

Secondary antibodies

Anti-rabbit IgG (H+L), F(ab´)2 Fragment (Alexa Fluor® 555 Conjugate), Cell Signaling Technology, #4413S
Anti-mouse IgG (H+L), F(ab´)2 Fragment (Alexa Fluor® 488 Conjugate), Cell Signaling Technology, #4408S

Antibodies used for the determination of pluripotency of iPSCs by fluorescence-activated cell sorting (FACS) were purchased from BioLegend (Fell).

SSEA4: Alexa Fluor® 647 anti-human #330408
TRA-1-60: PE anti-human TRA-1-60-R #330610
TRA-1-81: Alexa Fluor® 488 anti-human #330710

2.1.1.5 Media for Bacterial Culture

All prepared media were sterilised by autoclaving before use. For selection purposes, antibiotics were added to the media.

LB liquid medium	10 g/l tryptone 5 g/l yeast extract 10 g/l natrium chloride
LB agar plates	10 g/l tryptone 5 g/l yeast extract 10 g/l natrium chloride 12 g/l agar
Antibiotics	100 μg/ml ampicillin 30 μg/ml kanamycin

2.1.1.6 Media for Culturing Murine and Human Cells

MEFs and HEK293 cell line were cultured in DMEM medium supplemented with 10 % FBS and 1 % penicillin/streptomycin.

DMEM medium	10 % (v/v) foetal bovine serum 1 % (v/v) penicillin/streptomycin in DMEM, high glucose

Human embryonic stem cells (hESCs) and induced pluripotent stem cells (iPSCs) were cultured under feeder-dependent conditions in KSR medium or under feeder-independent conditions in the commercially available medium mTeSR™1 purchased from STEMCELL Technologies.

KSR medium	10 % knockout serum replacement
	2 mM glutamine
	1 % non-essential amino acids
	50 U/ml penicillin/streptomycin
	0.1 mM 2-Mercaptoethanol
	4 ng/ml basic fibroblast growth factor 2
	in DMEM/F-12

2.1.2 Organisms

2.1.2.1 DH5α Competent *E. coli*

The bacterial strain DH5α was purchased from Thermo Fisher Scientific (#18265-017). It was used for conventional cloning procedures and possesses the following genotype:
F- Φ80lacZΔM15 Δ(lacZYA-argF) U169 rec A1 end A1 hsdR17(rk-, mk+) phoA supE44 thi-1 gyrA96 relA1 λ-

2.1.2.2 Murine Embryonic Fibroblasts

In order to prevent differentiation of hESCs and iPSCs, mitotically inactivated MEFs were used for their cultivation under feeder-dependent conditions. MEFs were purchased from Applied StemCell (Milpitas, CA, USA), expanded in DMEM supplemented with 10 % FBS and 1 % penicillin/streptomycin, and mitotically inactivated by ionising irradiation with the dose of 40 Gray.

2.1.2.3 Human Embryonic Kidney Cells 293

Cells of the strain HEK293 were transfected with fluorescently labelled compounds or plasmids expressing GFP (green fluorescent protein) or YFP (yellow fluorescent protein) to test the quality of the fluorescence signal. They were also used for transfection with a plasmid carrying wildtype Cas9 together with plasmids carrying gRNAs to verify their efficiency. HEK293 cells were kindly provided by Dr. Stefan Heinrichs from the Institute for Transfusion Medicine, University Hospital Essen.

2.1.2.4 Human Embryonic Stem Cells

Cell line H1 and, in some cases, also H9 served as positive controls in experiments carried out to prove the pluripotency of iPSCs, which were generated in this study in cooperation with the group of Dr. Hannes Klump (Institute for Transfusion Medicine). The use of H1 and H9 is in compliance with the German Stem Cell Law and covered by permission AZ:3.04.02/0099. Both cell lines were purchased from WiCell Research Institute, Inc., Madison, WI, USA and their import is covered by permission AZ 1710-79-1-4-49. Human embryonic stem cells were first isolated from human blastocysts by James Thomson (Thomson 1998).

2.1.2.5 Induced Pluripotent Stem Cells

Cell lines AGI-0 and MCH2-10 were kindly provided by Prof. Dr. Stormy Chamberlain, Farmington, CT, USA (Chamberlain *et al.*, 2010). They represented positive iPSC controls in experiments performed with iPSCs generated in this study. AGI-0 is an iPSC line derived from a patient with Angelman syndrome carrying a large deletion of approximately 6 Mb on the maternal chromosome 15. MCH2-10 is a heathy control iPSC line.
For the purposes of this study, two cell lines were generated by reprogramming dermal fibroblasts with Yamanaka factors. Line AS_Δ3 is a patient-specific cell line, line M55045 is a healthy control line.

2.1.2.6 Nude mice

Immunodeficient NMRI nude mice Crl:NMRI-*Foxn1*^{nu} were used for teratoma formation assay to confirm the pluripotency of iPSCs studied in this project. The experiment was approved by the Committee on the Ethics of Animal Experiments of *Landesamt für Natur, Umwelt und Verbraucherschutz,* LANUV AZ 8.87-50.10.37.09.187 and AZ 84-04.04.2013.A350 and was performed by Dr. Diana Klein (Institute for Cell Biology, University Hospital Essen).

2.2 Methods

2.2.1. General Molecular Biology Methods

2.2.1.1 Small-Scale Preparation of Plasmid DNA

A single colony of *E. coli* transformed with the plasmid of interest was inoculated in 3 ml LB medium supplemented with appropriate antibiotics and cultivated at 37 °C at 250 rpm overnight (G25 Incubator Shaker, New Brunswick Scientific, Nürtingen). 1.5 ml of the cell suspension was centrifuged in a 1.5 ml reaction tube for 20 s at 14 000 rpm and the supernatant was discarded. The pellet was resuspended in 300 µl buffer P1 (4 °C, Qiagen). 300 µl buffer P2 (Qiagen) were added and the reaction tube was inverted several times to mix the sample. Incubation at RT followed for 3 min. 300 µl buffer P3 (Qiagen) were added to stop the lysis. The sample was mixed by inversion and centrifuged for 10 min at 13 000 rpm. The supernatant was transferred to a new reaction tube containing 500 µl 100 % ethanol, mixed well by vortexing and centrifuged for 10 min at 13 000 rpm. The precipitated DNA pellet was washed with 150 µl 70 % ethanol, centrifuged for 5 min at 13 000 rpm, the supernatant was removed and the pellet was left to air-dry for at least 10 min before it was resuspended in 30 µl H_2O.

2.2.1.2 Large-Scale Preparation of Plasmid DNA

Preparations of plasmid DNA in large amounts were performed with the ZymoPURE™ Plasmid Maxiprep Kit following the manufacturer's instructions. 250 ml to 500 ml overnight culture were used for the preparations.

2.2.1.3 Isolation of Genomic DNA

Cell pellet of maximum 5 x 10^6 cells was resuspended in 1 ml lysis buffer and, when needed, incubated at 56 °C until the solution appeared completely clear. 400 µl saturated 5 M NaCl were added, the sample was mixed by inversion several times and centrifuged for 7 min at 14 000 rpm. The supernatant was transferred to a fresh 1.5 ml reaction tube containing 840 µl 100 % isopropanol and inverted until DNA precipitate could be seen. The sample was centrifuged for 7 min at 14 000 rpm and the supernatant was discarded. The DNA pellet was washed with 750 µl 70 % ethanol, centrifuged for 7 min at 14 000 rpm, the supernatant was removed and the pellet was left to air-dry for at least 10 min. The DNA was then resuspended in 30 µl to 100 µl TE buffer, pH 8, depending on the size of the pellet.

Lysis buffer

TEN buffer	2 ml
SDS 10 %	1 ml
Proteinase K	0.5 ml
H_2O	6.5 ml

TEN buffer 10x

Tris-Cl, pH 8	0.1 M
EDTA pH 8	0.01 M
NaCl	1 M

2.2.1.4 Concentration Measurements of Nucleic Acids in Solution

To determine the concentration of nucleic acids in solution, photometric adsorption of the samples was measured at λ = 260 nm, λ = 280 nm and λ = 230 in an ND-1000 Spectrophotometer (NanoDrop Technologies). OD_{260} = 1 corresponds to a concentration of 50 µg/ml DNA or 40 µg/ml RNA. Ratios OD_{260} / OD_{280} and OD_{260} / OD_{230} indicate the purity of the sample. The former ratio equals 1.8 for pure DNA and 2.0 for pure RNA. The latter ratio lies between 2.0 and 2.2 for both pure DNA and RNA. Lower values are caused by the presence of proteins, phenol or other substances absorbing at λ = 280 nm or λ = 230 nm.

2.2.1.5 Bisulphite Conversion

In order to assess the methylation status of a specific DNA region, bisulphite conversion of 500 ng DNA was performed using EZ DNA Methylation-Gold™ Kit (Zymo Research). For low cell counts, EZ DNA Methylation-Direct™ Kit (Zymo Research) was used, which allows for direct conversion from the cells without prior DNA isolation, thereby reducing DNA loss. The application was carried out according to the manufacturer's instructions for the respective kits. Bisulphite-converted DNA was subsequently amplified by PCR and sequenced by Sanger sequencing or next-generation bisulphite sequencing.

2.2.1.6 PCR

Polymerase chain reaction was performed to amplify regions of interest from plasmid DNA, genomic DNA, bisulphite-converted DNA or cDNA. GoTaq G2 Hot Start Green Master Mix (Promega), GoTaq G2 Flexi (Promega), HotStarTaq Master Mix Kit (Qiagen), Q5® Hot Start High-Fidelity DNA Polymerase (NEB) and Q5® Hot Start High-Fidelity 2x Master Mix (NEB) were used. When not using a master mix, the reactions were performed in the buffer supplied by the manufacturer of the respective polymerases with $MgCl_2$ added if necessary, 400 nM to 1000 nM primers, 200 µM to 500 µM dNTP mix, 50 ng to 500 ng DNA template and 0.1 U to 0.5 U polymerase in total volumes of 25 µl or 50 µl.
The initial denaturation phase was followed by 25 to 45 cycles of denaturation, primer annealing and elongation, and a final elongation phase. The primer annealing temperatures

were given by Geneious, Primer3 or Primer Express software and are generally calculated using the formula published by Chester & Marshak, 1993. For applications using products from NEB, the annealing temperatures were calculated with the manufacturer's online tool http://tmcalculator.neb.com/#!/. PCR programmes are specified in the Appendix.

2.2.1.7 DNA Sequencing

Sequencing of plasmid DNA, PCR products or bisulphite-converted DNA was performed using BigDye® Terminator v1.1 Cycle Sequencing Kit (Thermo Fisher Scientific). 1 µl BigDye®, 1 µl reaction buffer, 0.5 µM primer and up to 500 ng template DNA were used in a total volume of 10 µl. Sequencing of bisulphite-converted DNA was performed with 4 µl BigDye® without the addition of reaction buffer. The sequencing PCR began with a denaturation phase at 96 °C for 1 min. 25 cycles of denaturation at 96 °C for 10 s, annealing at a temperature determined by the primer for 5 s, and elongation at 60 °C for 4 min ensued. The samples were filled up to 20 µl with H_2O and purified with sephadex columns. Sephadex (GE Healthcare) was filled into a MultiScreen-HV plate (Merck) using the MultiScreen 45 µl Loader (Millipore) and 300 µl H_2O were added to each well. Columns were incubated at 4 °C for at least 3 h. The plate was centrifuged at 900 x g for 5 min before use. The sequencing reactions were loaded onto the sephadex columns and centrifuged at 900 x g for 5 min into a Thermo-Fast 96 PCR Detection Plate (Thermo Fisher Scientific). 10 µl Hi-Di™ formamide (Thermo Fisher Scientific) were added to each well. The samples were analysed with Genetic Analyzer 3130xl (Thermo Fisher Scientific) and the results were analysed with the programmes Sequencing Analysis v6.0 and Geneious.

2.2.1.8 Next-Generation Bisulphite Sequencing

Samples prepared by bisulphite conversion and subsequent PCR amplification were further processed for analysis of DNA methylation on the 454 Roche Genome Sequencer Junior System. A Re-PCR was performed with MID primers that bind to tag sequences of primers used in the previous PCR. In addition to the tag sequence, the MID primers contain a multiplex identifier (hence the name) specific for the sample, an adaptor and a key sequence for sequencing on the platform. The Re-PCR reaction contained 2 µl to 6 µl PCR product

from the first PCR, and 0.2 µM forward and reverse primer each in HotStarTaq Master Mix (Qiagen) in a total volume of 50 µl. After initial denaturation at 95 °C for 15 min, 35 cycles of denaturation at 95 °C for 30 s and annealing/extension at 72 °C for 1 min ensued, followed by a final elongation phase at 72 °C for 5 min. In rare cases, three-step Re-PCR was performed with the usual annealing step in addition. The Re-PCR products were analysed by gel electrophoresis. In case it was necessary to purify the fragments of interest, gel excision and isolation with Wizard® SV Gel and PCR Clean-Up System (Promega) were performed. The volume of the samples was filled up to 45 µl with H_2O. The subsequent steps were executed by laboratory technicians Sabine Kaya, Melanie Heitmann or Claudia Mertel (Institute of Human Genetics, University Hospital Essen). The Re-PCR products were purified with Agencourt® AMPure® XP system (Beckman Coulter) following the instructions of Roche Diagnostics (Amplicon Library Preparation Method Manual). Then the samples were diluted, pooled and clonally amplified in single droplets in emulsion PCR (emPCR Amplification Method Manual – Lib-A). The droplets contain a single amplicon bound to one DNA capture bead and primers that bind to the adaptor sequence of the MID primers used in the Re-PCR. After amplification, the beads were washed, recovered, enriched and transferred to a microtiter plate (GS Junior Titanium PicoTiterPlate Kit, Roche), whose wells accommodate exactly one bead to ensure purity of the amplicons. The plate was then loaded onto the sequencing platform (GS Junior Titanium Sequencing Kit, Roche) and analysed. Evaluation of the results ensued using the Amplikyzer software (Rahmann *et al.*, 2013) with default settings but for rare cases.

2.2.1.9 DNA Precipitation

DNA solution was filled up to 100 µl with H_2O, 10 µl 3 M sodium acetate, 250 µl 100 % ethanol and optionally 1 µl glycogen were added and the sample was incubated at -20 °C for at least 2 h. Then it was centrifuged for 30 min at 14 000 rpm at 4 °C and the supernatant was discarded. The DNA precipitate was washed with 500 µl 70 % ethanol and centrifuged again for 30 min at 14 000 rpm at 4 °C. The pellet was left to air-dry for at least 10 min and then resuspended in H_2O.

2.2.1.10 DNA Purification

Purification of PCR products was performed using the DNA Clean & Concentrator Kit (Zymo Research) or Agencourt® AMPure® XP system (Beckman Coulter) according to the manufacturers' instructions.

2.2.1.11 Agarose Gel Electrophoresis

PCR products or DNA fragments generated by restriction digests were separated by size on 1 % to 2 % (w/v) agarose gels. Agarose was boiled in 1 x TAE buffer and cooled. 0.4 µg/ml ethidium bromide (EtBr) was added. Samples were mixed with loading dye prior to loading to the wells. DNA markers were used to determine the size of the fragments. Gels were run in 1 x TAE buffer containing 0.4 µg/ml EtBr at 60 V for Southern blots and at 120 V for all other applications. Fragments were visualised on a UV-transilluminator with λ = 312 nm.

Buffer for Gel Electrophoresis

1 x TAE Buffer	40 mM Tris
	40 mM acetic acid
	1 mM EDTA pH 8.0

2.2.1.12 Gel Extraction of DNA

DNA fragments of interest were excised from agarose gels after electrophoresis using the gel extraction tool X-Tracta II (Biozym) on a UV-transilluminator with λ = 312 nm. Wizard® SV Gel and PCR Clean-Up System (Promega) was used to purify the DNA according to the manufacturer's instructions.

2.2.1.13 Insertion of DNA Fragments into TOPO Vector

Fragments bearing 3'-overhangs added by the polymerase during PCR were inserted into pCR^{TM}2.1 using TA Cloning® Kit (Thermo Fisher Scientific) in a one-step ligation reaction.

2 µl PCR product and 2 µl pCR™2.1 were incubated with 4 U T4-ligase in 1 x ligation buffer in a final volume of 10 µl at 14 °C overnight.

2.2.1.14 Transformation of Competent Bacteria

Transformation was performed using Subcloning Efficiency™ DH5α™ (Thermo Fisher Scientific) following the manufacturer's instructions. Bacteria were plated onto agar plates supplemented with antibiotics and incubated at 37 °C overnight.

2.2.1.15 Restriction Digests

Genomic or plasmid DNA was digested by restriction enzymes suitable for the respective applications. Under optimal conditions, 1 U enzyme digests 1 µg DNA in 1 h. The restriction reactions were performed under conditions recommended by the manufacturer. The incubation times were 15 min to 20 h depending on the application.

2.2.1.16 Southern Blot

10 µg to 15 µg genomic DNA were digested with *Eco*RV and *Bam*HI at 37 °C for at least 16 h. The whole reaction was loaded onto a 1.0 % agarose gel and run at 60 V for 5 h to 6 h. A picture of the gel was taken with a fluorescent ruler on a UV-transilluminator with λ = 312 nm. The gel was denatured twice in denaturing solution (438 g NaCl and 100 g NaOH in 5 l) for 30 min. Southern blot assembly ensued. Three layers of Whatman paper (35 cm x 15 cm) were soaked in denaturing solution and placed over a block the size of an agarose gel set in a container half-filled with denaturing solution. Air bubbles were removed with a glass rod. The agarose gel was laid on the layer of Whatman papers and bubbles were removed again. Strips of Parafilm® M (Pechiney Plastic Packaging) were placed around the gel. Amersham Hybond™-XL membrane (GE Healthcare) soaked in denaturing solution was laid on the gel and bubbles were removed. Three additional Whatman paper were soaked in denaturing solution and layered over the blotting membrane. Bubbles were removed. A stack of paper towels was positioned at the top of the blot sandwich and weighted down with a metal block. The transfer of the DNA to the membrane ensued for at least 16 hours. The blot

was then disassembled, gel slots were marked on the membrane with a pencil and the membrane was soaked in 20 mM Na_2HPO_4. With the help of a glass rod, the membrane was transferred into a 50 ml Falcon tube and a hole was pierced in the lid of the tube. Pre-hybridisation in 4 ml pre-warmed Church buffer (7 % SDS, 1 mM EDTA, 0.5 M Na_2HPO_4/NaH_2PO_4 pH 7.2) ensued at 65 °C for 30 min. The probe was labelled with α-^{32}P-dCTP using the Megaprime DNA Labeling System, dNTP (GE) and purified with the QIAquick Nucleotide Removal Kit (Qiagen) by Dr. Laura Steenpass (Institute of Human Genetics). Hybridisation followed at 65 °C overnight in 4 ml fresh Church buffer with 15 µl probe added. The membrane was briefly rinsed with pre-warmed Church buffer, washed twice with Church buffer for 30 min, sealed and exposed to film.

2.2.1.17 Isolation of Total RNA

Total RNA was isolated from cells using TRIzol® (Thermo Fisher Scientific) according to the manufacturer's instructions or RNeasy® Mini Kit (Qiagen) also following the protocol supplied with the kit.

2.2.1.18 Reverse Transcription of RNA

In order to prevent false-positive results due to contamination with DNA, samples were treated with DNase using the RQ1 RNase-free DNase Kit (Promega) according to the manufacturer's instructions prior to performing reverse transcription reaction. 1 U DNase was used to treat 1 µg RNA. The reverse transcription reaction ensued with 500 ng RNA, 5 mM $MgCl_2$, 1 mM dNTP each, 2.5 µM random hexamers, 1 U/µl RNase inhibitor and 2.5 U/µl MuLV reverse transcriptase in PCR Buffer II in a total volume of 50 µl. A control reaction without the MuLV reverse transcriptase was performed. All substances were purchased from Thermo Fisher Scientific.

2.2.1.19 Reverse-Transcription PCR

To verify the specificity of selected primer pairs used in this project, PCR was performed on cDNA and the result was analysed by gel electrophoresis.

2.2.1.20 Quantitative Real-Time PCR

qRT-PCR was used to assess the expression of a number of genes relative to a stably expressed housekeeper gene most suitable for the respective assays, *GAPDH*, *RPL13A* or *ACTB*. The normalisation of the studied gene to a housekeeper gene also serves the purpose of correcting variations, which may occur during the process of preparing cDNA, and allows for the results of different qRT-PCRs to be compared between each other in a reliable manner. The $\Delta\Delta C_T$ method was used for calculation and the expression levels of the respective genes were set to 1 in the chosen reference sample. The result of a qRT-PCR is given as fold-difference in the expression of the studied gene. SYBR Green binds to the newly synthesised DNA strands, thus the fluorescence detected at the end of each cycle is proportionate to the amount of PCR products. The cycle in which the fluorescence crosses a set threshold is determined as the C_T (threshold cycle). This value is used to calculate the fold-change in the gene expression. Apart from not having to employ a labelled probe for each specific target, another advantage of performing qRT-PCR with SYBR Green is the possibility of verifying the specificity by subsequent melting curve analysis. The reactions contained 10 µl SYBR Green master mix, 0.5 µM forward and reverse primer each, and 10 ng cDNA in a total volume of 20 µl. The initial denaturation at 95 °C for 1 min was followed by 40 cycles of denaturation at 95 °C for 15 s and annealing/elongation at 60 °C for 30 s. The melting curve analysis ensued starting by denaturation at 95 °C for 1 min and annealing at 55 °C for 30 s, followed by a rise in temperature to 95 °C by 0.5 °C per step held for 30 s, after which the fluorescence was read. Plates were run on a CFX96™ Real-Time System C1000™ Thermal Cycler (Bio-Rad) and the generated data was analysed with the Bio-Rad CFX Manager 3.1 software.

2.2.1.21 Single-Nucleotide Primer Extension Assay

The three-base pair deletion in Angelman syndrome iPSCs was used as a SNP to determine the allelic ratios of *UBE3A*. Analysis of cDNA prepared from mRNA isolated from pluripotent cells, neural progenitors and terminally differentiated neurons was performed using the ABI PRISM® SNaPshot™ Multiplex Kit (Thermo Fisher Scientific). Genomic DNA served as reference. The samples were prepared and sequenced by Michaela Hiber

(Institute of Human Genetics) and the data were evaluated using the Gene Mapper 4.0 software (Applied Biosystems) by Dr. Laura Steenpass.

2.2.1.22 Quantitative Allele Distinction of *UBE3A*

To distinguish and quantify the expression from the wildtype paternal *UBE3A* allele and the maternal *UBE3A* allele harbouring a three-base pair deletion in Angelman syndrome iPSCs, qRT-PCR was employed utilising fluorescently labelled minor groove binding probes. The probes were designed with the Primer Express software to detect specifically the sequence with and without the triplet, respectively, and to match the Tm of 60 °C, while being as similar in length as possible. Artificial wildtype and mutant templates were developed by cloning a 280 bp cDNA fragment from Angelman syndrome iPSCs with the site of the deletion positioned in the middle into a vector. The presence or absence of the triplet was verified by Sanger sequencing. The respective plasmids were mixed in defined ratios from 0:100 to 100:0 to create a standard curve for both targets at a time detected by probes labelled with different fluorophores. When using probes labelled with the same fluorophore, two separate standard curves were calculated for the paternal and the maternal *UBE3A* allele, respectively.

2.2.2 Cell Culture

2.2.2.1 Reprogramming of Fibroblasts into iPSCs

Skin fibroblasts from a healthy control person were cultivated, expanded and subjected to reprogramming by a lentiviral vector expressing *POU5F1*, *SOX2*, *KLF4* and *MYC*, and a reporter fluorescent protein (Voelkel *et al*., 2010). 5 x 10^5 cells were seeded on a 10-cm dish and transduced with an MOI (multiplicity of infection) of 5, that is, in a ratio of five virus particles per cell. Seven days later, cells expressing the reporter protein were isolated by fluorescence-activated cell sorting and 1000 cells/cm^2 were plated on 10-cm dishes or 6-well plates in KSR medium supplemented with Rho-associated protein kinase (ROCK) inhibitor Y-27632 (Sellekchem), which enhances the recovery of freshly thawed cells or cells passaged as single cells. Colonies were isolated approximately four weeks later. Skin fibroblasts from

an Angelman syndrome patient were reprogrammed by Kristin Stolp in the laboratory of Dr. Hannes Klump at the Institute of Transfusion Medicine.

2.2.2.2 Thawing Cryopreserved Cells

Cells were stored at -80 °C for short-term storage and at -195 °C for long-term storage in liquid nitrogen. Frozen aliquots were thawed quickly in a water bath heated to 37 °C and diluted in 9 ml pre-warmed culture medium. Cells were centrifuged at 1000 rpm for 4 min, the pellet was resuspended in 1 ml culture medium and transferred to appropriate culture vessels. Stem cells were plated on a well of a 6-well plate (Nunc™ Cell Culture Treated Multidishes, Thermo Fisher Scientific) coated either with 0.2 % gelatine and a layer of feeder cells, or with Vitronectin XF™ (STEMCELL Technologies) containing 1 ml culture medium. The culture medium was supplemented with ROCK inhibitor. MEFs were transferred into a 75 cm^2 culture flask after thawing (Greiner).

2.2.2.3 Maintenance

Cells were cultured in KSR medium or in mTeSR™1 at 37 °C and 5 % CO_2 in a humidified incubator. When they reached confluency, they were passaged using Collagenase Type IV (STEMCELL Technologies), if grown under feeder-dependent conditions, Gentle Cell Dissociation Reagent (STEMCELL Technologies), if grown under feeder-free conditions, or StemPro® Accutase® Dissociation Reagent (Thermo Fisher Scientific), if single cells were needed.

KSR medium	10 % knockout serum replacement
	2 mM glutamine
	1 % non-essential amino acids
	50 U/ml penicillin/streptomycin
	0.1 mM 2-Mercaptoethanol
	4 ng/ml FGF2
	in DMEM/F-12

2.2.2.4 Cryopreservation of Cells

Cells were dissociated in the same manner as for passaging, centrifuged at 1000 rpm for 4 min and the pellet was resuspended in freezing medium. 1 ml cell suspension was transferred to each cryo tube (Nunc™ CryoTubes™, Thermo Fisher Scientific) and incubated on ice for 20 min. The cells were kept in a polystyrene box at -80 °C for at least a week before being transferred to a liquid nitrogen tank.

Freezing Medium	90 % foetal bovine serum
	10 % DMSO

2.2.2.5 Neuronal differentiation

2.2.2.5.1 Dual SMAD Inhibition by Koch *et al.*

Cell clumps were transferred to a 10-cm low-attachment dish and kept in basic medium. The medium was changed on day 2. On day 4, neuronal differentiation was initiated by dual SMAD inhibition; neural differentiation medium (NDM) was changed every other day. On day 12, embryoid bodies (EBs) were plated on a matrigel-coated 10-cm dish in NDM; medium change ensued every other day. On day 18, rosettes and neuroectodermal islands were isolated, treated with trypsin or TrypLE Express (Thermo Fisher Scientific) to obtain a single-cell suspension and seeded on a matrigel-coated well of a 6-well plate at high density. Neural progenitors were then differentiated further in NDM to terminally differentiated neurons (day 48). Alternatively, the cells were cultured in lt-NES medium to maintain them in the neural progenitor stage (Koch *et al.*, 2009).

NDM	50 % DMEM/F12 (120.5 ml)
	50 % Neurobasal (120.5 ml)
	2 mM glutamine
	0.4 g glucose
	100 U/ml penicillin/streptomycin

	0.5 % N2 supplement
	0.5 % B27 supplement
	0.75 µg cAMP
	0.25 µM LDN-193189
	10 µM SB-431542
Lt-NES	2 mM glutamine
	0.4 g glucose
	100 U/ml penicillin/streptomycin
	1 % N2 supplement
	0.1 % B27 supplement
	10 ng/ml EGF
	10 ng/ml FGF2
	238.5 ml DMEM/F12 (filled up to 250 ml)

2.2.2.5.2 Dual SMAD Inhibition by Chambers *et al*.

Single cells were subjected to neuronal differentiation when confluency reached 90 % by changing the culture medium to SRM. On day 4, the medium was changed to SRM:N2 mixed in a ratio of 3:1, on day 6 to SRM:N2 mixed in a ratio of 1:1 and on day 8 to SRM:N2 mixed in a ratio of 1:3. On day 10, three wells of a 6-well plate were transferred to one well of a 6-well plate in BASF medium and cultured for six days. The medium was replaced with BAGTC on day 17 and the cells were cultured for seven more days. BASF and BAGTC media were changed every other day (Chambers *et al.*, 2009). Samples for the extraction of RNA were harvested on day 0, day 5, day 10, day 17 and day 24.

SRM	15 % knockout serum replacement
	2 mM glutamine
	1 % non-essential amino acids
	0.5 mM 2-Mercaptoethanol
	100 nM LDN-193189
	10 µM SB-431542

	in Knockout DMEM
N2	1 % N2 supplement 2 mM glutamine 100 nM LDN-193189 10 µM SB-431542 in Neurobasal
BASF	2 % B27 supplement without retinoic acid 1 % N2 supplement 2 mM glutamine 20 ng/ml BNDF 200 µM ascorbic acid 50 ng/ml SHH 100 ng/ml FGF8 in Neurobasal
BAGTC	2 % B27 supplement without retinoic acid 1 % N2 supplement 2 mM glutamine 20 ng/ml BNDF 200 µM ascorbic acid 20 ng/ml GDNF 1 ng/ml TGFβ-III 500 µM dbcAMP in Neurobasal

2.2.2.5.3 Neuronal Differentiation by STEMdiff™ Neural Induction Medium

Single cells were plated on a matrigel-coated well of a 6-well plate in STEMdiff™ Neural Induction Medium (STEMCELL Technologies) and cultured for 11 days. Medium was

changed every day. The cells were split and seeded on a new matrigel-coated well of a 6-well plate at the density of 2 x 10^5 cells/cm^2 when they reached confluency, that is, on day 7 to 9.

2.2.2.5.4 Dual SMAD Inhibition by Boissart *et al*.

Neuronal induction was initiated by plating cell clumps on a matrigel-coated well of a 6-well plate in induction medium supplemented with ROCK inhibitor. Medium was changed every other day. On day 10, the monolayer was replated on a new matrigel-coated well of a 6-well plate in expansion medium, cultured for four more days and harvested on day 14 (Boissart *et al.*, 2013).

Induction medium	50 % DMEM/F12
	50 % Neurobasal
	0.5 % N2 supplement
	0.5 % B27 supplement
	100 nM LDN-193189
	20 µM SB-431542
	4 ng/ml FGF2
Expansion medium	50 % DMEM/F12
	50 % Neurobasal
	0.5 % N2 supplement
	0.5 % B27 supplement
	10 ng/ml EGF
	10 ng/ml FGF2

2.2.2.6 Transfection of HEK Cells and iPSCs

Cells were transfected using Lipofectamine® RNAiMAX Transfection Reagent (Thermo Fisher Scientific) following the manufacturer's protocol. Methylated oligonucleotides, single-stranded in vitro-methylated DNA or plasmid DNA, and lipofectamine were diluted in Opti-MEM medium separately, then combined and incubated at RT for 5 min to allow for

complexes to form. The mixture was added dropwise to the cells. Medium was changed 24 hours later. The efficiency of the transfection was analysed the following day by microscopy.

2.2.2.7 Nucleofection of iPSCs

Cells were nucleofected using the Amaxa™ Nucleofector™ Technology (Lonza) and the Human Stem Cell Nucleofector® Kit 2 according to the manufacturer's instructions. The appropriate volume of the supplement and the Nucleofector® Solution were combined just prior to performing nucleofection. Cells were dissociated by StemPro® Accutase® Dissociation Reagent (Thermo Fisher Scientific) and the cell count was determined. The required number of cells was centrifuged at 1000 rpm for 4 min and the pellet was resuspended in the prepared Nucleofector® Solution in a ratio of 100 µl per 800 000 cells. DNA to be delivered into the cells was added to the cell suspension and the sample was mixed gently. 100 µl were transferred to a cuvette supplied with the kit without bubbles, the cuvette was closed and inserted into the Nucleofector™ 2b (Lonza), and the programme B016 was applied. 500 µl culture medium were added to the cuvette and the cell suspension was gently transferred into a prepared 24-well plate with the supplied plastic pipettes. The efficiency of the nucleofection was analysed the following day by microscopy.

2.2.2.8 Electroporation of iPSCs

Cells were electroporated using the Neon® Transfection System (Thermo Fisher Scientific) following the protocol recommended by the manufacturer. Cells were dissociated by StemPro® Accutase® Dissociation Reagent (Thermo Fisher Scientific) and the cell count was determined. The required number of cells was centrifuged at 1000 rpm for 4 min and the pellet was resuspended in Opti-MEM to reach the density of 5×10^5 cells per 10 µl. DNA to be electroporated into the cells was added to the cell suspension and the sample was mixed gently. 10 µl cell suspension were taken into the Neon® Pipette tip, set into the pipette holder and the electric pulse of 1100 V was applied for 30 ms. Electroporation was performed by Sebastian Vogt (Department of Medical Oncology, University Hospital Essen). Cells were then seeded into prepared wells of 6-well or 24-well plates. The efficiency of the electroporation was analysed the following day by microscopy and on the third day by FACS.

2.2.2.9 Pluripotency Tests

2.2.2.9.1 Alkaline Phosphatase Staining

Colonies of hESCs and iPSCs were tested for the activity of alkaline phosphatase, whose high activity is a general marker of pluripotency, using the Alkaline Phosphatase Detection Kit (EMD Millipore) according to the manufacturer´s instructions.

2.2.2.9.2 Immunocytochemistry

Immunofluorescent antibody staining was performed using StemLight™ Pluripotency Antibody Kit (Cell Signaling Technology). Primary and secondary antibodies are listed in the section Materials. Cells were washed with PBS and fixed with 4 % paraformaldehyde for 15 min. Washing thrice with PBS followed. Cells to be stained with nuclear markers were treated with 0.3 % Triton X-100 for 5 min and washed thrice with PBS. Blocking was performed for 30 min to 60 min with blocking buffer (48.5 ml PBS with 1.5 ml goat serum). Primary antibodies were diluted in antibody dilution buffer (49.5 ml PBS with 0.5 ml goat serum) as follows: Oct-4A, Sox2 and SSEA4 1:200, Nanog, TRA-1-60(S) and TRA-1-81 1:100. Incubation ensued at 4 °C overnight. Cells were washed thrice with PBS and secondary antibodies diluted 1:1000 were added. After incubation at RT for 2 h in the dark, cells were washed thrice with PBS and incubated with DAPI diluted 1:200 at RT for 30 min in the dark. Finally, the cells were washed thrice with PBS and stored in 500 µl PBS at 4 °C in the dark until pictures were taken.

2.2.2.9.3 Fluorescence-Activated Cell Sorting (FACS)

Cells were dissociated with StemPro® Accutase® Cell Dissociation Reagent (Thermo Fisher Scientific) and feeder removal was performed with Feeder Removal MicroBeads (Miltenyi) according to the manufacturer's instructions. 1 x 10^5 cells in 100 µl FACS buffer (90 % PBS, 10 % FBS) were used per staining with antibodies or isotype controls. The volume of the respective antibodies and isotype controls added to the cells was either given by the manufacturer, or calculated using the general rule of 1 µg antibody per 1 x 10^6 cells.

Incubation at 4 °C for 20 min in the dark ensued. 1 ml FACS buffer was added and the samples were centrifuged at 700 x g for 5 min. The pellet was resuspended in 200 µl FACS buffer and transferred to FACS tubes for analysis on ARIA III (BD). BD FACSDiva™ software V8.0.1 and FlowJo® V10 (FlowJo LLC) software were used for evaluation of the results. Anika Neureiter performed the analysis and evaluation of the pluripotency assays.

2.2.2.9.4 Quantitative Real-Time PCR

cDNA prepared by reverse transcription of RNA was used for comparing expression levels of pluripotency marker genes *POU5F1, SOX2, KLF4, MYC, NANOG, LIN28, DNMT3B* and *REX1* in hESCs and iPSCs. *RPL13A* and *GAPDH* were used for normalisation by the $\Delta\Delta C_T$ method. Expression levels in hESCs were set to 1. QuantiFast SYBR Green PCR Kit was purchased from Qiagen and samples were analysed using BIORAD software. Detailed description of the method can be found in section 2.2.1.20.

2.2.2.9.5 EB Formation Assay

8 000 cells to 15 000 cells per well were seeded into V-bottom or U-bottom 96-well plates (Nunc™ 96-well Polystyrene V-bottom or U-bottom MicroWell™ Plates, Thermo Fisher Scientific), in 100 µl AggreWell™ EB Formation Medium (STEMCELL Technologies). On day 6, the formed embryoid bodies were transferred to 6-well plates with or without coating with 0.2 % gelatine and cultured until day 14 when they were harvested. Culture medium was changed every other day. EBs were analysed by qRT-PCR.

2.2.2.9.6 Teratoma Assay

For teratoma formation assay, cells were dissociated with StemPro® Accutase® Cell Dissociation Reagent (Thermo Fisher Scientific), centrifuged at 1000 rpm for 4 min, resuspended in DMEM/F-12 medium in a ratio of 50 µl medium per 1 x 10^6 cells and kept on ice. 50 µl growth factor reduced Matrigel (BD) were added per 50 µl medium and 100 µl (equals 1 x 10^6 cells) were injected into both hind limbs of two immunodeficient NMRI nude mice Crl:NMRI-*Foxn1*^{nu}. Teratomas were explanted when skin lesions appeared or after the

maximum of 67 days. They were fixed, embedded in paraffin and cut into microsections. The assay was performed by Dr. Diana Klein. Staining with haematoxylin and eosin ensued at the Institute of Pathology, University Hospital Essen. Microscopic analysis for the presence of all three germ layers was performed by Prof. Dr. Agnes Bankfalvi (Institute of Pathology).

2.2.2.10 Integrity Tests

2.2.2.10.1 Karyotyping

Cells were treated with 100 ng/ml colcemid (Roche) for at least four hours, then dissociated with StemPro® Accutase® Cell Dissociation Reagent (Thermo Fisher Scientific), centrifuged at 1000 rpm for 10 min, resuspended in 8 ml pre-warmed KCl solution (0.3 g KCl, 0.02 g EGTA, 0.48 g HEPES in 96 ml H_2O) and incubated at 37 °C for 20 min. 1.5 ml freshly prepared fixative (methanol : acetic acid = 1:3) was added, the sample was mixed by inversion and centrifuged at 1000 rpm for 10 min. The supernatant was discarded and the pellet was washed thrice with 8 ml fixative. Finally, the pellet was resuspended in 250 µl to 500 µl fixative and stored at -20 °C. Metaphase spreads were prepared by dropping the cell suspension onto glass slides, which were stored in 100 % ethanol at -20 °C and rinsed well with water prior to use. The slides were dried briefly on a plate heated to 60 °C, then baked overnight at 60 °C, treated with 2.5 % trypsin for 4 min, washed thrice in 0.9 % NaCl solution, stained with 10 % Giemsa solution for 3 min to 5 min, rinsed with water, air-dried and sealed with coverslips. Most metaphases were prepared and analysed by Elke Jürgens (Institute of Human Genetics) with an Axioskop microscope (Zeiss) and Ikaros software v5.8 (MetaSystems).

2.2.3. Methylation Induction

2.2.3.1 Methylated Oligonucleotides

Artificial methylated oligonucleotides are protected from degradation by cellular nucleases by a phosphorothioate backbone. One non-bridging oxygen atom on the phosphate backbone is replaced by a sulphur atom, thus forming a phosphorothioate bond. The delivery of the

oligonucleotides into the cells was performed by transfection with Lipofectamine® RNAiMAX (Thermo Fisher Scientific) at the following concentrations: 0.5 µM, 2.0 µM, 5.0 µM and 10.0 µM. The cells were harvested 24 h, 48 h and 72 h post transfection and analysed for the induction of DNA methylation at the targeted locus by Sanger sequencing of bisulphite-converted DNA. The concentration of 2.0 µM proved to be optimal for cell survival after treatment and was used in subsequent experiments. Three to six consecutive transfections were used to deliver the oligonucleotides into the cells every other day, or every three days. The cells were analysed microscopically for the presence of a fluorescence signal from one of the oligonucleotides 24 h post transfection and harvested after the third or the sixth round of treatment, respectively. Analysis of the targeted locus ensued by Sanger sequencing of bisulphite-converted DNA. As an alternative, nucleofection using the Amaxa™ Nucleofector™ Technology (Lonza) was employed for delivery in otherwise identical experimental settings.

2.2.3.2 In Vitro-Methylated DNA Fragments

DNA fragments were methylated in vitro using the *M.Sss*I CpG methyltransferase (NEB) or during PCR with methylated dCTPs. For the former application, up to 4 µg DNA were incubated with 1 U/µl *M.Sss*I methyltransferase and 320 µM SAM as the donor of the methyl group in NEB Buffer 2 in a total volume of 20 µl at 37 °C for 4 h. Then, fresh SAM was added to the reaction and the incubation continued overnight. For the latter application, plasmid DNA containing the required fragment was used as template and methylated dCTPs (Zymo Research) were added to the reaction. The ratio of methylated dCTPs to unmethylated dCTPs was 60:40. GoTaq G2 Flexi polymerase (Promega) was used for amplification. The success of the methylation was validated by restriction digest of 200 ng DNA with the methylation-sensitive enzyme *Hpa*II. DNA fragments that had been methylated in vitro either by *M.Sss*I CpG methyltransferase, or by PCR with methylated dCTPs were denatured at 95 °C for 5 min and incubated on ice for at least 2 min prior to transfection. They were delivered into the cells by three to six consecutive rounds of transfection with Lipofectamine® RNAiMAX (Thermo Fisher Scientific) and harvested for analysis after the third, fourth, fifth and sixth round of transfection. DNA was subjected to bisulphite conversion and analysed by Sanger sequencing or next-generation bisulphite sequencing.

2.2.3.3 Modified CRISPR/Cas9 System

The wildtype variant of the Cas9 protein was engineered to induce methylation of the targeted sequence instead of double-strand breaks. It was fused with the active domains of DNMT3A and DNMT3L. Four different gRNAs were designed to target the sequence covered by the amplicon used for next-generation bisulphite sequencing. All constructs were kindly provided by Dr. Pavel Bashtrykov from the laboratory of Prof. Dr. Albert Jeltsch, Stuttgart. Plasmids carrying the modified Cas9 construct were delivered into the cells by nucleofection using the Amaxa™ Nucleofector™ Technology (Lonza) together with one or two plasmids containing the gRNAs. Alternatively, the plasmid DNA was delivered into the cells by electroporation using the Neon® Transfection System (Thermo Fisher Scientific). Altogether, 5 µg plasmid DNA were used for a single delivery. Cells were harvested three days post treatment, sorted by fluorescence-activated cell sorting by the expression of YFP by Hannah de Oliveira Kessler (Institute for Transfusion Medicine) and either analysed directly for the presence of DNA methylation, or seeded and harvested seven and fourteen days later for analysis.

2.2.3.3.1 T7 assay

HEK cells were transfected with 2 µl Lipofectamine® 2000 (Thermo Fisher Scientific) diluted in 25 µl Opti-MEM medium combined with 500 ng plasmid carrying wildtype Cas9 and 120 ng plasmid containing gRNA also diluted in 25 µl Opti-MEM medium. Cells were lysed 48 h later. PCR was performed using Q5® Hot Start High-Fidelity 2x Master Mix (NEB), 0.5 µM forward and reverse primer each, and 100 ng DNA as template. PCR products were purified using DNA Clean & Concentrator Kit (Zymo Research) and the concentration of the samples was adjusted to 20 ng/µl. The subsequent annealing reaction contained 2 µl NEB Buffer 2 and 18 µl purified PCR product. Initial denaturation at 95 °C for 10 min was followed by five steps of lowering the temperature from 95 °C to 85 °C by 2 °C/s, then by 600 steps of lowering the temperature from 85 °C to 25 °C by 0.1 °C/s. Restriction digest by T7 Endonuclease I ensued. 1 µl enzyme was added to each of the annealed samples and the reaction was incubated at 37 °C for 15 min. The result was analysed by agarose gel electrophoresis.

3. Results

Some results presented in this thesis are included in the paper Stanurova *et al*. 2016 published in cooperation with Anika Neureiter. After reprogramming fibroblasts from an Angelman syndrome patient into induced pluripotent stem cells by Kristin Stolp (Institute for Transfusion Medicine), characterisation of eight patient-derived clones ensued. Clones D, F and H were assayed at the Institute of Human Genetics as part of my PhD project; clones B1, W, Y, Q and P, and the human embryonic stem cell line H1 representing the gold standard for pluripotency were analysed by Anika Neureiter within her PhD project at the Institute for Transfusion Medicine. Alkaline phosphatase staining, immunohistochemistry, qRT-PCR, EB formation assay and teratoma assay were executed separately. FACS of all eight clones was done jointly at the Institute for Transfusion Medicine and evaluated by Anika Neureiter. Sequencing, Southern blot and karyotyping of all eight clones were performed at the Institute of Human Genetics. Based on the result of the Southern blot, clones D, H, B1 and P with a single virus integration site were selected for further experiments. Ten healthy control clones isolated after reprogramming were first subjected to Southern blot analysis to choose those with a single virus integration site. Only then did their characterisation follow. Both selected control clones 42 and 645 were characterised at the Institute of Human Genetics, but for FACS analysis and evaluation done by Anika Neureiter. Neuronal differentiation according to the protocol from Koch *et al*. was carried out with patient-derived clones D and H, and previously published cell lines AGI-0 and MCH2-10 (Chamberlain *et al.*, 2010) at the Institute of Human Genetics. Experiments on neuronal differentiation employing the protocol from Chambers *et al*. were performed separately; patient-derived clones D and H, and healthy control clones 42 and 645 were assayed at the Institute of Human Genetics. Experiments relying on the STEMdiff™ protocol and the protocol from Boissart *et al*. were conducted both at the Institute of Human Genetics and the Institute for Transfusion Medicine with the four patient-derived clones, the two control clones and human embryonic stem cell lines H1 and H9. Further work on neuronal differentiation optimisation was done by Anika Neureiter. Samples obtained with her protocol were processed for single-nucleotide primer extension assay at the Institute of Human Genetics. Quantitative allele distinction assay, methylation

analyses of imprinted and pluripotent loci, and methylation induction experiments were performed at the Institute of Human Genetics. Results displayed here are generally restricted to patient-derived clone D, healthy control clone 645 and human embryonic stem cell line H1 for comparison. Patient-derived clone D, along with patient-derived clone H, exhibited the best results regarding methylation stability at imprinted loci among patient-derived clones. The healthy control clone 645 showed a higher potential for differentiation than clone 42. Thus, patient-derived clone D and healthy control clone 645 were chosen as representative examples.

3.1 Reprogramming of Skin Fibroblasts

Fibroblasts from a skin biopsy of a healthy control person were reprogrammed with a lentiviral vector as described in 2.2.2.1 and 48 iPSC colonies were isolated manually approximately four weeks post selection by FACS. Of these clones, six were selected for further analysis; the rest was cryopreserved. Fibroblasts from a skin biopsy of an Angelman syndrome patient carrying a three-base pair deletion in the *UBE3A* maternal allele (Horsthemke *et al.*, 2011) were reprogrammed by Kristin Stolp and eight iPSC clones were selected. The reprogramming efficiencies were comparable (Stanurova *et al.*, 2016).

3.2 iPSC Characterisation

The isolated iPSC clones were characterised by various tests in order to validate their pluripotency. Pluripotency was verified by AP staining, immunocytochemistry, fluorescence-activated cell sorting, qRT-PCR, EB formation assay and teratoma assay.

3.2.1 Pluripotency Verification

3.2.1.1 Alkaline Phosphatase Staining

Alkaline phosphatase is a hydrolase enzyme, which catalyses dephosphorylation of substrates such as nucleotides under alkaline conditions. It is highly expressed in pluripotent stem cells and the activity of the enzyme is a general marker of pluripotency. If alkaline phosphatase converts the colourless substrate, the colonies exhibit a pink/red colour. iPSC colonies were tested using the Alkaline Phosphatase Detection Kit and all clones stained positive for the activity of alkaline phosphatase. Results are shown in Fig. 4A.

3.2.1.2 Immunocytochemistry

Immunofluorescent staining was used to verify the presence of nuclear pluripotency markers OCT4, NANOG and SOX2, and surface pluripotency markers SSEA4, TRA-1-60 and TRA-1-81. All clones stained positive for all markers. Results are shown in Fig. 4B.

3.2.1.3 Fluorescence-Activated Cell Sorting

The presence of surface pluripotency markers SSEA4, TRA-1-60 and TRA-1-81 was proved by FACS, as seen in Fig. 4C. Results were analysed by Anika Neureiter. All clones exhibited pluripotency in these experiments.

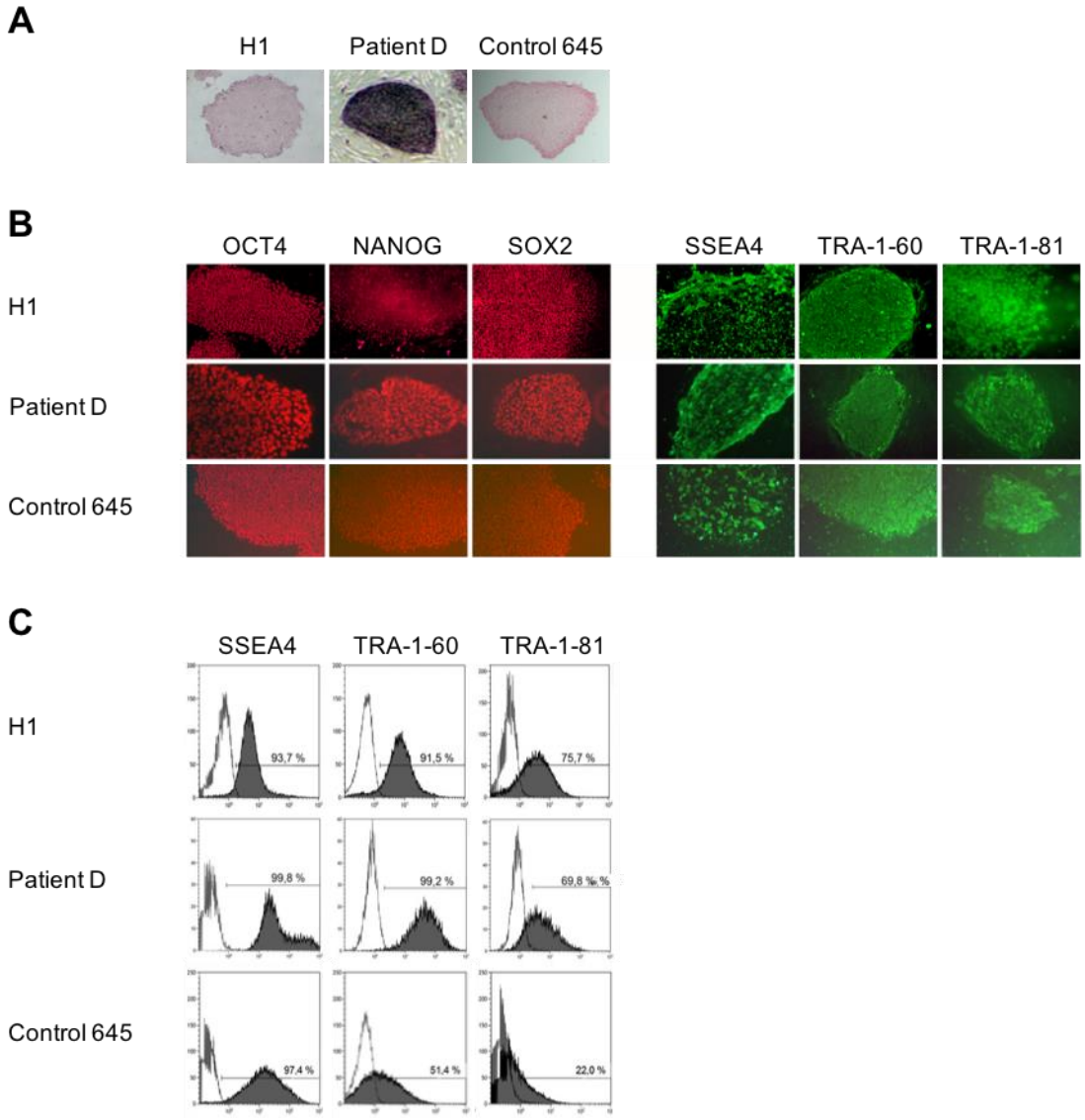

Figure 4. Characterisation of patient-derived and control iPSCs in comparison with hESCs H1. A) Patient-derived line D and control line 645 exhibit high activity of alkaline phosphatase. hESCs H1 are shown for comparison. **B)** Immunofluorescent staining of nuclear markers OCT4, NANOG and SOX2 (red), and surface markers SSEA4, TRA-1-60 and TRA-1-81 (green) confirm expression of pluripotency markers in patient-derived line D and control line 645 in comparison to hESCs H1. **C)** FACS analysis of surface markers SSEA4, TRA-1-60 and TRA-1-81 shows the comparison of isotype controls in white with the staining with a specific antibody in grey. A positive result is indicated by a shift of the assayed population to the right. hESCs H1 are depicted for comparison. hESCs H1 analyses, and FACS analysis and evaluation were performed by Anika Neureiter. The figure was adapted from Stanurova *et al.*, 2016.

3.2.1.4 Quantitative Real-Time PCR

qRT-PCR was employed to assess the expression of eight pluripotency markers: *POU5F1* coding for the pluripotency marker OCT4, *SOX2*, *KLF4*, *MYC*, *NANOG*, *LIN28*, *DNMT3B* and *REX1* coding for the pluripotency marker ZFP42. Housekeeper genes *RPL13A* and *GAPDH* were used for normalisation. Results are shown in Fig. 5. All genes showed expression levels comparable to those in hESCs H1 in all clones.

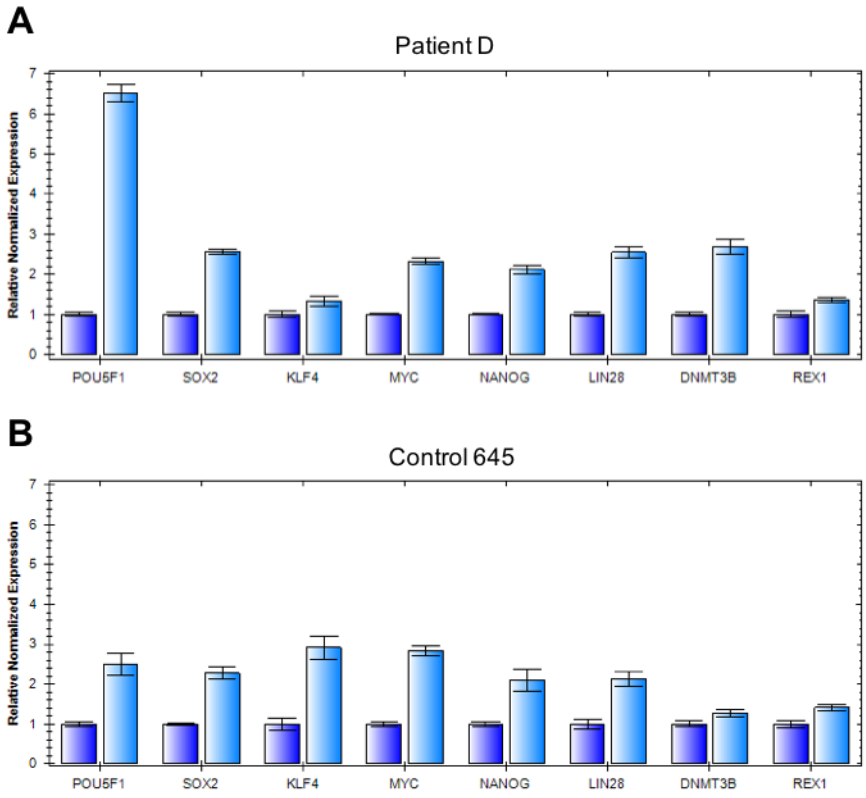

Figure 5. Pluripotency confirmation of patient-derived and control iPSCs by qRT-PCR. Expression of eight selected markers associated with pluripotency was analysed by qRT-PCR. Results for the assayed lines are shown relative to hESCs H1. Both **A)** the patient-derived line D and **B)** the control line 645 are similar to hESCs H1 in expression levels of all evaluated markers (iPSCs in light blue, hESCs H1 in dark blue). Standard deviation of three technical replicates is indicated.

3.2.1.5 EB Formation Assay

iPSCs were assayed for their ability to differentiate into all three germ layers. Upon initial cultivation in suspension, iPSCs form three-dimensional aggregates and start to differentiate. Further cultivation in suspension gives rise to different types of tissue than adherent

cultivation on gelatine. The samples were analysed by qRT-PCR for the expression of a pluripotency marker *POU5F1*, an ectodermal marker *PAX6*, a mesodermal marker *BRACHYURY*, and an endodermal marker *SOX17*. Their expression was normalised to *ACTB*. Results are shown in Fig. 6. All clones showed a loss of pluripotency manifested by the decrease of *POU5F1* expression and the increase in expression of the markers representing the respective germ layers.

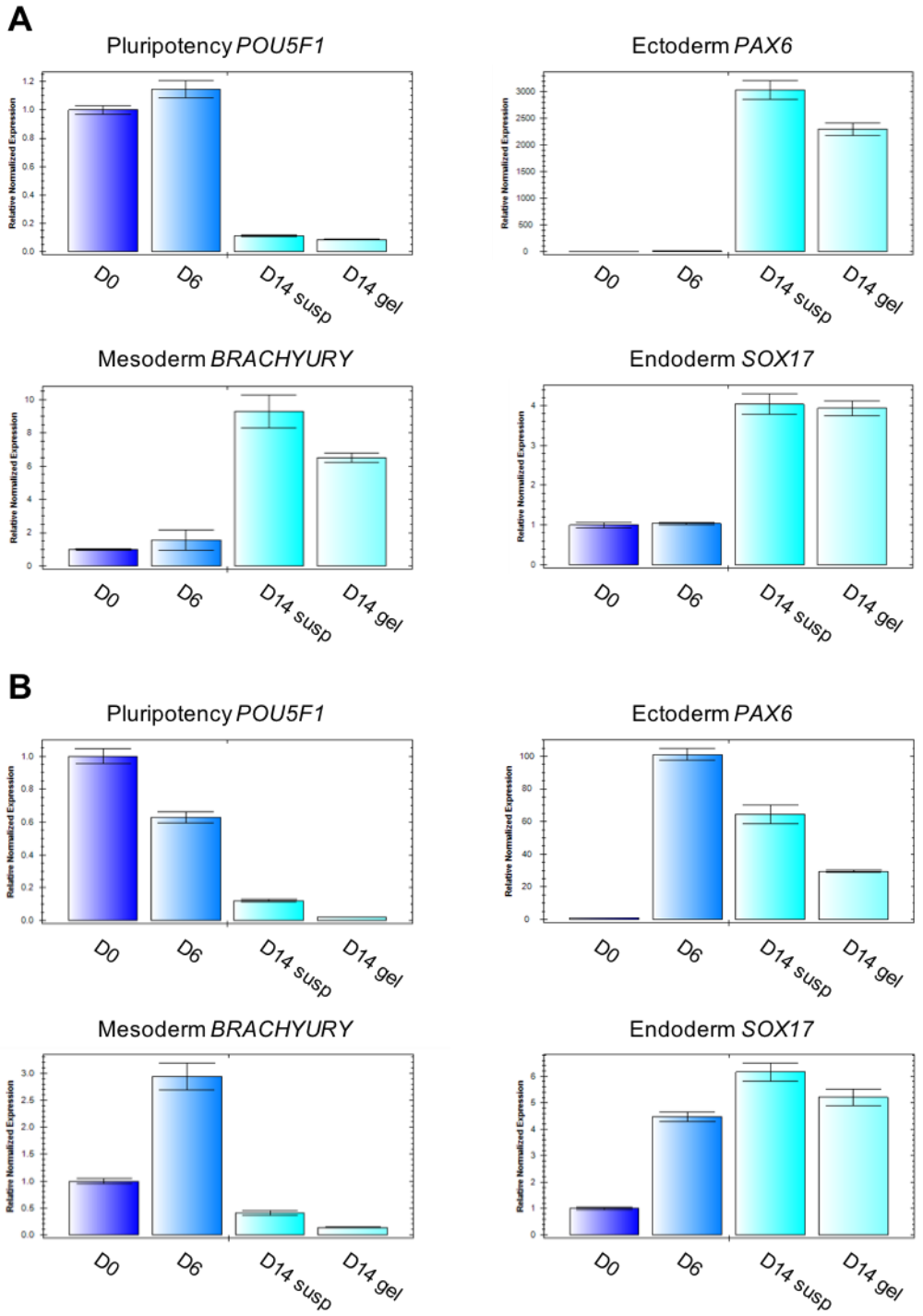

Figure 6. Differentiation potential of patient-derived and control iPSCs. Expression of the pluripotency marker *POU5F1* and markers representative of the three germ layers was assessed by qRT-PCR. **A)** Decreasing levels of *POU5F1* indicate the loss of pluripotency within 14 days of differentiation in patient-derived line D. Expression of the three differentiation markers rises confirming the pluripotency of patient-derived iPSCs. **B)** Pluripotency is lost during 14 days of differentiation, as shown by the reduction in *POU5F1* expression in

control line 645. The ectodermal and endodermal markers are upregulated. The expression level of the mesodermal marker rises temporarily. Susp – cultivation in suspension, gel – cultivation on gelatine.

3.2.1.6 Teratoma Assay

Teratoma formation assay was performed as the most stringent test of pluripotency. Cells were injected into immunodeficient NMRI nude mice Crl:NMRI-*Foxn1*^{nu} and tumours were explanted when skin lesions appeared or after a maximum of 67 days. All clones formed tumours with 100 % efficiency. Tumours were explanted, fixed, embedded in paraffin, cut into microsections, stained with haematoxylin and eosin (H&E), and analysed microscopically for the presence of derivatives of the respective germ layers. All tested clones proved to be pluripotent. Pictures with examples representative of each germ layer are shown in Fig. 7.

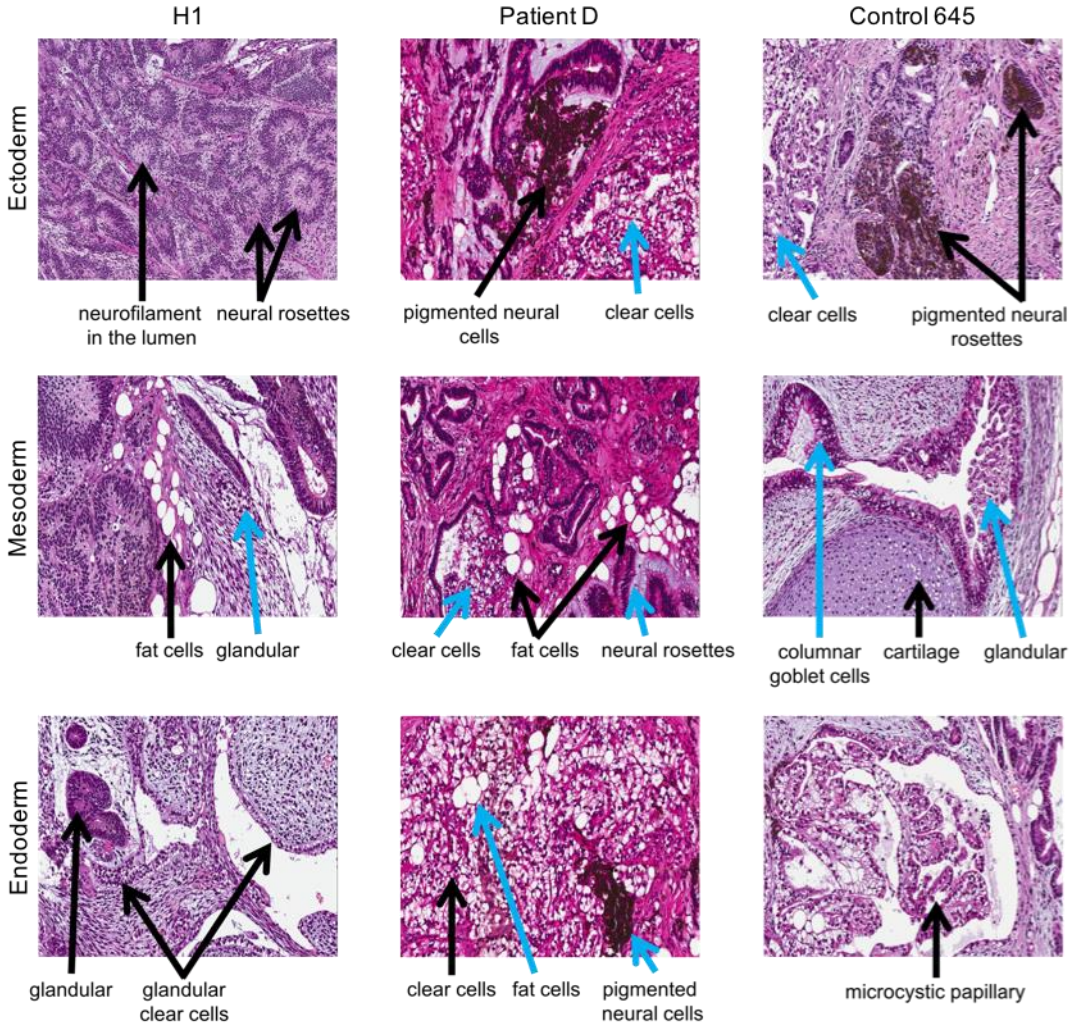

Figure 7. Teratoma assay of patient-derived and control iPSCs. H&E staining of teratomas formed by hESCs H1, patient-derived line D and control line 645. Derivatives of all three germ layers are present. Structures typical for the indicated germ layer are marked by black arrows, such as neuroectodermal rosettes for ectoderm, fat cells for mesoderm, and clear cells for endoderm. Other structures found in the image but not characteristic for the given germ layer are marked by blue arrows.

All analysed clones passed all applied pluripotency tests. In addition, their Epi-Pluri-Score was assessed in the laboratory of Prof. Dr. Wolfgang Wagner (Helmholtz Institute for Biomedical Engineering, RWTH Aachen), and a TaqMan array was performed (Stanurova *et al.*, 2016). Also in these experiments, the pluripotency of the studied iPSCs was verified successfully.

3.2.2 Quality and Identity Tests

Identity and quality of the iPSCs derived in this study were tested by sequencing for the presence of the three-base pair deletion in case of the Angelman syndrome iPSCs, Southern blot and karyotyping. Furthermore, high-resolution HLA typing was conducted to verify the genetic identity between iPSCs and the primary fibroblasts they had been derived from (Stanurova *et al*., 2016).

3.2.2.1 Sequencing

Eight patient-derived iPSC clones were sequenced to verify the presence of the three-base pair deletion causing Angelman syndrome in the patient. All eight clones (Stanurova *et al*., 2016) proved to bear the mutation as is shown in Fig. 8A.

3.2.2.2 Southern Blot

The number of virus integration sites was determined by Southern blot. Eight patient-derived clones were analysed along with ten healthy control clones. Clones with a single integration site were selected for further experiments. These clones are indicated in Fig. 8B.

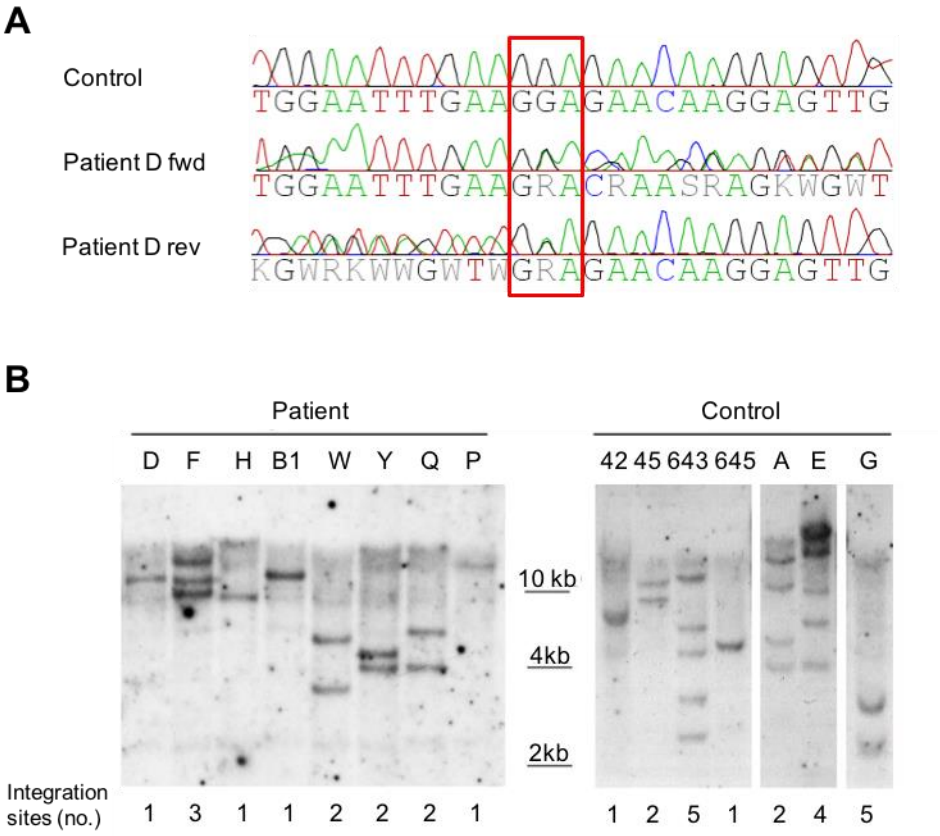

Figure 8. Sanger sequencing and Southern blot. A) Patient-derived clones display presence of the three-base pair deletion, as shown by Sanger sequencing. Forward and reverse sequencing of clone D is depicted in comparison with a normal healthy control at the top. A GGA triplet marked by the red rectangle is deleted, which is indicated by the ambiguity of the sequence starting at the site of the deletion. **B)** Southern blot of patient-derived and control iPSCs determined the number of integration sites of the lentiviral vector used for reprogramming. The results are given beneath the image. DNA isolated from patient-derived clones was digested with *Bam*HI, while DNA extracted from control clones was subjected to restriction by *Eco*RV. The figure was adapted from Stanurova *et al*., 2016.

3.2.2.3 Karyotyping

To evaluate whether the studied clones possess a normal karyotype, at least eleven metaphase spreads were analysed per sample. Both healthy control clones and three out of four patient-derived clones displayed a normal female karyotype 46, XX as shown in Fig. 9A. The exception was the patient-derived clone H exhibiting a marker chromosome, whose nature was determined by whole-chromosome painting as isochromosome 12p (Stanurova *et al*., 2016) (Fig. 9B). Due to this abnormality, this clone was excluded from further analyses.

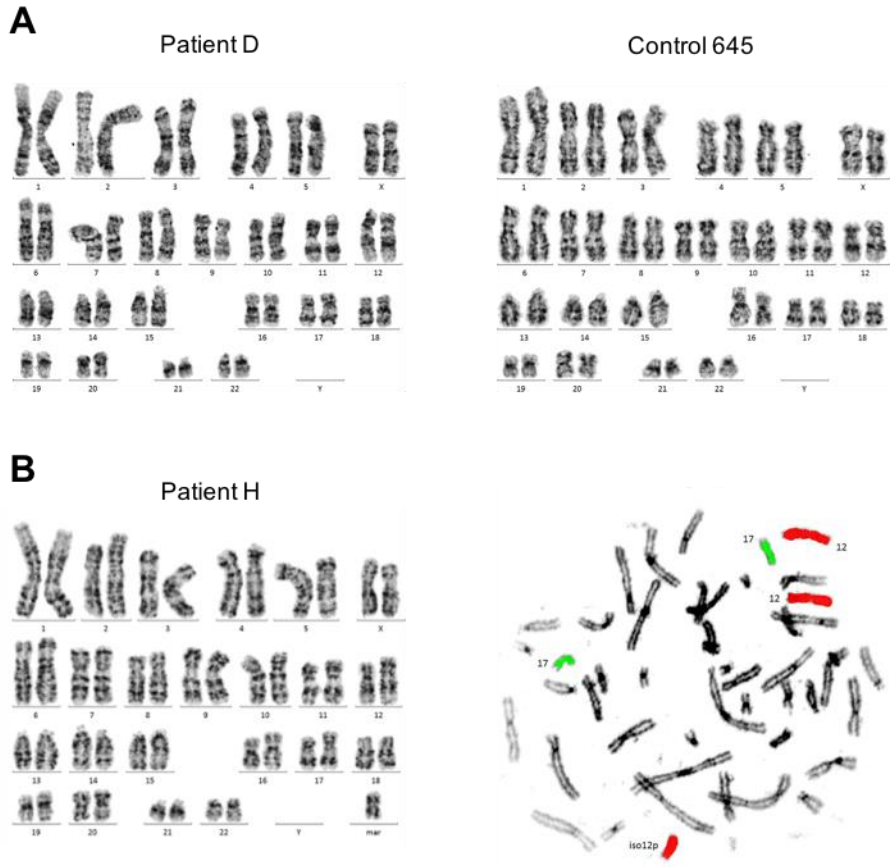

Figure 9. Karyotyping. A) Normal female karyotype 46, XX of patient-derived clone D (left) and control clone 645 (right). **B)** Patient-derived clone H exhibits a marker chromosome identified by whole-chromosome painting as i12p (right). Chromosome 12 is depicted in red, chromosome 17 in green. The figure was taken from Stanurova *et al*., 2016.

3.3 Neuronal Differentiation

Direct differentiation of iPSCs or hESCs into terminally differentiated neurons via embryoid bodies using the protocol published by Koch *et al*. was successful and yielded neural networks intertwined with axons. The progress of the development is shown in Fig. 10. Cell clumps were kept in suspension forming embryoid bodies upon induction of neuronal differentiation by dual SMAD inhibition in NDM containing N2, B27, the BMP signalling inhibitor LDN-193189 and TGFβ signalling inhibitor SB-431542. On day 12, embryoid bodies were plated on a matrigel-coated dish. Rosettes and neuroectodermal islands were

isolated and plated as single cells at high density on a matrigel-coated well of a 6-well plate on day 18. Further cultivation in NDM generated terminally differentiated neurons.

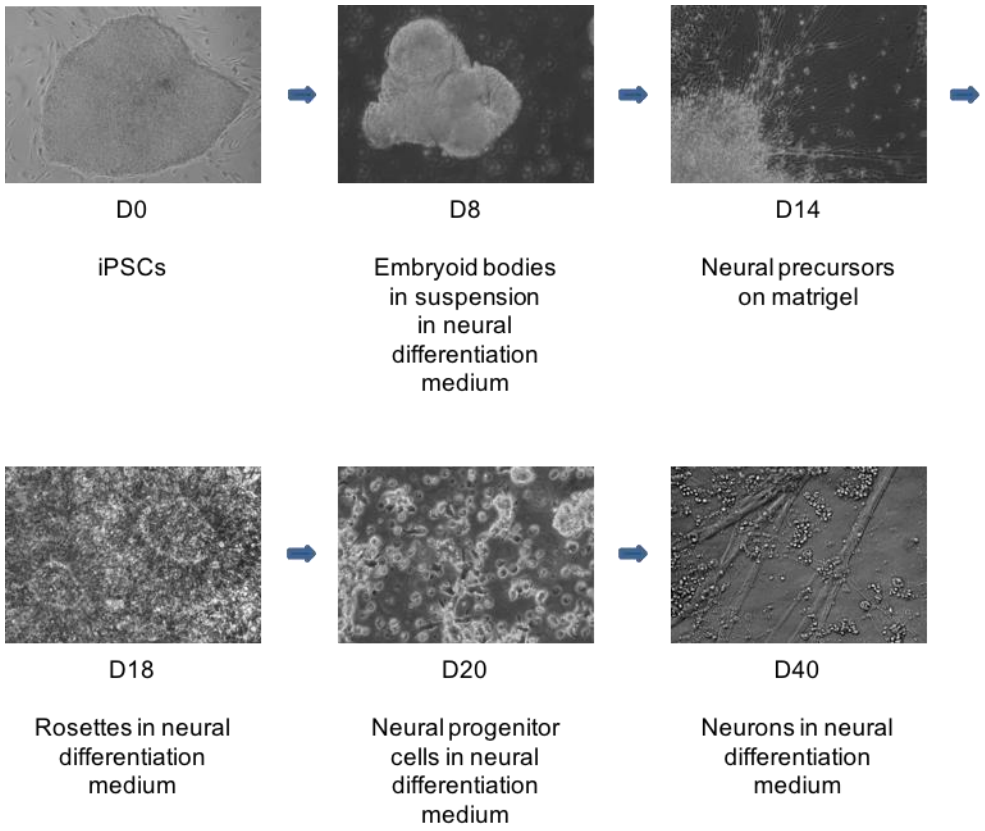

Figure 10. Neuronal differentiation according to the protocol by Koch *et al*.. iPSCs form embryoid bodies in differentiation medium on D8. Neural precursors visible on D14 organise into rosettes occurring on D18. Neural progenitors observed on D20 develop outgrowths that establish complex intertwined networks upon further culture in differentiation medium, as seen on D40.

Since it takes rather long to obtain mature neurons (four weeks for terminal differentiation of neural progenitors), I aimed to establish a neural progenitor culture with this protocol, which I could expand and subject to terminal differentiation any time. The attempts to culture neural progenitors in lt-NES medium containing N2, B27, EGF and FGF2 instead of NDM starting from day 18 failed repeatedly. They only yielded non-neuronal cells, whose identity I did not specify more closely. Most likely, these cells were neural crest cells, as this lineage tends to proliferate more quickly than neurons. Not even a gradual transition by plating the progenitors on day 18 in NDM and then replacing a quarter, a half and three quarters of NDM by lt-NES on consecutive days led to a stable neural progenitor culture.

Since the first approach resulted in successful differentiation of iPSCs into mature neurons but not the development of a long-term culture of neural progenitors, we tried to reproduce neuronal differentiation with the protocol described by Chambers *et al*. used to derive neurons from the iPSC lines AGI-0 and MCH2-10. Neural induction of single cells was induced by SRM containing LDN-193189 and SB-431542, and its gradual replacement by N2 medium containing N2 and both inhibitors. On day 10, three wells were combined into one and cultured further in BASF medium containing BDNF, ascorbic acid, SHH (sonic hedgehog) and FGF2. On day 17, the medium was changed to BAGTC containing BDNF, ascorbic acid, GDNF, TGFβ-III and dbcAMP. Samples for analysis were collected on the days when one medium replaced the other completely, that is, on day 0, day 5, day 10, day 17 and day 24 at the end of the experiment. The results between clones analysed by qRT-PCR differed substantially. For instance, the patient-derived clone D displayed considerable upregulation of neuronal markers *NURR1*, *TH* and *TUJ3* (Fig. 11A) and an obvious increased expression of neural markers *NESTIN*, *PAX6* and *SOX1*. On the contrary, the control clone 645 manifested hardly any significant change in the expression of the assayed genes (Fig. 11B, note the scale).

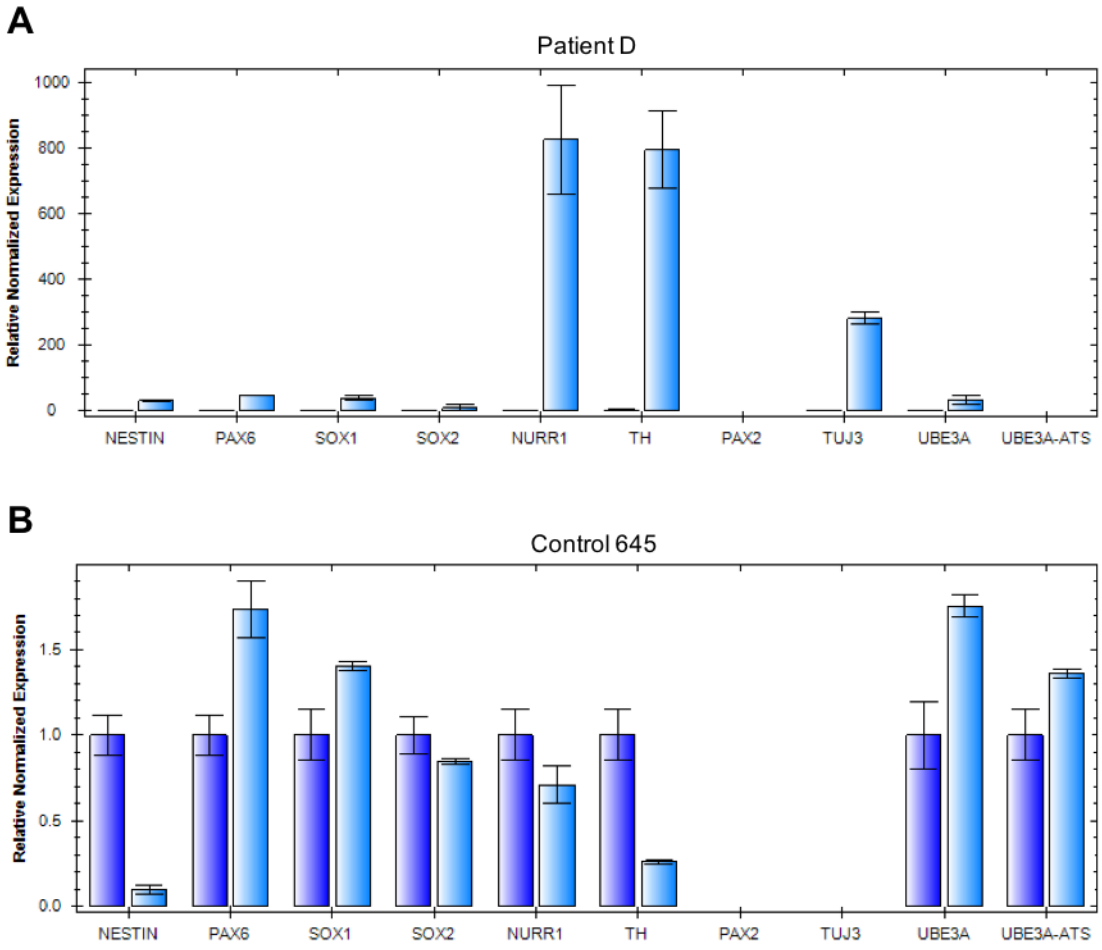

Figure 11. Neuronal differentiation according to the protocol by Chambers *et al*.. A) qRT-PCR analysis of patient-derived clone D shows a very strong upregulation of neuronal markers *NURR1*, *TH* and *TUJ3*, and an increase in expression of neural markers *NESTIN*, *PAX6* and *SOX1*. Dark blue = D0, light blue = D24. **B)** qRT-PCR analysis of control clone 645 exhibits virtually no neural induction. Dark blue = D0, light blue = D24.

Therefore, we performed neural induction of single cells with the commercially available STEMdiff™ Neural Induction Medium. The composition of the medium is defined and relies on a mechanism of neural induction other than dual SMAD inhibition. Cells were harvested for analysis on day 11 (Fig. 12). With this method, we did not obtain a stable neural progenitor culture and decided to return to neural induction by dual SMAD inhibition.

Neural induction by dual SMAD inhibition using the protocol by Boissart *et al*. was initiated by plating cell clumps on a matrigel-coated well of a 6-well plate in induction medium containing N2, B27, both inhibitors and FGF2. On day 10, the cells were replated on a new matrigel-coated well and cultured in expansion medium containing N2, B27, EGF and FGF2. The cells were harvested for analysis on day 14. qRT-PCR analysis of the samples obtained

by neural induction with STEMdiff™ Neural Induction Medium and by utilising the protocol by Boissart *et al*. showed virtually no consistency among the assayed clones and the outcome for single clones was not reproducible between biological replicates (Fig. 12). For example, in the first replicate, the patient-derived clone D exhibited no presence of the neural marker *PAX6* neither with the STEMdiff™ medium, nor with the expansion medium according to Boissart *et al*. (Fig. 12A). In the second replicate, the upregulation of *PAX6* was massive with both media (Fig. 12B, note the scale). Similarly, the neural marker *PLZF* showed a decrease with STEMdiff™ medium and a slight increase with the expansion medium according to Boissart *et al*. in the first replicate (Fig. 12A). An increase in the expression level of *PLZF* even more prominent than that of *PAX6* could be observed in the second replicate (Fig. 12B).

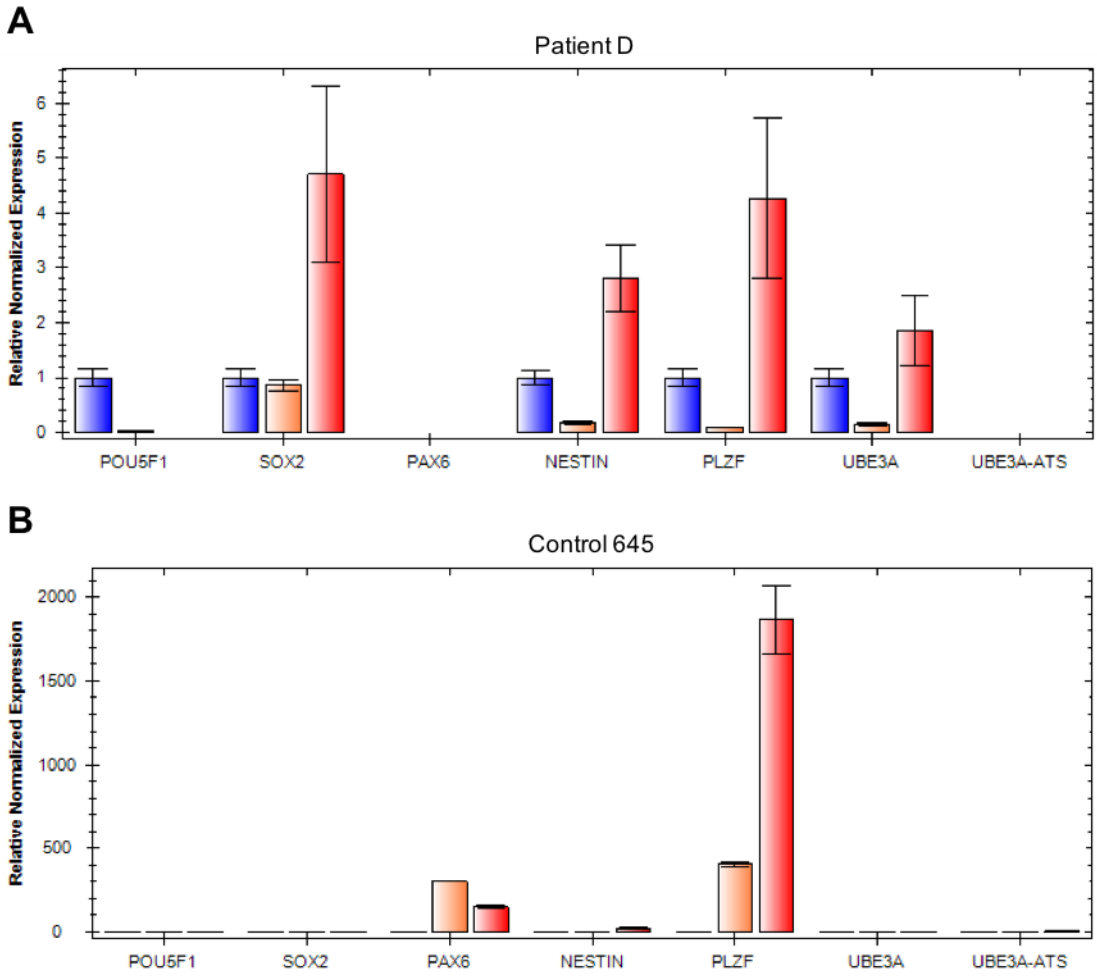

Figure 12. Neuronal differentiation using STEMdiff™ and the protocol by Boissart *et al*.. A) As determined by qRT-PCR, neural marker *PAX6* is absent in the first biological replicate of differentiation of patient-derived clone D with both STEMdiff™ and the expansion medium according to Boissart *et al*.. Neural marker *PLZF* shows a decrease in expression with STEMdiff™ and a mild increase in the expansion medium according to Boissart *et al*.. **B)** In the second biological replicate of neuronal differentiation, *PAX6* exhibits

considerable upregulation with both protocols and the increase in expression levels of *PLZF* is even more pronounced. Blue = D0, orange = STEMdiff™ protocol, D11, red = protocol from Boissart *et al*., D14.

Employing the protocol from Boissart *et al*. without optimisation led neither to reproducible results, nor to the establishment of a stable neural progenitor culture. Only after applying positive selection using magnetic anti-PSA-NCAM MicroBeads on day 13 did we obtain a rather stable culture of neural progenitors. Their further differentiation for another three weeks on poly-D/L-ornithine and laminin yielded terminally differentiated neurons on day 35 (Stanurova *et al.*, 2016). The positive selection and terminal differentiation were performed by Anika Neureiter.

3.4 Single-Nucleotide Primer Extension Assay

Expression of *UBE3A* and *SNHG14* was determined by RT-PCR in a commercially available cDNA from adult human lung tissue and human foetal brain tissue, cDNA generated from lymphoblastoid cell lines (LCLs) from a Prader-Willi patient and an Angelman syndrome patient, both carrying a large deletion on their paternal and maternal chromosome 15, respectively, and neurons obtained by neuronal differentiation of patient-derived clone D for 35 days. *UBE3A* transcripts should be present in all samples. In lung, both the maternal and the paternal allele are expressed. In foetal brain, the analysis detected maternally expressed *UBE3A*. The same holds true for PWS LCLs. AS LCLs display paternally expressed *UBE3A*. Neurons obtained by differentiation express *UBE3A* from the maternal allele. Indeed, I observed *UBE3A* transcripts in all samples (Fig. 13). Since the expression of *SNHG14* is restricted to the brain, it should only be detected in foetal brain and in generated neurons, if the neuronal differentiation had been successful. Presence of *SNHG14* transcripts in foetal brain but not in lung and the LCL lines demonstrates the specificity of the primers I utilised for the analysis (Fig. 13). By proving *SNHG14* expression in neurons harvested on day 35 of our experiment, I was able to verify successful derivation of mature neurons (Fig. 13).

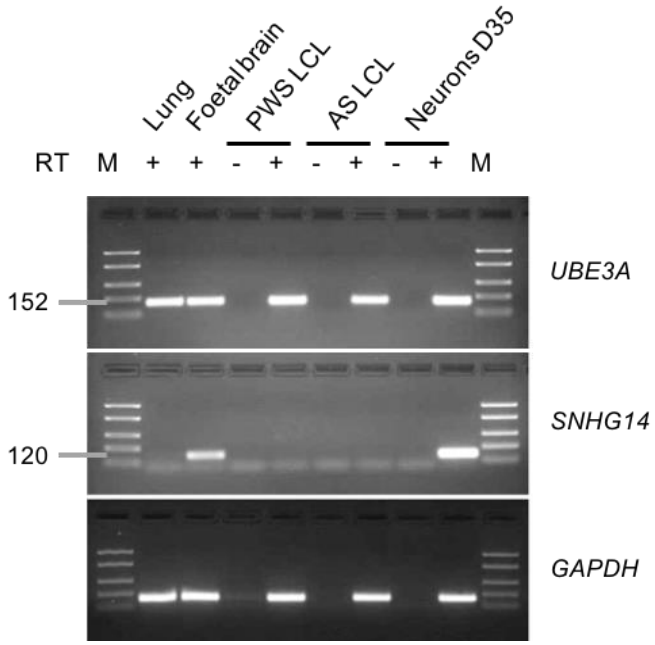

Figure 13. Expression of *UBE3A* and *SNHG14* in different tissues. *UBE3A* is expressed in lung, foetal brain, PWS LCL, AS LCL and neurons obtained by differentiation for 35 days (top). Expression of *SNHG14* is only detectable in foetal brain and generated neurons indicating primer specificity, successful neuronal differentiation and upregulation of *SNHG14* expression in the neurons (middle). Housekeeper gene *GAPDH* was included to confirm cDNA integrity (bottom). –RT samples are the negative controls for the respective cDNA preparatory reactions.

Samples obtained on day 0, day 14, day 21, day 28 and day 35 of neuronal differentiation of Angelman syndrome iPSCs were subjected to qRT-PCR analysis in order to assess the expression of *UBE3A* and *SNHG14* during the course of the experiment. As shown in Fig. 14, expression levels of *UBE3A* are slightly elevated already at the neural progenitor stage on day 14. In more mature neurons on day 28 and day 35, the upregulation of *UBE3A* is even stronger. Expression levels of *SNHG14* rise gradually throughout neuronal differentiation (Fig. 14). Increased expression was detected early into differentiation at the neural progenitor stage on day 14. The more differentiated the neurons were, the more enhanced the expression levels of *SNHG14* became. From one week to the next, upregulation of *SNHG14* increased by an order of magnitude throughout the whole experiment.

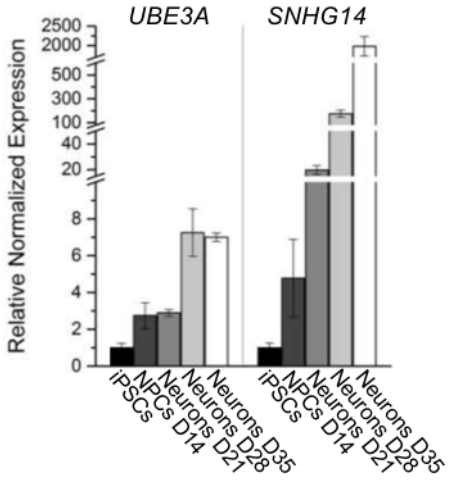

Figure 14. *UBE3A* and *SNHG14* expression levels during neuronal differentiation. Mild upregulation of *UBE3A* is observed already at the neural progenitor (NPC) stage of differentiation on D14 and the expression level further increases in more mature neurons on D28 and D35, as shown by qRT-PCR. Levels of *SNHG14* rise gradually throughout neuronal differentiation from mild upregulation at the neural progenitor stage to a very strong increase in expression on D35. The figure was adapted from Stanurova *et al*., 2016.

Single-nucleotide primer extension assay (SNaPshot) was employed to determine when silencing of the paternal *UBE3A* allele occurs during the process of neuronal differentiation. The three-base pair deletion in the maternal allele of the Angelman syndrome iPSC clone D served as a SNP by that the expression from the parental alleles was distinguished. In the reaction, the primer is extended either by a G, if it annealed to the wildtype paternal allele, or by an A, if it annealed to the maternal allele carrying the deletion. The G/A ratio is calculated and normalised to the G/A ratio of genomic DNA, which stays constant. In pluripotent cells on day 0, the ratio should equal approximately 1, since the expression of *UBE3A* is expected to be biallelic. As shown in Fig. 15, this is indeed the case. On day 14 at the stage of neural progenitors, as well as on day 21 at the stage of early neurons, the G/A ratio remained unaltered. On day 28, the G/A ratio decreased to 0.82 indicating a weaker expression from the paternal allele. On day 35, the reduction in the G/A ratio became more pronounced declining to 0.66. Based on these results, I conclude that silencing of the paternal *UBE3A* allele by *SNHG14* only begins in rather mature neurons at around day 28.

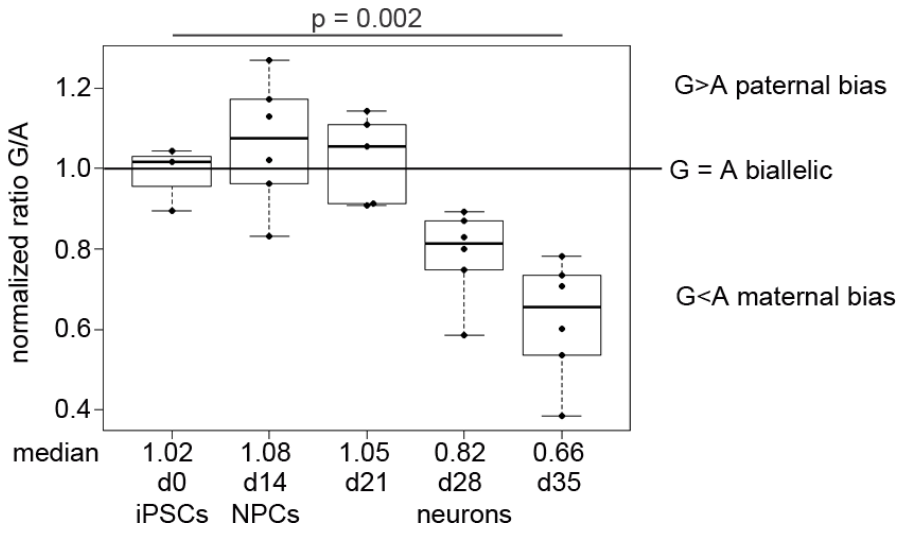

Figure 15. SNaPshot analysis. Ratio of the paternal (G) to the maternal (A) allele suggests biallelic expression of *UBE3A* in iPSCs, neural progenitors (NPC) and early neurons up to D21 of neuronal differentiation. On D28, the ratio decreases to 0.82 indicating a weaker expression from the paternal allele. The effect of silencing by *SNHG14* becomes even more prominent on D35 of differentiation when the ratio further drops to 0.66. The figure was taken from Stanurova *et al*., 2016.

3.5 Quantitative Allele Distinction of *UBE3A*

Results from the single-nucleotide primer extension assay indicated skewing of *UBE3A* expression towards the maternal allele starting on day 28 of neuronal differentiation due to the silencing of the paternal *UBE3A* allele by *SNHG14* (see Fig. 15). Nonetheless, I showed by qRT-PCR that the overall expression of *UBE3A* rises during the course of differentiation in spite of the silencing taking place (Fig. 14) and by Western blot that the protein level does not change throughout the experiment (Stanurova *et al*., 2016). To demonstrate that the silencing does occur and the expression from the maternal allele rises to compensate for the loss of the expression from the paternal allele in order to maintain a stable protein level, I designed an assay to quantify the contributions of the respective parental alleles to the pool of *UBE3A* mRNA molecules in the cells. Minor groove binding (MGB) probes were designed to bind to the site of the mutation on the maternal allele and to its corresponding healthy paternal counterpart, respectively. 280 bp cDNA fragments from Angelman syndrome iPSCs containing the target sequences of the probes in the middle were cloned into a vector.

Plasmids verified by Sanger sequencing for the absence (mat) or presence (pat) of the triplet, respectively, were mixed in the following ratios to create a standard curve for both probes: 0:100, 10:90, 25:75, 50:50, 75:25, 90:10, 0:100. The first calibration multiplex qRT-PCR with a FAM-labelled paternal probe and a TET-labelled maternal probe showed substantial differences in the probes' fluorescence capacities. While the FAM-labelled probe's capacity was satisfactory, the TET-labelled probe hardly showed any (Fig. 16A). A test with the TET-labelled probe treated with DNase I prior to qRT-PCR to release the full fluorescence potential did not yield a better result. To rule out the possibility of target or probe interference, a singleplex qRT-PCR experiment was performed. The fluorescence signal of the TET-labelled probe did not display any improvement in comparison with the multiplex qRT-PCR, so interference of any kind could not have been the issue. The TET-labelled probe was replaced by an MGB probe labelled with Yakima Yellow (YY) to obtain a stronger fluorescence signal. However, the substitution of the fluorescent dye did not lead to a satisfactory result either (Fig. 16B).

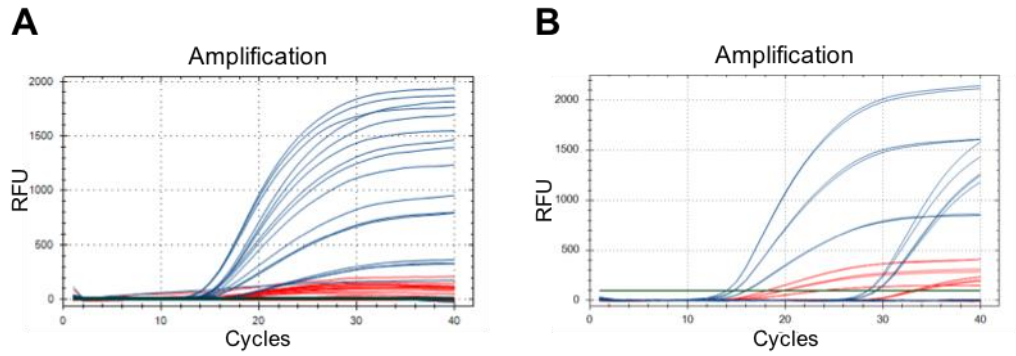

Figure 16. Quantitative allele distinction optimisation. A) Multiplex qRT-PCR plot of all standard mixes using a FAM-labelled paternal probe (blue) and a TET-labelled maternal probe (red) shows a great difference between the fluorescence capacities of the probes. **B)** Multiplex qRT-PCR plot of standard mixes pat:mat = 75:25, 50:50 and 25:75 using a FAM-labelled paternal probe (blue) and a YY-labelled maternal probe (red) displays a better, yet still insufficient performance of the new maternal probe in comparison with the original one. RFU = relative fluorescence unit.

I turned to the analysis of the assay design itself because the probability that two probes synthesised at different times would contain a mismatch in the sequence was rather low. I first examined the specificity and the efficiency of the primers. qRT-PCR with SYBR Green and the same set of templates and primers as in the multiplex qRT-PCR confirmed the presence of a single product and no variation between template mixes (Fig. 17A), which was expected, since the amount of the target sequence is equal in all of them. A different set of primers

originally used for cloning the 280 bp cDNA fragment yielded similarly convincing results (not shown). Next, I utilised a 10-fold serial dilution of cDNA from Angelman syndrome iPSCs as template. The amount of cDNA input corresponded to 10 ng, 1 ng, 0.1 ng and 0.01 ng reverse-transcribed RNA. Perfect doubling each cycle yields curves separated by 3.32 cycles and an efficiency of 100 %. In the primer test, the curves were separated by 3.36 cycles and the efficiency reached 98 %. The efficiency of the reaction was stable over three orders of magnitude and the sensitivity only reached its limits with the last dilution (Fig. 17A and 17B).

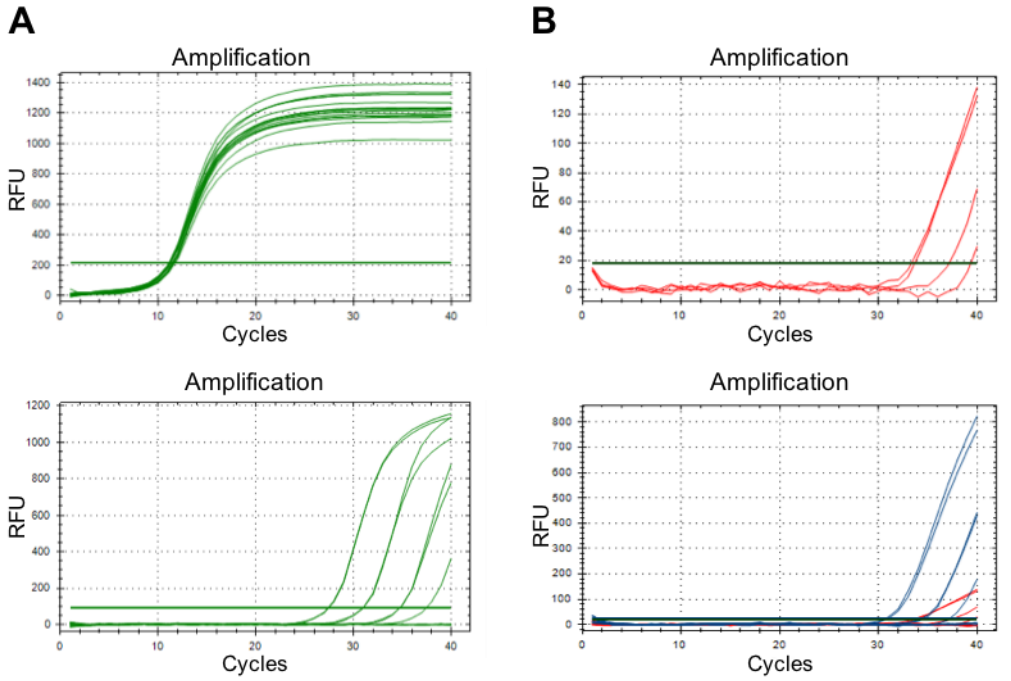

Figure 17. Quantitative allele distinction optimisation. A) qRT-PCR analysis of the standard mixes with SYBR Green confirms the reliability of the standard mixes in terms of overall DNA concentration (top). A 10-fold serial dilution of cDNA prepared from patient-derived clone D assayed with SYBR Green displays a very good efficiency over at least three orders of magnitude validating the primers (bottom). **B)** Multiplex qRT-PCR with a 10-fold serial dilution of cDNA prepared from patient-derived clone D indicates a moderately satisfactory detection by the YY-labelled maternal probe (top). Multiplex view (bottom) illustrates the disparity between the probes, as the signal from the FAM-labelled paternal probe (blue) is much stronger than the one from the YY-labelled maternal probe (red). Note the different scales. RFU = relative fluorescence unit.

However, the test with cDNA dilutions drew my attention to the plasmid templates again. As the test with SYBR Green showed, the curves coming from the reactions containing plasmid mixes entered the logarithmic phase about 15 cycles earlier than those coming from the cDNA dilution samples (Fig. 17A). I obtained similar results with the respective templates and the fluorescent probes. However, in this case, the curves of the plasmid mixes flattened

with decreasing target concentration (Fig. 16) indicating that the efficiency of the reaction drops, unlike with the cDNA samples (Fig. 17B). It would mathematically be possible to derive the respective target concentrations from a standard curve calculated from mixes containing much more target than the samples subjected to evaluation. In other words, a big difference in C_T values between the standards and the analysed samples is, of course, not preferable but it is acceptable provided that the efficiencies of the reactions are equal or close to 100 %. Since the plasmid mixes did not fulfil this essential condition in combination with the fluorescent probes, I speculated that perhaps the vectors are in a supercoiled state, which might interfere with the binding of the probes. Therefore, I performed enzymatic restriction with a single cutter and I used the linearised plasmids in the qRT-PCR. There was no difference between the untreated and the treated templates (not shown), so steric hindrance did not explain the problem with the efficiency.

Lastly, I replaced the probe detecting the maternal allele with a FAM-labelled MGB probe in order to determine, whether the fluorescence signal would finally match the one of the paternal probe. I utilised both the plasmid mixes and the cDNA serial dilutions for this analysis as templates.

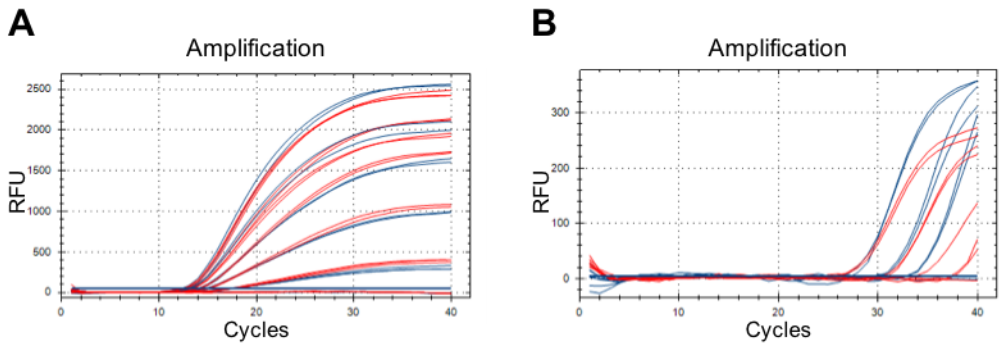

Figure 18. Quantitative allele distinction optimisation. A) Multiplex qRT-PCR plot of standard mixes using a FAM-labelled paternal probe (blue) and a FAM-labelled maternal probe (red) exhibits a perfect overlay of the signals. **B)** Multiplex qRT-PCR with a 10-fold serial dilution of cDNA prepared from patient-derived clone D indicates satisfactory reliability of the reactions with both the paternal and the maternal probe and their sufficient similarity in terms of detection and fluorescence potential. RFU = relative fluorescence unit.

If the sequence of the maternal probe is correct, the signals from both probes should overlay, since there is no difference between the strength of the fluorophores and the amounts of the respective target sequences should be equal as well. In case of the plasmid mixes, the amounts of targets are inversely correlated, so the expectation still holds true. Indeed, I observed

a perfect overlay of the curves originating from the reactions containing the respective parental probes. This applied to both template variants (Fig. 18). Since now the analysis of the respective parental alleles had to be performed separately due to the labelling of the probes with the same fluorophore, the idea of a single standard curve for both probes at a time became irrelevant. Therefore, to construct a standard curve for each parental probe, 10-fold serial dilutions of the plasmids carrying the paternal and the maternal target, respectively, were prepared and analysed by qRT-PCR. The curves of the maternal standard samples were separated by 3.32 cycles, the efficiency reached 99 % and was stable over seven orders of magnitude. Similarly, 3.45 cycles spacing was observed between the curves of the paternal standard samples, the efficiency equalled 94 % and was also stable over seven orders of magnitude. The precise overlay of the curves generated by the respective parental standard samples is shown in Fig. 19.

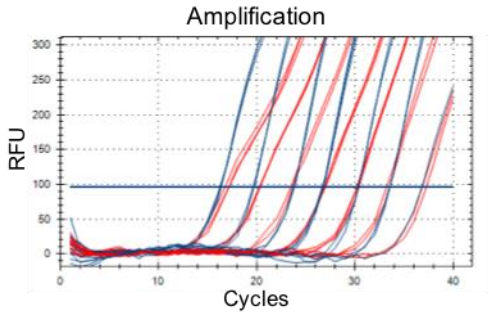

Figure 19. Quantitative allele distinction optimisation. qRT-PCR plot of 10-fold serial dilutions of the plasmids carrying the respective parental targets using a FAM-labelled paternal probe (blue) and a FAM-labelled maternal probe (red) exhibits a perfect overlay of the signals. The efficiencies of the respective reactions were stable over seven orders of magnitude. RFU = relative fluorescence unit.

The standard curves can be used to calculate the exact contributions of the respective parental alleles to the pool of *UBE3A* mRNA molecules in analysed samples, since the size of the plasmids is known and so is the number of copies present in each reaction. In comparison with single-nucleotide primer extension assay, the output of quantitative allele distinction analysis provides much more precise and therefore more valuable information. While the result obtained by single-nucleotide primer extension assays theoretically allows for ambiguous interpretation, the developed method facilitates accurate quantification of the expression dynamics of both parental alleles in an exact manner.

3.6 Methylation Analyses

Stability of DNA methylation at the gametic ICRs of six imprinted loci was examined in two healthy control clones, four patient-derived clones, the parental fibroblasts, two hESC lines, and iPSC lines AGI-0 and MCH2-10 (Chamberlain *et al*., 2010) by next-generation bisulphite sequencing. The results are depicted in Fig. 20 and 21. The status was determined at PWS-SRO, whose methylation regulates the expression of *UBE3A*; ICR1 and ICR2, which regulate the expression of *IGF2*/*H19* and the *KCNQ1OT1* locus, respectively; NESPAS of the *GNAS* locus; CpG85 of *RB1*; and IG-DMR of *DLK1/MEG3* locus. Since one allele is methylated and the other one is not, a level of approximately 50 % methylation is expected at imprinted loci. Such levels were observed at PWS-SRO in all samples but for AGI-0, which correctly showed no methylation, since it harbours a large deletion on the maternal chromosome 15 including the PWS-SRO (Fig. 21). At ICR1, 50 % methylation levels were detected with the exception of patient-derived clone B, which exhibited a loss of methylation, and hESC line H9, which displayed a gain of methylation at a higher passage (Fig. 21). ICR2 showed only one deviation from the otherwise stable methylation level of 50 % in patient-derived clone P, whose methylation was lost at this region (Fig. 20). A loss of methylation at NESPAS was detected in both healthy control clones, patient-derived clones B1 and P, and MCH2-10; all other samples showed 50 % methylation levels (Fig. 20 and Fig. 21). CpG85 exhibited a consistent gain of methylation in almost all lines; the sole exception was a 50 % methylation level in the healthy control fibroblasts (Fig. 20). A gain of methylation was observed at IG-DMR in both H1 and H9 hESC lines, both healthy control clones and both iPSC lines published by Chamberlain *et al*., whereas all four patient-derived clones displayed 50 % methylation levels. Patient fibroblasts, which had been immortalised due to poor growth in culture (Stanurova *et al*., 2016), showed a complete loss of methylation at IG-DMR (Fig. 20). Differential methylation was detected at both CpG85 and IG-DMR in an additional analysis of the patient's blood sample and healthy control fibroblasts from two other independent healthy donors, although the methylation levels were moderately elevated at both loci in one of the fibroblast samples (Fig. 21).

Both hESC lines H1 and H9 showed a gain of methylation at CpG85 and IG-DMR, and an expected level of methylation of approximately 50 % at all other loci. Control fibroblasts

exhibited a 50 % methylation level at all loci. Both iPSC clones derived from these fibroblasts displayed a loss of methylation at NESPAS and a gain of methylation at CpG85 and at IG-DMR. Patient-specific immortalised fibroblasts showed a gain of methylation at CpG85 and a loss of methylation at IG-DMR, whereas expected levels of methylation were detected at all other loci. Patient-derived clones D and H exhibited 50 % methylation at all loci but CpG85, which was hypermethylated. Patient-derived clones B1 and P displayed a loss of methylation at ICR1 and ICR2, respectively. Both clones also showed a gain of methylation at CpG85, and a loss of methylation at NESPAS (Fig. 20). In lines AGI-0 and MCH2-10, moderately elevated levels of methylation were observed at ICR1; CpG85 and IG-DMR were hypermethylated. In MCH2-10, also a loss of methylation at NESPAS was detected (Fig. 21).
In addition, I determined methylation status at two pluripotency loci, *POU5F1* and *NANOG*, in the cell lines. Products of both genes, OCT4 and NANOG, are key players in pluripotency maintenance. Upon differentiation when downregulation of their expression is required, their promoters acquire methylation. Therefore, higher levels of methylation are expected at these loci in differentiated cells than in pluripotent cells. Indeed, I observed low levels of methylation in all pluripotent samples, whereas in fibroblasts, methylation levels were high (Fig. 20 and Fig. 21).

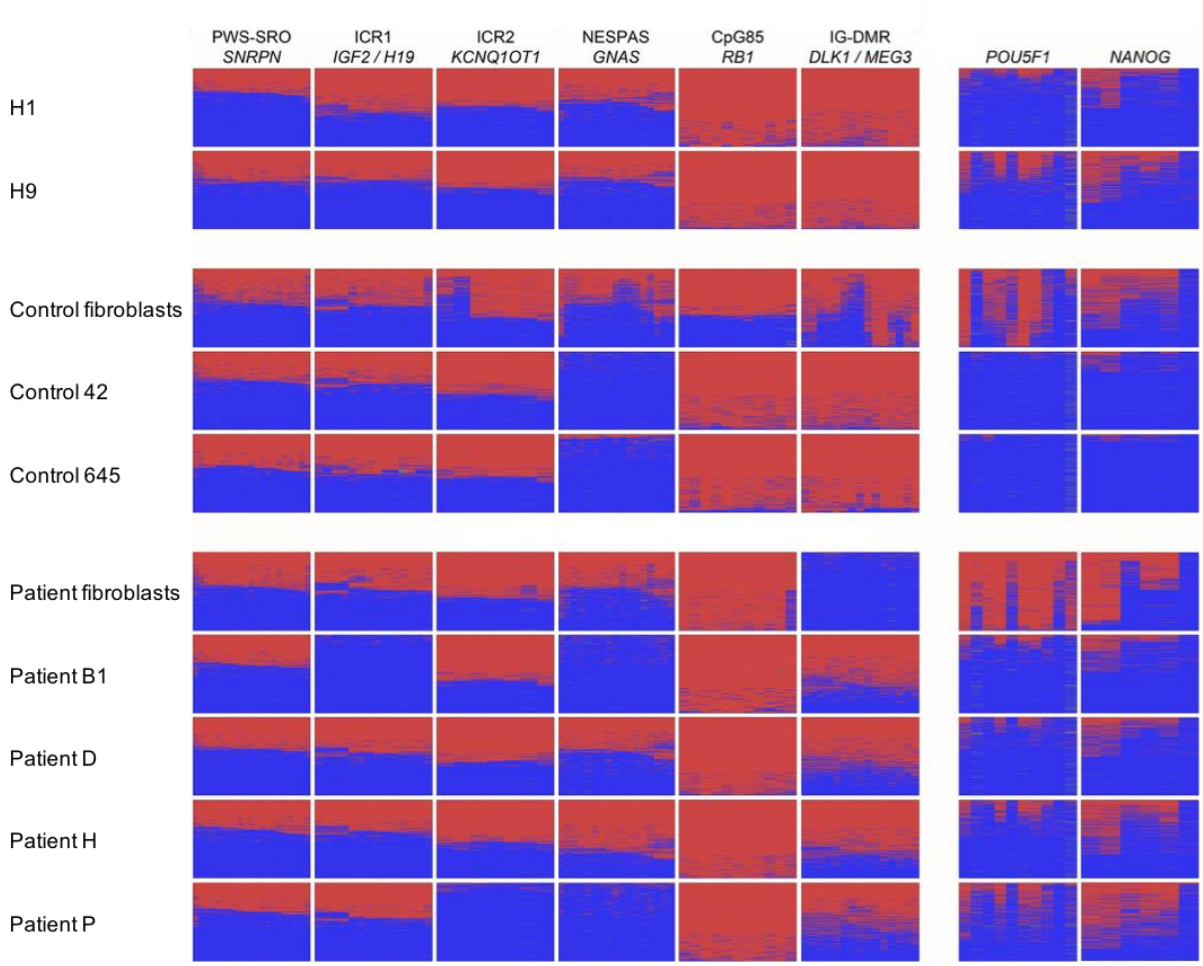

Figure 20. Methylation status of six imprinted ICRs and two pluripotent loci. A level of 50 % methylation is expected at imprinted loci. This is true for PWS-SRO without exception. ICR1 and ICR2 show one loss of methylation each. NESPAS exhibits a loss of methylation in four samples. CpG85 displays a consistent gain of methylation in all samples but one. Methylation levels are elevated at IG-DMR in four samples; one sample manifests a loss of methylation. Pluripotent loci *POU5F1* and *NANOG* acquire methylation upon differentiation. Accordingly, the levels of methylation in fibroblasts are higher than in hESCs and iPSCs. The figure was taken from Stanurova *et al.*, 2016.

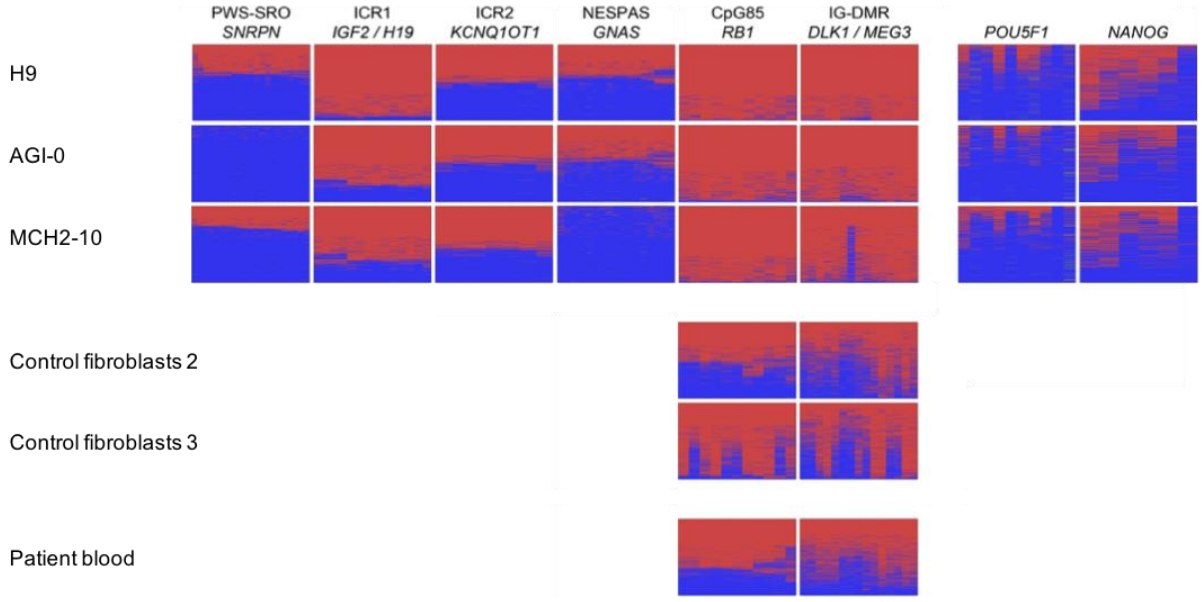

Figure 21. Additional methylation analyses of six imprinted ICRs and two pluripotent loci. PWS-SRO shows hypomethylation in AGI-0 due to the loss of the maternal allele. ICR1 exhibits a gain of methylation in hESCs H9 at a higher passage. Methylation at ICR2 is preserved. NESPAS displays one loss of methylation. CpG85 and IG-DMR manifest a gain of methylation in pluripotent cells. In two additional fibroblast samples and the patient's blood sample, differential methylation at CpG85 and IG-DMR is maintained. Levels of methylation at pluripotent loci *POU5F1* and *NANOG* in pluripotent samples are lower than in fibroblasts; compare with the previous figure. The figure was adapted from Stanurova *et al*., 2016.

3.7 Methylation Induction

To establish the induction of methylation, I used the iPSC line AGI-0 for all experiments. As described above, the methylation level at PWS-SRO in this cell line is zero or close to zero due to the large deletion on the maternal chromosome 15 including the PWS-SRO. Presence of only the unmethylated paternal allele makes the cell line especially suitable for studying induction of methylation at PWS-SRO. The analysis is straightforward and the results clearly show whether the induction of methylation had been successful or not.

3.7.1 Methylation Induction by Artificial Methylated Oligonucleotides

Methylated oligonucleotides have successfully been used to induce methylation at targeted loci. They are protected from degradation by cellular nucleases by phosphorothioate backbones. Replication or transcription are required to facilitate annealing of the

oligonucleotides to their target sequence, since only then do the DNA strands transiently separate. Upon annealing, a hemi-methylated stretch of DNA is formed that is targeted by DNMT1, which methylates the endogenous DNA strand. As the endogenous DNA strands reanneal, the hemi-methylated portion of DNA is methylated by DNMT1 fully. Delivery of the oligonucleotides into the cells was performed by transfection with Lipofectamine® RNAiMAX or by nucleofection using the Amaxa™ Nucleofector™ Technology. The position of the nucleotides in the genome is indicated in Fig. 22A. Success of the delivery was verified by microscopy one day post transfection, since one of the oligonucleotides was fluorescently labelled (Fig. 22B). The transfection efficiency reached approximately 50 %. DNA isolated from cells harvested at different time points was subjected to bisulphite conversion and sequenced. Single deliveries of the oligonucleotides at various concentrations did not lead to an induction of methylation at the targeted region. The results were independent from the time of harvest. Therefore, the concentration of 2 μM that proved to be optimal for cell survival after the treatment was used for multiple rounds of transfection every two or three days. However, neither three, nor six rounds of transfection yielded methylation of the target sequence. These results were also independent from the time point, at which the cells were harvested for analysis. The frequency of transfection did not influence the output, since there was no difference in the samples transfected every two or three days. An example of a fully converted sample is shown in Fig. 22C.

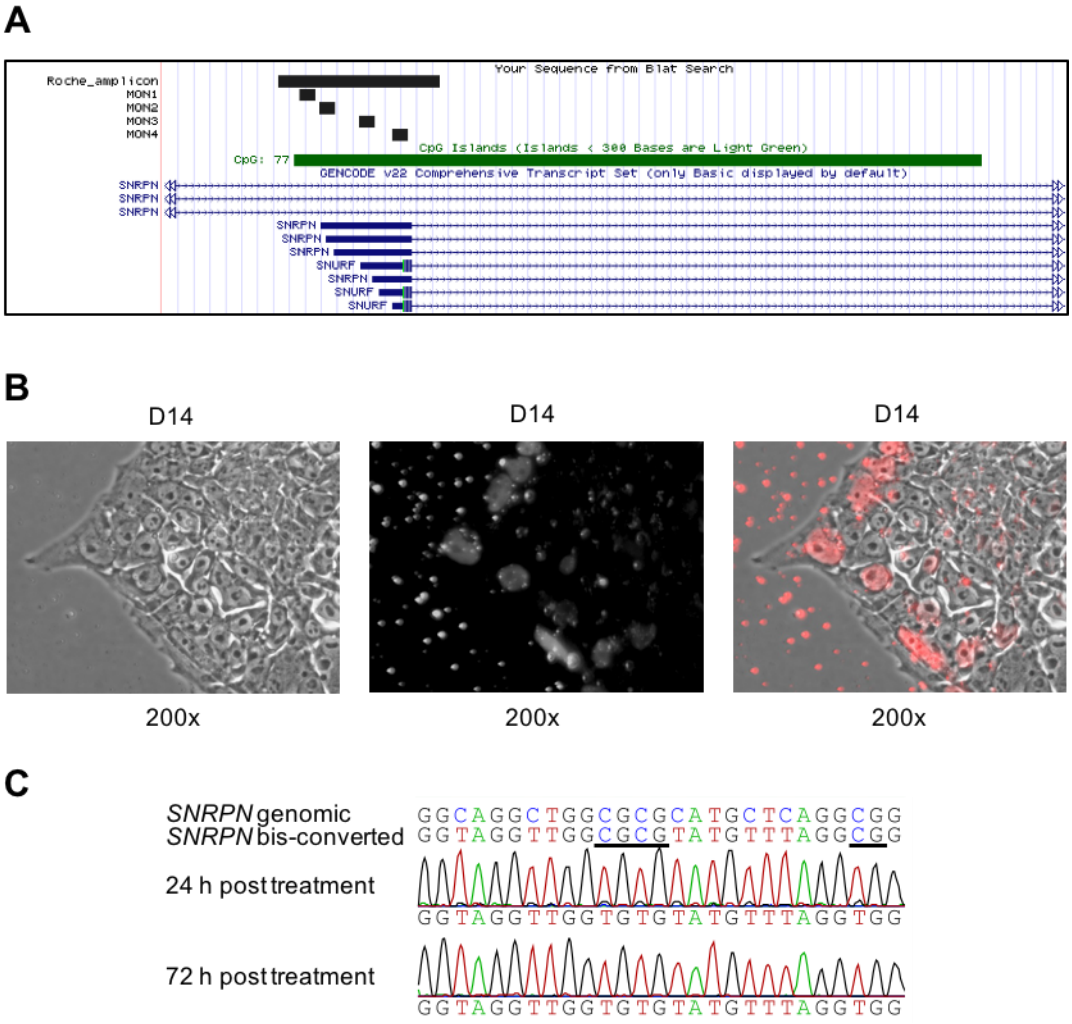

Figure 22. Artificial methylated oligonucleotide treatment. A) The designed methylated oligonucleotides all lie within the amplicon analysed by next-generation bisulphite sequencing indicated by the upper black bar. **B)** Methylated oligonucleotides are absorbed by the cells. **C)** 24 h or 72 h after treatment, cells exhibit no induced methylation at the targeted region. CpG dinucleotides in the sequence are indicated by black bars.

3.7.2 Methylation Induction by In Vitro-Methylated DNA Fragments

3.7.2.1 *M.Sss*I-Methylated Fragments

Fragments methylated in vitro by *M.Sss*I methyltransferase have been shown to efficiently induce methylation leading to downregulation of transcription at the targeted loci. Similarly to the previous method, this approach also relies on separation of the endogenous DNA strands during replication or transcription, and methylation by DNMT1. A 1413-bp DNA fragment

encompassing the whole CpG77 at the *SNURF-SNRPN* promoter (Fig. 23) was amplified by PCR from a plasmid, purified and 4 µg DNA were methylated in vitro by *M.Sss*I methyltransferase. The success of the methylation was validated by restriction digest with *Hpa*II as shown in Fig. 24A. Methylated DNA is resistant to digestion with *Hpa*II, as the enzyme's restriction sites C˅CGG are blocked by methylation present on the second cytosine. Hence, a fully methylated fragment should not be cut by *Hpa*II. Apart from the intact full-length fragment, smaller restriction products can be observed indicating incomplete methylation. Approximately 80 % methylation of the fragment was achieved. Denatured DNA was delivered into the cells by three rounds of transfection with Lipofectamine® RNAiMAX. Genomic DNA was isolated from harvested cells, subjected to bisulphite conversion and sequenced. The result displayed a partial methylation of the targeted region (not shown). To determine the extent of the methylation precisely, analysis by next-generation bisulphite sequencing ensued. The level of methylation induced by this method reached 38.6 % as shown in Fig. 25. In order to verify that the observed induction was not a false-positive result originating from the transfected DNA fragment, reads were separated by a SNP that had been introduced into the sequence beforehand by site-directed mutagenesis by Nadja Utz (Institute of Human Genetics). Since there were no reads present for the sequence containing the substitute nucleotide, the detected methylation came exclusively from the endogenous DNA.

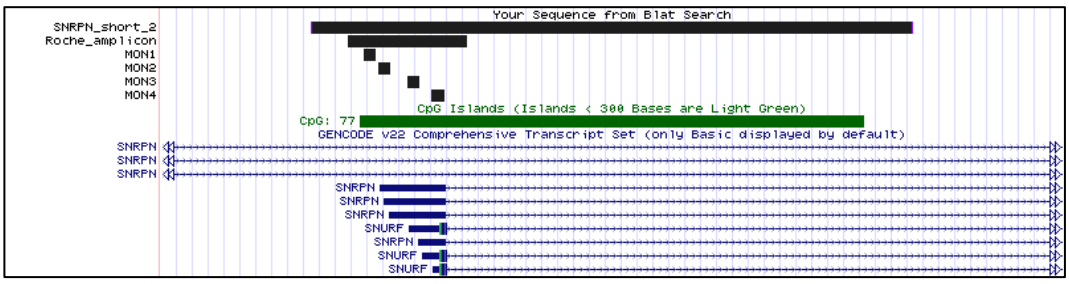

Figure 23. Position of the selected fragment in the genome. The DNA fragment chosen for induction of methylation encompasses the whole CpG77. Methylated oligonucleotides and the region analysed by next-generation bisulphite sequencing are included for comparison.

In a follow-up experiment, cells that had already been transfected thrice were either treated with three more rounds of transfection and harvested for analysis after each of them, or left untreated and harvested at the same time points as the treated cells. Methylation analysis by

next-generation bisulphite sequencing followed. As shown in Fig. 25, treated cells maintained approximately the same level of methylation, whereas the previously induced level was not retained in untreated controls, decreasing to 11.7 % within a week.

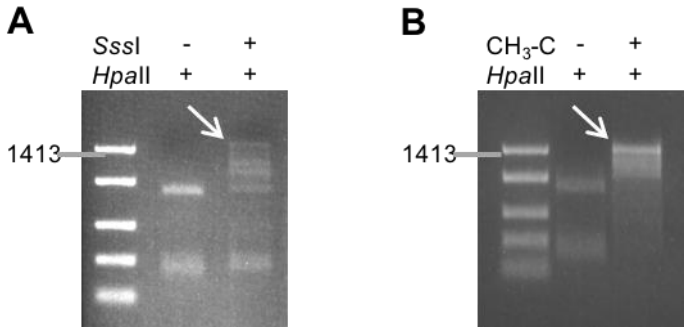

Figure 24. Methylation validation of *M.Sss*I-methylated and PCR-methylated fragments by methylation-sensitive *Hpa*II restriction. A) Fragments do not become completely methylated by *M.Sss*I, as shown by the presence of restriction products smaller than the full-length fragment marked by an arrow. **B)** PCR-methylated fragments exhibit methylation to a higher extent than *M.Sss*I-methylated fragments.

Since a pool of cells was analysed, I tested whether the decline of induced methylation was caused by a general loss in the whole population, or because the subpopulation of cells carrying methylation got overgrown by unmethylated cells. These cells might proliferate more quickly because they had not been transfected, which confers a selection advantage per se, or because they lose or remove the methylation, which might lead to faster growth in comparison to methylated cells. After three rounds of treatment, single cells were seeded at a low density to allow for the isolation of single subclones. 24 subclones that formed large colonies and 24 subclones that formed small colonies were isolated manually, expanded and assayed for the presence of methylation. If a subpopulation overgrowth was the reason for the overall decline of methylation, clones with large colonies would expectedly display no methylation, whereas clones forming small colonies would show methylation to at least some extent. Since all analysed clones exhibited a complete loss of methylation (not shown), I conclude that the induced methylation only remains stable upon additional treatment and is gradually lost upon its withdrawal.

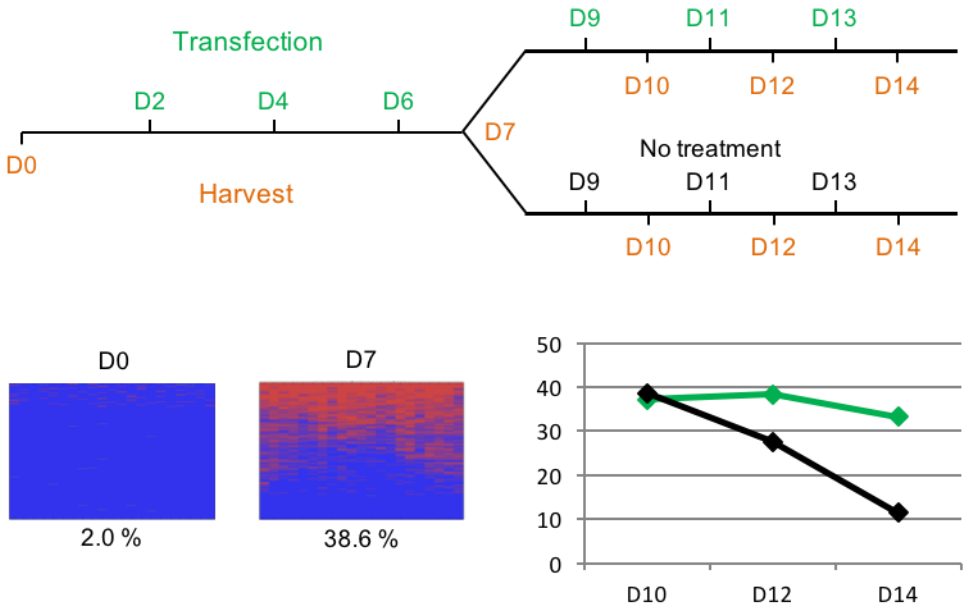

Figure 25. Induction and stability of methylation by *M.Sss*I-methylated fragments. Top: experimental workflow. Green = days of transfection, orange = days of harvest, black = days without treatment. Bottom: after three rounds of transfection, the level of methylation increases to 38.6 % on D7. Methylation status of 2.0 % assessed prior to treatment on D0 is displayed for comparison. Level of methylation induced by three rounds of transfection is maintained upon additional treatment (green line). Untreated cells lose methylation gradually (black line).

3.7.2.2 PCR-Methylated Fragments

A 1413-bp DNA fragment was amplified from a plasmid by PCR with methylated dCTPs. The ratio of methylated to unmethylated dCTPs was 60:40. The methylated fragment was purified and the rate of methylation was determined by restriction digest with *Hpa*II as shown in Fig. 24B. Denatured DNA was then delivered into the cells by three rounds of transfection with Lipofectamine® RNAiMAX. Genomic DNA was isolated from harvested cells, subjected to bisulphite conversion and sequenced. A follow-up experiment was conducted in the same settings as with the *M.Sss*I-methylated fragments. The delivery of the PCR-methylated fragments did not lead to any induction of methylation in the treated cells (not shown).

3.7.3 Methylation Induction by a Modified CRISPR/Cas9 System

Four different gRNAs were designed by Dr. Pavel Bashtrykov, Institute of Biochemistry, University of Stuttgart, to target the region analysed by next-generation bisulphite sequencing (Fig. 26). The efficiency of single gRNAs was evaluated in HEK293 cells by their co-transfection with a plasmid encoding wildtype Cas9 and subsequent T7 assay. gRNA forms a ribonucleoprotein complex with Cas9 and guides it to its target sequence. Cas9 induces double-strand breaks in the DNA that are repaired by the cell rendering the DNA non-perfectly matched. After amplification of the targeted region and subsequent annealing of the fragments, restriction by T7 endonuclease ensues. The enzyme recognises and cleaves segments containing mismatches. As shown by the presence of restriction products, all four gRNAs proved to target the desired sequence efficiently (Fig. 27).

Plasmids encoding Cas9 protein fused with the active domains of DNMT3A and DNMT3L were delivered into the cells together with one or two plasmids each containing one gRNA. Cells were inspected microscopically for the expression of YFP from the plasmid carrying the modified Cas9 one day post treatment. Delivery by transfection with Lipofectamine® RNAiMAX was successful in HEK293 cells with an efficiency of approximately 60 %. However, the method did not work for iPSCs, as no cells expressing YFP were found (not shown). The delivery by Amaxa™ Nucleofector™ Technology was evaluated by FACS but yielded hardly any cells positive for the YFP signal (25 cells out of 10 000 input cells; not shown).

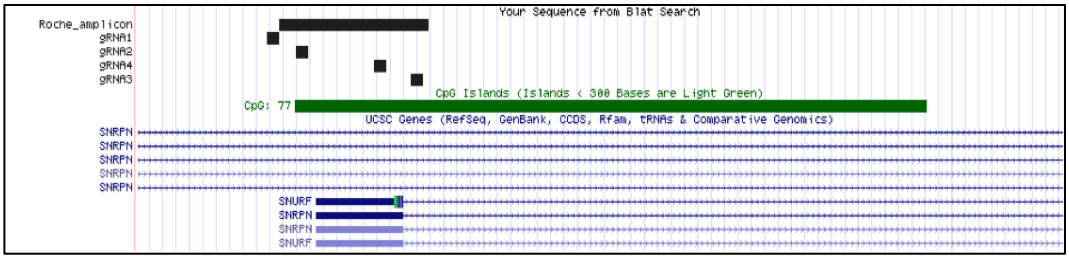

Figure 26. gRNA design for methylation induction by a modified CRISPR/Cas9 system. Four gRNAs target the region analysed by next-generation bisulphite sequencing, which is shown for comparison.

Electroporation using the Neon® Transfection System proved to be the most successful approach, although still with significant limitations. The viability of iPSCs after

electroporation (defined as the ratio of live cells as determined by FACS to the number of input cells on the day of electroporation) did not reach 10 %. No more than a fifth of the sorted live cells was positive for the expression of YFP. These cells were either directly subjected to analysis by next-generation bisulphite sequencing to quantify the induction of DNA methylation, or cultured further and harvested for analysis seven or fourteen days later, respectively (Fig. 28). The viability of the cells after sorting posed another problem, since only about 1 % of the seeded cells survived.

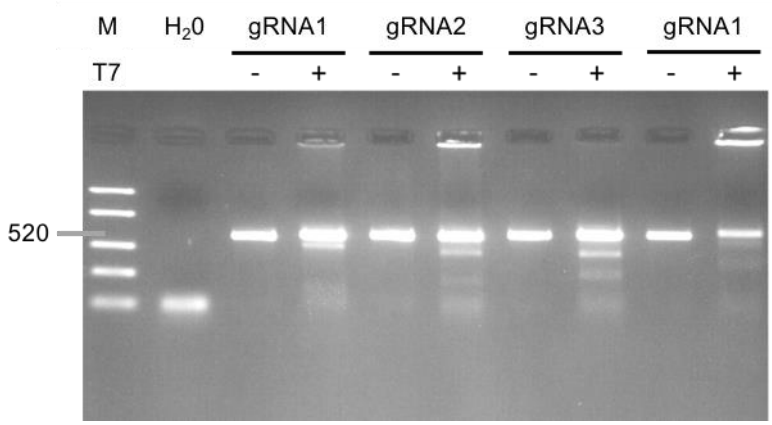

Figure 27. T7 assay with gRNAs targeting CpG77. gRNAs target the desired region effectively, as confirmed by the presence of restriction products in the respective reactions containing T7 endonuclease (lanes marked by +). Unrestricted fragments (lanes marked by -) are shown for comparison.

A follow-up assay was planned in the same settings as with the *M.Sss*I-methylated or PCR-methylated fragments but scaling up the experiment failed to deliver the required number of cells. Therefore, the sampling of cells to investigate the stability of induced DNA methylation over the period of two weeks had to be reduced to two time points, 7 and 14 days after seeding of sorted cells on day 0. As expected, no methylation was induced by electroporation of the plasmid carrying the fusion protein alone at any analysed time point (Fig. 28). Combining gRNA1 and gRNA3 with the Cas9-DNMT3A-DNMT3L construct resulted in an increase in methylation to 15.7 % on day 7 and an additional rise to 30.0 % on day 14. By applying gRNA2 and gRNA4 instead, methylation level was induced to 5.6 % on day 7 and further to 11.8 % on day 14.

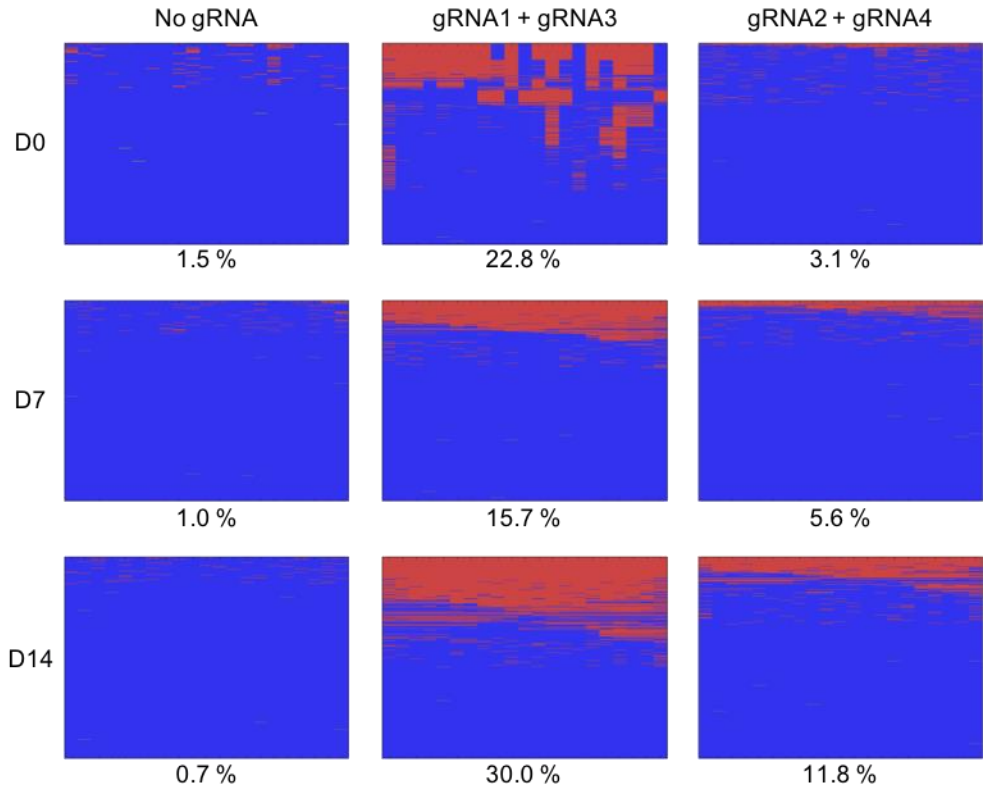

Figure 28. Induction of methylation by a modified CRISPR/Cas9 system and its stability. Control samples with only the vector used for electroporation remain unmethylated at all three time points analysed. Combination of gRNA1 and gRNA3 with the plasmid induces methylation to 15.7 % on D7 that further rises to 30.0 % on D14. Application of gRNA2 and gRNA4 together with the construct yields less notable results with an increase in methylation to 5.6 % on D7 and 11.8 % on D14.

4. Discussion

4.1 Characterisation of iPSCs

Reprogramming of patient and control fibroblasts in order to obtain iPSCs occurred with a similar efficiency. Hence, we conclude that the *UBE3A* mutation has no effect on reprogramming. Based on the result of the Southern blot analysis, four patient-specific and two control lines were selected for further work that harboured only a single integration site of the lentiviral vector used for reprogramming. The six lines were subjected to a number of pluripotency tests to verify their pluripotency and to choose the most suitable ones for the final experiments. Pluripotency of the analysed lines was confirmed by alkaline phosphatase staining, immunohistochemical staining, FACS, qRT-PCR, EB formation assay, TaqMan array, Epi-Pluri-Score analysis and teratoma formation assay. High-resolution HLA typing and sequencing for the presence of the three-base pair deletion in the patient-specific iPSC lines proved the identity of the cells. Karyotyping revealed a normal 46, XX karyotype in three patient-derived lines and both control lines, and an aberrant karyotype in patient iPSC line H. The additional marker chromosome was identified by whole-chromosome painting as isochromosome 12p. The gain of chromosome 12 or isochromosome 12p has been described as a frequent anomaly in hESCs and iPSCs (Buzzard *et al.*, 2004; Draper *et al.*, 2004; Pera, 2004; Mitalipova *et al.*, 2005; Mayshar *et al.*, 2010). Genes located on 12p are associated with pluripotency and proliferation. Their increased expression supposedly confers a selection advantage to single cells, which corresponds to the recurrent presence of isochromosome 12p in tumours and clonally isolated cell lines. Isochromosome 12p in a mosaic state leads to Pallister-Killian syndrome, a severe developmental disorder characterised by distinct craniofacial features, pigmentation anomalies, epilepsy, congenital heart defects and intellectual disability (Mauceri *et al.*, 2000). The severity of this disorder depends on the level of mosaicism and is thought to be lethal in non-mosaic state. Because of the abnormality in its karyotype, patient iPSC line H was excluded from subsequent analyses performed with other unaffected lines.

The existing Angelman syndrome cell line AGI-0 harbours a large deletion on the maternal chromosome 15 encompassing many genes (Chamberlain *et al.*, 2010), which makes it difficult to attribute certain phenotypes to the loss of *UBE3A*. The newly published cell lines derived from a patient with a paternal uniparental disomy of chromosome 15 (Takahashi *et al.*, 2017) add a further tool for studying AS in vitro. In these cells, both alleles exhibit the paternal pattern of expression. Accordingly, *SNURF-SNRPN*, *SNORD116*, *SNORD115* and *SNHG14* are expressed biallelically. Hence, *UBE3A* is silenced by *SNHG14* on both alleles. Therefore, phenotype attribution is not less complicated than in AGI-0. Similarly, cell lines carrying an imprinting defect are not more informative in this respect. Both alleles carry the paternal imprint, so the expression pattern at the locus resembles that of paternal uniparental disomy. The most promising cell lines in this regard are the newly published cell lines obtained by genetic engineering via CRISPR/Cas (Fink *et al.*, 2017). The engineering resulted in a one-base pair insertion in both *UBE3A* alleles preventing successful splicing and translation of the UBE3A protein. Therefore, in these cells, the expression pattern at the locus is similar to the physiological state but for the expression of *UBE3A*. This does allow for phenotype attribution but the expression dynamics cannot be studied in these cells. Identification of interaction partners of UBE3A is not possible either.

The cell lines we established have both parental *UBE3A* alleles present. Moreover, the molecular defect they harbour is an in-frame deletion in the maternal *UBE3A* gene (Horsthemke *et al.*, 2011) giving rise to a UBE3A protein only missing a single amino acid in comparison with its healthy counterpart. Therefore, our cell lines feature two significant advantages in comparison with the cell lines described above. First, the expression pattern at the locus is completely true to the physiological state including *UBE3A* expression. This facilitates faithful analysis of the expression dynamics of both parental *UBE3A* alleles during neuronal differentiation. Second, the UBE3A protein is present in the cells, which allows for the identification of interaction partners of UBE3A and the attribution of all observed phenotypic manifestations directly to the loss of the protein function. Our cells represent a very valuable tool to study Angelman syndrome and to develop potential therapy.

4.2 Allelic Expression of *UBE3A* during Neuronal Differentiation

Development of a reliable protocol for neuronal differentiation was the aim of the doctoral thesis of Anika Neureiter and will be described there in detail. Utilising the protocol outlined in Stanurova *et al.*, 2016, we were able to generate terminally differentiated neurons, as confirmed by immunofluorescent staining for MAP2 and β-III-TUBULIN, both markers of post-mitotic neurons. In particular, I was interested in the development of *UBE3A* expression during neuronal differentiation because the silencing of the paternal allele takes place during this process (Chamberlain *et al.*, 2010; Sato & Stryker, 2010; Judson *et al.*, 2014; Fink *et al.*, 2017). Since my goal was to interfere with the silencing of the paternal *UBE3A* allele by *SNHG14*, I first needed to determine when exactly during neuronal differentiation the process occurs. I assessed expression levels of *UBE3A* and *SNHG14* in embryoid bodies after 14 days of differentiation by qRT-PCR. This period of time proved to be insufficient to observe significant changes in expression. During neuronal differentiation over 35 days, I observed a gradual increase in expression of both *UBE3A* and *SNHG14*. The latter corresponds with the onset of silencing of the paternal *UBE3A* allele. The former can be explained by enhancing *UBE3A* expression from the maternal allele to compensate for the loss of expression from the paternal allele due to its silencing. This is in accordance with no decrease in overall mRNA expression and unaltered level of UBE3A protein in iPSCs and neurons (Chamberlain *et al.*, 2010; Stanurova *et al.*, 2016). To address the phenomenon in more detail, single-nucleotide primer extension assay was employed. The three-base pair deletion in the maternal *UBE3A* allele was utilised as a SNP to assess the expression dynamics of both parental *UBE3A* alleles during neuronal differentiation. In iPSCs, neural progenitors and early neurons, a ratio of about 1 was detected indicating biallelic expression of *UBE3A*. Only on day 28 of differentiation did we observe a decrease in the ratio to 0.82 that became more pronounced on day 35, dropping to 0.66. This correlates with the onset of silencing of the paternal *UBE3A* allele by *SNHG14* (Fig. 15). The evidence implies that silencing of the paternal *UBE3A* allele might be tightly coupled to neuron maturation, which is in line with the results based on the mouse model of Angelman syndrome (Sato & Stryker, 2010; Judson *et al.*, 2014).

4.3 Quantitative Allele Distinction

Single-nucleotide primer extension assay is a useful method and the output is a valuable piece of information in itself. However, the result may potentially be misinterpreted, since no absolute figures are available. If a ratio rises or drops, it might be due to a change in the numerator, or the denominator, or both at a time. In case of the *UBE3A* gene, I observe a decrease in the ratio of the paternal to the maternal allele. The outcome may occur due to a decrease in the paternal allele expression (numerator) brought upon by silencing, or because of an increase in the maternal allele expression (denominator) caused by compensation, or as a combination of both effects. The results indicate that the latter variant is true. Silencing of the paternal *UBE3A* allele has been described (Chamberlain *et al.*, 2010; Stanurova *et al.*, 2016) and I observed an overall gradual rise of *UBE3A* expression throughout the course of neuronal differentiation by qRT-PCR and a stable protein level by Western blot (Stanurova *et al.*, 2016). Theoretically though, a ratio decrease determined by single-nucleotide primer extension assay might not be caused by silencing of the paternal allele, but merely by an increase of the maternal allele expression instead, while the paternal allele expression remains stable. Given all the indications, this is a rather unlikely scenario but I wanted to establish an analysis to follow the development at the locus as accurately as possible. I designed the quantitative allele distinction assay to study the behaviour of both parental *UBE3A* alleles separately and to precisely quantify their contributions to the pool of *UBE3A* mRNA molecules in the cells during neuronal differentiation when the silencing of the paternal allele takes place.

The generation of a standard curve is an essential prerequisite for any method utilised for absolute quantification. I designed two MGB probes to specifically detect the site of the mutation on the maternal *UBE3A* allele and its healthy counterpart on the paternal *UBE3A* allele by quantitative real-time PCR. 280 bp cDNA fragments from Angelman syndrome iPSC clone D containing the respective target sites were cloned into a vector. The plasmids were screened for accuracy of the inserted sequence and the two selected ones carrying the respective target sequences were mixed in defined ratios as templates for the standard curve. At first, I encountered a problem with the detection capacity of the TET-labelled probe detecting the maternal allele. The fluorescence signal was so weak that it was hardly possible

to evaluate the samples with the highest concentration of the target. A DNase I digestion test to release the full fluorescence potential of the probe did not lead to any improvement in the readout. qRT-PCR in multiplex and in singleplex settings excluded interference between the probes that would hinder the binding of one or the other probe to its target, as there was no difference between the outputs. Furthermore, the addition of salmon sperm DNA to the reactions verified that the probes only bind to their designated targets and not somewhere else on the vectors. The results with a requested replacement probe labelled with a stronger fluorophore, Yakima Yellow, were still unsatisfactory. Since it is very improbable that two different probes would contain a mismatch, I re-examined the assay design thoroughly. There was no way to alter the design of the probes because they had to fulfil a number of criteria that gave no room for adjustment. I first confirmed the primer specificity by using SYBR Green and the same set of templates as before. The expected output was an overlay of all curves because the amount of the target sequences should be equal in all reactions. Indeed, I observed an overlay without exception and the melting curve analysis proved the presence of a single PCR product. A 10-fold serial dilution of cDNA from Angelman syndrome iPSCs demonstrated primer efficiency of 98 % over four orders of magnitude. My experiment with SYBR Green not only showed that the primers were well designed but also that the plasmid mixes serve as appropriate templates, since the curves exhibited an overlay and a perfect sigmoid shape. However, when the respective probes were used with the standard samples, the curves flattened progressively with the decreasing amount of target. This indicates impaired efficiency of the reactions. My speculation that the phenomenon might be caused by a supercoiled structure of the plasmids restricting the access of the probes to their respective targets proved incorrect. Vectors linearised by enzymatic digestion with a single cutter did not differ from the untreated samples, so possible steric hindrance does not influence the accessibility of the targets.

Lastly, I replaced the YY-labelled maternal probe with a FAM-labelled one to assay, whether its fluorescence signal would match that of the paternal probe. I tested the probe on both sets of templates. Signals of equal strength were anticipated from the probes because the fluorophores were the same, the target concentrations in the standard mixes are inversely correlated, and the amounts of targets in the cDNA serial dilution samples should be at least comparable, if not identical. Indeed, the result of the analysis displayed a perfect overlay of the signals generated by the respective probes with both sets of templates. Since the idea of a single standard curve for both probes at a time became irrelevant due to the labelling of both

probes with the same fluorophore, two separate standard curves were constructed instead. 10-fold serial dilutions of the plasmids carrying the respective target sequences displayed the same sigmoid shape at all dilutions without any signs of flattening. Efficiencies of almost 100 % were stable over seven orders of magnitude. The decreasing efficiency of the standard samples in mixed ratios was most likely only apparent. A feasible explanation of the phenomenon is that the PCR reaction occurs on both templates in the mix simultaneously at a joint efficiency reaching or nearing 100 %. Since only a defined portion of the reactions is detected by the respective probe, it appears as a decrease in efficiency when a lower amount of the target is available because the rest is omitted. Under such conditions, a standard curve cannot be created.

The successful construction of a reliable standard curve for each probe allows for an exact calculation of the respective target amounts in analysed samples over a wide range of concentrations. The output obtained by the technique is much more informative than that of single-nucleotide primer extension assay. It facilitates the monitoring of expression dynamics of both parental *UBE3A* alleles in a very precise and unambiguous manner. If a fluorophore is developed that would match FAM in its fluorescence potential, multiplex qRT-PCR could be used for target detection to simplify the method.

4.4 Methylation Analyses of Imprinted ICRs

Since our aim was to establish a reliable model of Angelman syndrome and also to manipulate the methylation level at PWS-SRO, its stability and thus retained functionality with regard to *UBE3A* expression dynamics was an essential prerequisite for my work. Imprinted loci are expected to have a methylation level of 50 %. However, defects in maintenance during reprogramming or upon prolonged culture may occur (Pick *et al.*, 2009; Nazor *et al.*, 2012; Johannesson *et al.*, 2014; Ma *et al.*, 2014b). I analysed the methylation level at six imprinted loci. PWS-SRO proved to be the sole ICR with stable differential methylation in fibroblasts, iPSCs derived from them, hESC lines and the control iPSC line MCH2-10. Line AGI-0 harbours a large deletion on the maternal chromosome 15 including the imprinting centre, which is in concert with only unmethylated reads detected in the analysis (Fig. 25). My findings on the stability of the methylation level at PWS-SRO during

reprogramming are in line with previously published results (Chamberlain *et al.*, 2010; Ma *et al.*, 2014b). At ICR1, I observed a loss of methylation in patient iPSC line B1 and a gain of methylation in hESC line H9. Aberrant methylation towards both a loss and a gain of methylation have been reported (Nazor *et al.*, 2012; Johannesson *et al.*, 2014; Ma *et al.*, 2014b). ICR2 showed expected levels of methylation but for one exception in patient iPSC line P, in which the methylation was lost. A loss of methylation at NESPAS was detected in five out of 13 samples analysed. This result corresponds with previously published evidence on variable methylation at NESPAS in hESCs and iPSCs (Grybek *et al.*, 2014). CpG85 only exhibited differential methylation in four out of 16 assayed samples. Methylation was consistently elevated in all other samples. Variation at this locus between tissues has been observed with an obvious trend towards hypermethylation (Kanber, Institute of Human Genetics, unpublished data). IG-DMR showed a gain of methylation in seven out of 16 samples. This observation is in agreement with its reported susceptibility to acquiring methylation (Stadtfeld *et al.*, 2012; Johannesson *et al.*, 2014; Ma *et al.*, 2014b). I detected a loss of methylation at IG-DMR in immortalised fibroblasts of the patient but not in three other fibroblast samples. Therefore, this result is most likely the consequence of immortalisation. Alterations in methylation at imprinted loci and in the expression of imprinted genes have been described in immortalised lymphoblastoid cell lines and fibroblasts (Saferali *et al.*, 2010; Okamura *et al.*, 2011).

My results indicate a tendency towards either a loss of methylation, or its gain at a certain locus. I detected only a loss of methylation at ICR2 and at NESPAS, while solely a gain of methylation at CpG85 and at IG-DMR was observed. ICR1 was an exception to this trend showing both an increase and a decrease of methylation in different samples. Mechanisms favouring a loss or a gain of methylation at an ICR in hESCs or in iPSCs have not been understood so far. Imprint stability is expected in hESCs because imprints are already set in the parental germline, protected during the global wave of reprogramming in early embryonic development and passed on to daughter cells upon division. iPSCs are generated by reprogramming differentiated cells, whose imprints should be stable as well. Anomalies in methylation at imprinted loci therefore probably occur due to a defective maintenance during the cultivation of hESCs, fibroblasts and iPSCs, or as a result of reprogramming (Rugg-Gunn *et al.*, 2007; Johannesson *et al.*, 2014; Ma *et al.*, 2014b). In general, my observations on the stability of the analysed ICRs in hESCs and in iPSCs are in line with previous reports. Most

importantly, I confirmed the stability of the methylation at PWS-SRO in the cells and thereby their adequacy for the purposes of the study.

4.5 Methylation Induction

Successful targeting of selected regions by artificial methylated oligonucleotides (MONs) in order to interfere with the expression of a certain gene or RNA has previously been described (Yao *et al.*, 2003; Zhu *et al.*, 2004; Hoffman & Hu, 2006; Ma *et al.*, 2010). In theory, the method relies on the annealing of the MONs to their target during mitosis or transcription. The hemi-methylated stretch of DNA is recognised by the maintenance methyltransferase DNMT1 and the newly synthesised strand is methylated. Once the MONs dissociate and the DNA double helix is formed, DNMT1 completes the methylation. Several groups demonstrated efficient induction of methylation and a subsequent silencing of gene expression. For instance, in a model of hepatocellular carcinoma, expression levels of the targeted gene decreased rapidly upon methylation induction. Moreover, the survival of rats treated with MONs was significantly prolonged in comparison with negative controls (Yao *et al.*, 2003). Successful results were obtained using various cell lines but neither hESCs nor iPSCs were among them. I employed transfection and nucleofection to deliver the MONs into the cells and tested a range of MONs concentrations to determine the most suitable one. Although the delivery was rather efficient, the method did not induce methylation at the targeted PWS-SRO (Fig. 22). Prolonging the time of the treatment before harvest did not lead to any improvement in the outcome. I performed repeated delivery every two or three days involving six rounds of transfection at most. The region remained unmethylated when targeted by a single MON as well as by a combination of MONs.

The efficiency of the MONs delivery into the cells was probably not the limiting factor of the technique, though it is often an issue. In case of nucleofection, the viability of the cells was strongly impaired after the treatment but the surviving cells did absorb additional MONs during subsequent rounds of transfection. It is feasible that a combination of other aspects prevented the successful application of the approach. Even at a high concentration, it is unlikely for the MONs to find their target. Experiments on the plasticity of nuclear organisation in embryonic stem cells and fibroblasts demonstrated high stability of the

chromatin structure in differentiated cells, while the positions of the chromatin domains fluctuated substantially within 40 minutes in embryonic stem cells (Strickfaden *et al.*, 2010; Cremer, personal communication). The increased plasticity does not favour the binding of the MONs. Furthermore, mitosis of hESCs and iPSCs is a fast process (Becker *et al.*, 2006), which does not contribute to the MONs annealing either. There is only a very short time frame for the pairing to occur. In addition, methylation by DNMT1 is a process much slower than replication, so the probability that DNMT1 acts at the correct moment is low. All the described circumstances make the approach ineffective. If methylation is induced to a small extent, it is most likely not maintained or even actively removed by TET enzymes, whose activity is rather high in hESCs and iPSCs because it is required for maintaining pluripotency (Tahiliani *et al.*, 2009; Pastor *et al.*, 2011; Gao *et al.*, 2013). It would be worthwhile to try applying the method in neural progenitors.

Induction of methylation at a targeted locus using in vitro-methylated fragments has been published (Hsiao *et al.*, 2010; Hsu *et al.*, 2011; Teng *et al.*, 2011). Adjustments to the method described in the article were required, since methylation by *M.Sss*I was not working efficiently. Gel elution proved to be an unsuitable means of purifying the desired fragment after PCR. Probably, impurities present in the eluate inhibited the *M.Sss*I activity. Purification by the Agencourt® AMPure® XP system produced an eluate of sufficient purity. Optimisation of the methylation reaction yielded fragments methylated to approximately 80 %. After the initial problems I encountered with MONs, I resorted to multiple transfections from the beginning, as indicated in the publication (Hsiao *et al.*, 2010). By employing this approach, I accomplished an increase of 38.6 % methylation at the targeted region after three rounds of transfection. I pursued the development of the methylation after three rounds of transfection with and without additional delivery. When transfection ensued, the methylation level remained stable (Fig. 25). When no further substrate was provided, I observed a rapid decrease of the methylation level by roughly 5 % per day. The loss could have been general in the whole population, or due to clonal expansion of cells that had not been transfected and thereby possessed a selection advantage. The analysis of single clones confirmed the former hypothesis, since all analysed clones exhibited a complete loss of methylation. It is possible that the gradual loss of methylation is caused simply by the lack of its maintenance and it passively gets diluted out. Alternatively, it can be removed by the activity of TET enzymes. Since the approach did not induce stable methylation, I decided not to work with it further.

Therefore, I did not determine the exact mechanism of the methylation loss. It would have been possible to employ TET inhibitors to identify whether it is an active or a passive process. However, considering that my aim was to develop a means of therapy, an additional treatment in the form of TET inhibitors would be highly undesirable.

The experiment with the PCR-methylated fragments surprisingly led to no induction of methylation at the targeted locus. Based on the *Hpa*II validation result, it seemed to be more promising than the *M.Sss*I approach, even though the fragments were not methylated to full extent by this method either (Fig. 24). Considerable optimisation was required to obtain a PCR product at all because methylated cytosine is not a substrate polymerases recognise readily. Since the methylated cytosines are incorporated by the polymerase on a random basis during PCR, they occur in the sequence not only in the context of CpG dinucleotides. The presence of methylated cytosines outside of this context is not physiological. Such a piece of DNA might therefore be interpreted as potentially deleterious and eliminated.

Especially type II CRISPR/Cas system relying on Cas9 has been widely adopted as a tool for genetic and epigenetic engineering. Fusion proteins of the inactivated nucleases with histone deacetylases, transcription repressors or enhancers represent only some of the possible options the technology offers (Hilton *et al.*, 2015; Kearns *et al.*, 2015; Thakore *et al.*, 2015). The CRISPR/Cas9 fusion construct with DNMT3A and DNMT3L active domains was shown to be an efficient tool to induce methylation at targeted loci (Jurkowska *et al.*, 2008; Rajavelu *et al.*, 2012; Siddique *et al.*, 2013; Emperle *et al.*, 2014; McDonald *et al.*, 2016; Vojta *et al.*, 2016; Stepper *et al.*, 2017). The published experiments were performed in differentiated cells and not in iPSCs. Transfection of HEK293 cells was successful and I proved the specificity and efficiency of the designed gRNAs by T7 assay (Fig. 27). However, the delivery of the constructs into iPSCs proved to be an issue difficult to deal with. Delivery by transfection yielded no cells positive for YFP, although HEK293 cells are not larger in size than hESCs or iPSCs. hESCs as well as iPSCs are cells generally difficult to transfect by any means of delivery (Eiges *et al.*, 2001; Gerrard *et al.*, 2005; Liu *et al.*, 2005; Braam *et al.*, 2008; Hohenstein *et al.*, 2008; Siemen *et al.*, 2008). Moreover, the plasmids carrying the constructs are larger than 12 kb, which itself is a hindrance. Nucleofection that proved to be more efficient for the delivery of MONs into the iPSCs than conventional transfection yielded virtually no YFP-positive cells. Also in this case, the size of the construct was presumably the critical factor because I observed a delivery efficiency of up to 60 % with a smaller GFP-

expressing plasmid provided with the kit as positive control. Electroporation was the sole method by that I obtained YFP-positive cells, although also this approach was rather inefficient. Approximately 10 % of the input cells survived the treatment. Out of the remaining cells, no more than 9.6 % were positive for YFP, as determined by FACS. Merely 1 % of the cells was viable after sorting when seeded for expansion. The limited efficiency and the poor viability of the cells after electroporation and especially after sorting cannot be improved with current methods. Scaling up as the only means of retrieving a number of cells sufficient for the planned analyses was extremely inefficient, the output after sorting being 0.03 % at best. This was most probably due to technical reasons, as the experiment took a considerable amount of time and the viability of the cells decreases rapidly, if they do not adhere to the surface of the culture vessel as soon as possible. When it is compromised by electroporation in addition, the likelihood of survival is low. Alternatively, lentiviral transduction, though a laborious and time-consuming method, represents another possibility of delivery into cells difficult to transfect. However, the overall size of the vector is restricted to around 10 kb and the insert should not exceed 6 kb, which is a condition that the constructs I employ do not fulfil, even if the minimal necessary portion were used. Moreover, the method would lead to the integration of the vector into the genome.

Methylation levels detected in electroporated cells immediately after sorting, that is, three days after treatment, were unexpectedly low. Since the cells were positive for YFP, the fusion protein was also present in the cells. The surprising outcome could have been caused by diverse reasons or, more likely, their combination. First, technical issues associated with sorting may have been a problem. Doublet exclusion is essential because doublets with only one cell positive for YFP are interpreted as a positive event. If these doublets are not excluded, unmethylated cells are carried over and bias the results. Even with proper gating and careful analysis, doublets may escape the negative selection. Second, the efficiency of gRNAs is dose-dependent. When the gRNA-protein complexes are formed, probing of DNA sequence neighbouring the PAM triplet begins. If the complex does not find its target, it disintegrates and loses its methylation potential. As 5'-NGG-3' PAM sites are very abundant in the genome, a lot of the fusion protein is needed to target the correct sequence. Even when large amounts of the protein are available in the cells, the methylation capacity might be dissipated before the gRNA-protein complex reaches the target sequence. Third, it is generally rather difficult to methylate promoters of actively transcribed genes, which is likely also the case of *SNURF-SNRPN*. The region is probably occupied by transcription factors and

RNA polymerase complexes. This creates steric hindrance, which inhibits the access of the gRNA-protein complexes to the target. Moreover, TET enzymes are active at such promoters, which further decreases the probability that the region would acquire methylation and retain it (Pastor *et al.*, 2011; Wu *et al.*, 2011).

The best result I obtained by electroporation was 30.0 % methylation at the targeted locus after two weeks of cultivation post sorting. The level of methylation nearly doubled within a week from 15.7 % on day 7. It is difficult to estimate the development of the methylation between day 0, which shows 22.8 % methylation, and day 7. Since only very few cells were available for DNA isolation on day 0, the results are affected by a strong bias. An obvious clonal expansion and a patchy pattern of methylation indicate the inaccuracy of the outcome on day 0. Most likely, the cells exhibit significantly lower levels of methylation than suggested by the analysis. I probably would have been able to see an increase in methylation from day 0 to day 7, had it been possible to analyse more material. On day 7 and day 14, the pattern of the induced methylation was not patchy, which would imply its active removal by TET enzymes. On the contrary, it was evenly distributed indicating that methylation is not restricted to regions directly neighbouring the binding sites of the gRNAs but gets spread beyond the targeted segments of DNA. This is a very promising result because I observe reads with all CpGs methylated despite occasional template switching. Also, the stability of the methylation is exceptional especially considering the rapid decrease of methylation induced with *M.Sss*I-methylated fragments.

It is possible that the gain of methylation to 30.0 % occurred due to the lasting presence of the vectors in the cells. Nevertheless, methylation spreading and self-propagation is plausible and even quite feasible, since the plasmids do get diluted out over time. Another explanation of the gain in methylation may be the clonal expansion of cells, whose *SNURF-SNRPN* expression had been abolished due to the introduced repressive methylation. This might confer a selection advantage to the cells that would then overgrow the population of unmethylated cells. Further long-term time-course assays and qRT-PCR analyses of *SNURF-SNRPN* expression to test the biological effects of the induced methylation are required to determine the true mechanism.

Although an increase of 30 % in methylation is a very good result, it would be desirable to achieve a higher level of methylation for experimental purposes. Positive selection by applying kanamycin represents one of the ways to accomplish this. The process would yield only cells carrying the plasmid; however, there are certain drawbacks to the method. When

selection conditions suitable for healthy cells are applied to cells with impaired viability due to electroporation, they may as well not survive the stringent pressure. Another possibility would be to indirectly induce DNA methylation by histone modifications, for instance by employing complexes containing the SET domain catalysing H3K9 trimethylation (Xiao *et al.*, 2003). Transcriptional regulation is a sophisticated mechanism involving an interplay of diverse factors including chromatin remodelling, so this process would most likely also contribute. Alternatively, artificial reporter constructs could be implemented to induce DNA methylation. Such systems may contain *Sss*I methyltransferase, Krüppel-associated suppression box (KRAB) that functions as a strong transcriptional repressor (Witzgall *et al.*, 1994), and a reporter to monitor the effects (Ma *et al.*, 2014a). Both described options rely on large complexes that would pose a problem with delivery into the cells similar to the one I encountered with the CRISPR/Cas9 system. Probably the most reliable method of inducing stable methylation would be the generation of stable cell lines with any of the fusion proteins integrated into the genome and constantly expressed. The most important reason why I did not resort to creating stable cell lines was that my goal was to develop a means of therapy. However, establishing stable cell lines to prove my hypothesis might contribute to a better understanding of the methylation dynamics and support optimisation of the non-integrative approaches.

I chose to induce methylation in iPSCs rather than in neurons for various reasons. At the time the study was initiated, the published methods of accomplishing methylation induction all required mitosis to function and iPSCs certainly are mitotically active. On the contrary, the more mature neurons become, the more they cease to proliferate, so it would have hardly been possible to use them for my experiments. Moreover, neurons exhibit very high levels of TET enzymes (Kriaucionis & Heintz, 2009; Globisch *et al.*, 2010; Szwagierczak *et al.*, 2010), which would also have been counterproductive for my purposes. Lastly, neurons are fragile, challenging to obtain and generally demanding to work with. As I experienced difficulties delivering constructs into the iPSCs, I considered employing neural progenitors instead. The reason was that all of the described approaches relied on differentiated cells and neural progenitors would probably be more suitable in this regard than iPSCs. Also, unlike neurons, they are still mitotically active. On the other hand, the activity of TET enzymes is high in neural progenitors as well (Hahn *et al.*, 2013; Lister *et al.*, 2013; Zhang *et al.*, 2013). I did not perform the methylation induction in neural progenitors because a stable culture had not yet been established. It would definitely be worthwhile to proceed with research on inducing

methylation in neural progenitors. The modified CRISPR/Cas9 system was only developed recently. Although there are particular disadvantages to the approach, its indisputable advantage in comparison with the other methods is its independence from mitosis. Thus, its application in neural progenitors or even terminally differentiated neurons is well practicable. Optimisation of delivery would surely be necessary but the combination could yield very interesting results and is unquestionably worth further investigation.

5. Conclusion

In this study, an iPSC model of Angelman syndrome was developed. iPSCs were generated from an Angelman syndrome patient harbouring a three-base pair deletion in the maternal *UBE3A* allele and from a healthy control person. The maternal *UBE3A* allele is expressed but the protein UBE3A is not functional. Therefore, the cells exhibit normal expression of all genes at the PWS/AS locus. In comparison with all iPSC lines generated as a model of Angelman syndrome so far, this is a significant advantage because all observed effects may be attributed directly and solely to the inactive UBE3A protein.

Using lentiviral transduction, we reprogrammed fibroblasts from the patient and from the healthy control person, and isolated several clones. Their thorough characterisation followed confirming their pluripotency, identity and integrity by various methods. Based on the results, clones most suitable for further analyses were selected. The stability of the imprint at the PWS/AS locus is a critical prerequisite for the faithful analysis of imprinted expression and for the induction of DNA methylation on the paternal allele. Therefore, the methylation status at six imprinted loci and two pluripotent loci was determined in the iPSCs generated at the beginning of this project, their parental fibroblasts, in hESCs H1 and H9, and in published cell lines AGI-0 and MCH2-10 that represented iPSC controls. Most importantly, I observed an exceptional stability of the methylation imprint at PWS-SRO. Three imprinted loci showed a tendency towards a loss of methylation and two exhibited susceptibility to acquiring methylation. Both pluripotent loci displayed a higher level of methylation in differentiated cells than in pluripotent cells. My results on the stability of the assayed loci upon reprogramming are in agreement with previously reported observations.

In cooperation with Anika Neureiter from the Institute for Transfusion Medicine, iPSCs were differentiated into neurons. We determined by single-nucleotide primer extension assay that silencing of the paternal *UBE3A* allele by *SNHG14* occurs late during the process of neuronal differentiation. These findings are also in line with previously published results. I developed a quantitative qRT-PCR analysis to follow the expression dynamics of the maternal and the paternal *UBE3A* allele separately in the generated iPSCs during differentiation. The method

allows for a much more precise evaluation of the respective alleles' expression than single-nucleotide primer extension assay.

In the second part of the study, I aimed to induce methylation at the paternal PWS-SRO in the cell line AGI-0, which only harbours the unmethylated paternal allele. I observed a transient increase of methylation at the paternal PWS-SRO to 38.6 % upon transfecting the cells with methylated DNA fragments. By employing the modified CRISPR/Cas9 system fused with DNMT3A and DNMT3L, I was able to induce methylation at the paternal PWS-SRO in AGI-0 to 30.0 %. Not only was the methylation stable at the locus over the course of two weeks but its level also increased during the time. The result is especially valuable because the approach does not require mitosis for its functioning and could therefore potentially be used even in non-dividing cells such as neurons.

It would certainly be worthwhile to pursue the stability of the induced methylation in a longer time-course experiment. Also, the investigation of a direct biological impact in the form of a qRT-PCR assay of *SNURF-SNRPN* expression would be of importance. The effect of the methylation on the expression of *SNHG14* in neurons is even more relevant for my purposes and so is the subsequent impact on the expression of *UBE3A*. Should the methylation lead to abolishment of *SNHG14* expression and thereby prevent silencing of the paternal *UBE3A* allele in neurons, it would be a significant step towards possible compensation for the loss of maternal *UBE3A* by the intact paternal allele. Therefore, further optimisation of the method and its application in iPSCs generated in this study ought to be performed.

6. Zusammenfassung

In dieser Arbeit wurde ein iPS-Zellmodell für das Angelman-Syndrom etabliert. Wir generierten iPS-Zellen von einem Angelman-Syndrom Patienten mit einer Deletion von 3 bp im mütterlichen *UBE3A* Allel, sowie von einer gesunden Kontrollperson. Durch diese definierte Mutation im mütterlichen *UBE3A* Allel exprimieren die Zellen *UBE3A*, aber das daraus hergestellte Protein ist nicht funktionell. Die Zellen zeigen somit eine normale Expression aller Gene im PWS/AS Genlokus. Im Vergleich mit allem bisher als Modell für das Angelman-Syndrom generierten iPS-Zelllinien ist das ein bedeutsamer Vorteil, denn so können beobachtete Effekte direkt und ausschließlich auf das inaktive UBE3A-Protein zurückgeführt werden.

Mithilfe lentiviraler Transduktion wurden sowohl patienten-spezifische Fibroblasten, als auch Kontrollfibroblasten in iPS-Zellen reprogrammiert und anschließend einige Klone isoliert. Ihre Charakterisierung mittels verschiedener Methoden bestätigte die Pluripotenz, Identität und Integrität der Zellen. Die meistgeeigneten Klone wurden für weitere Analysen ausgewählt. Eine kritische Voraussetzung für die Analyse der geimprinteten Expression und der Induktion von DNA-Methylierung auf dem väterlichen Allel ist die Stabilität des Methylierungsimprints des PWS/AS-Genlokus. Daher wurde der Methylierungsstatus an sechs geimprinteten Lozi und zwei mit Pluripotenz assoziierten Lozi in den in dieser Studie generierten Zelllinien, in deren elterlichen Fibroblasten, in den humanen embryonalen Stammzelllinien H1 und H9, sowie in den publizierten iPS-Zelllinien AGI-0 und MCH2-10, welche iPS-Kontrollen darstellten, bestimmt. Der Imprint des PWS-SROs erwies sich als außergewöhnlich stabil. Drei der geimprinteten Lozi wiesen eine Tendenz zur Hypomethylierung auf, während die zwei anderen Lozi eine Neigung zur Hypermethylierung zeigten. Die Methylierung an den beiden mit Pluripotenz assoziierten Lozi war in differenzierten Zellen höher als in pluripotenten Zellen. Die Ergebnisse bezüglich Stabilität geimprinteter Lozi unter Reprogrammierung entsprechen zuvor publizierten Erkenntnissen.

Die Differenzierung von iPS-Zellen in Neurone erfolgte in Kooperation mit Anika Neureiter aus dem Institut für Transfusionsmedizin. Mithilfe der *single-nucleotide primer extension* Methode wurde festgestellt, dass die Stilllegung des väterlichen *UBE3A* Allels durch

SNHG14 erst spät während der neuronalen Differenzierung auftritt. Auch diese Ergebnisse stehen im Einklang mit früheren Beobachtungen. Es wurde eine quantitative qRT-PCR-Analyse entwickelt, die die Untersuchung der Expressionsdynamik beider elterlichen Allele getrennt in den generierten iPS-Zellen während neuronaler Differenzierung zulässt. Diese Methode ermöglicht eine Evaluierung der Expression der jeweiligen *UBE3A*-Allele, die viel präziser ist als die der *single-nucleotide primer extension* Analyse.

Im zweiten Teil des Projektes wurden Experimente zur Einführung von Methylierung am väterlichen PWS-SRO der Zelllinie AGI-0, die nur das unmethylierte väterliche Allel enthält, durchgeführt. Transiente Methylierung von 38.6 % wurde mittels Transfektion der Zellen mit methylierten DNA-Fragmenten erzielt. Durch den Einsatz eines modifizierten CRISPR/Cas9-Systems, in dem Cas9 fusioniert mit DNMT3A und DNMT3L vorliegt, wurde Methylierung von 30.0 % am väterlichen PWS-SRO induziert. Die Methylierung war über zwei Wochen stabil und das Ausmaß nahm in dieser Zeitspanne zu. Dieses Ergebnis ist von Bedeutung vor allem wegen der Unabhängigkeit des Verfahrens von Mitose, durch die die Verwendung der Methode in sich nicht teilenden Zellen wie Neuronen sehr vielversprechend ist.

Es wäre interessant die Stabilität der induzierten Methylierung über einen längeren Zeitraum zu verfolgen. Weiterhin wäre die Erforschung direkter biologischer Auswirkung der Methylierung auf die Expression von *SNURF-SNRPN* von Bedeutung. Die Auswirkung auf die Expression von *SNHG14* in Neuronen wäre noch wichtiger und gleichermaßen der nachfolgende indirekte Einfluss auf die Expression von *UBE3A*. Sollte die Methylierung die Expression von *SNHG14* unterdrücken und dadurch die Stilllegung des väterlichen *UBE3A* Allels verhindern, wäre das ein wichtiger Schritt zur potentiellen Kompensierung des Verlustes des mütterlichen *UBE3A* Allels durch das intakte väterliche Allel. Deshalb sollte eine weitere Optimierung der Methode und deren Einsatz in den in dieser Studie generierten iPS-Zellen unbedingt verfolgt werden.

7. References

Albrecht, U., Sutcliffe, J. S., Cattanach, B. M., Beechey, C. V., Armstrong, D., Eichele, G., & Beaudet, A. L. (1997). Imprinted expression of the murine Angelman syndrome gene, Ube3a, in hippocampal and Purkinje neurons. *Nat Genet, 17*(1), 75-78. doi:10.1038/ng0997-75

Amit, M., Carpenter, M. K., Inokuma, M. S., Chiu, C. P., Harris, C. P., Waknitz, M. A., Itskovitz-Eldor, J., & Thomson, J. A. (2000). Clonally derived human embryonic stem cell lines maintain pluripotency and proliferative potential for prolonged periods of culture. *Dev Biol, 227*(2), 271-278. doi:10.1006/dbio.2000.9912

Arand, J., Spieler, D., Karius, T., Branco, M. R., Meilinger, D., Meissner, A., Jenuwein, T., Xu, G., Leonhardt, H., Wolf, V., *et al.* (2012). In vivo control of CpG and non-CpG DNA methylation by DNA methyltransferases. *PLoS Genet, 8*(6), e1002750. doi:10.1371/journal.pgen.1002750

Armstrong, D. K. (2004). Topotecan dosing guidelines in ovarian cancer: reduction and management of hematologic toxicity. *Oncologist, 9*(1), 33-42.

Barlow, D. P. (2011). Genomic imprinting: a mammalian epigenetic discovery model. *Annu Rev Genet, 45*, 379-403. doi:10.1146/annurev-genet-110410-132459

Barlow, D. P., & Bartolomei, M. S. (2014). Genomic imprinting in mammals. *Cold Spring Harb Perspect Biol, 6*(2). doi:10.1101/cshperspect.a018382

Bartolomei, M. S., & Ferguson-Smith, A. C. (2011). Mammalian genomic imprinting. *Cold Spring Harb Perspect Biol, 3*(7). doi:10.1101/cshperspect.a002592

Bartolomei, M. S., Webber, A. L., Brunkow, M. E., & Tilghman, S. M. (1993). Epigenetic mechanisms underlying the imprinting of the mouse H19 gene. *Genes Dev, 7*(9), 1663-1673.

Barton, S. C., Surani, M. A., & Norris, M. L. (1984). Role of paternal and maternal genomes in mouse development. *Nature, 311*(5984), 374-376.

Baubec, T., Colombo, D. F., Wirbelauer, C., Schmidt, J., Burger, L., Krebs, A. R., Akalin, A., & Schubeler, D. (2015). Genomic profiling of DNA methyltransferases reveals a role for DNMT3B in genic methylation. *Nature, 520*(7546), 243-247. doi:10.1038/nature14176

Becker, K. A., Ghule, P. N., Therrien, J. A., Lian, J. B., Stein, J. L., van Wijnen, A. J., & Stein, G. S. (2006). Self-renewal of human embryonic stem cells is supported by a shortened G1 cell cycle phase. *J Cell Physiol, 209*(3), 883-893. doi:10.1002/jcp.20776

Bell, A. C., & Felsenfeld, G. (2000). Methylation of a CTCF-dependent boundary controls imprinted expression of the Igf2 gene. *Nature, 405*(6785), 482-485. doi:10.1038/35013100

Bernstein, D. L., Le Lay, J. E., Ruano, E. G., & Kaestner, K. H. (2015). TALE-mediated epigenetic suppression of CDKN2A increases replication in human fibroblasts. *J Clin Invest, 125*(5), 1998-2006. doi:10.1172/JCI77321

Bestor, T. H. (2000). The DNA methyltransferases of mammals. *Hum Mol Genet, 9*(16), 2395-2402.

Bhaya, D., Davison, M., & Barrangou, R. (2011). CRISPR-Cas systems in bacteria and archaea: versatile small RNAs for adaptive defense and regulation. *Annu Rev Genet, 45*, 273-297. doi:10.1146/annurev-genet-110410-132430

Bikard, D., Jiang, W., Samai, P., Hochschild, A., Zhang, F., & Marraffini, L. A. (2013). Programmable repression and activation of bacterial gene expression using an engineered CRISPR-Cas system. *Nucleic Acids Res, 41*(15), 7429-7437. doi:10.1093/nar/gkt520

Boissart, C., Poulet, A., Georges, P., Darville, H., Julita, E., Delorme, R., Bourgeron, T., Peschanski, M., & Benchoua, A. (2013). Differentiation from human pluripotent stem cells of cortical neurons of the superficial layers amenable to psychiatric disease modeling and high-throughput drug screening. *Transl Psychiatry, 3*, e294. doi:10.1038/tp.2013.71

Bolotin, A., Quinquis, B., Sorokin, A., & Ehrlich, S. D. (2005). Clustered regularly interspaced short palindrome repeats (CRISPRs) have spacers of extrachromosomal origin. *Microbiology, 151*(Pt 8), 2551-2561. doi:10.1099/mic.0.28048-0

Borowczyk, E., Mohan, K. N., D'Aiuto, L., Cirio, M. C., & Chaillet, J. R. (2009). Identification of a region of the DNMT1 methyltransferase that regulates the maintenance of genomic imprints. *Proc Natl Acad Sci U S A, 106*(49), 20806-20811. doi:10.1073/pnas.0905668106

Bourc'his, D., Xu, G. L., Lin, C. S., Bollman, B., & Bestor, T. H. (2001). Dnmt3L and the establishment of maternal genomic imprints. *Science, 294*(5551), 2536-2539. doi:10.1126/science.1065848

Boyer, L. A., Lee, T. I., Cole, M. F., Johnstone, S. E., Levine, S. S., Zucker, J. P., Guenther, M. G., Kumar, R. M., Murray, H. L., Jenner, R. G., *et al.* (2005). Core transcriptional regulatory circuitry in human embryonic stem cells. *Cell, 122*(6), 947-956. doi:10.1016/j.cell.2005.08.020

Braam, S. R., Denning, C., van den Brink, S., Kats, P., Hochstenbach, R., Passier, R., & Mummery, C. L. (2008). Improved genetic manipulation of human embryonic stem cells. *Nat Methods, 5*(5), 389-392. doi:10.1038/nmeth.1200

Brockdorff, N. (2011). Chromosome silencing mechanisms in X-chromosome inactivation: unknown unknowns. *Development, 138*(23), 5057-5065. doi:10.1242/dev.065276

Brouns, S. J., Jore, M. M., Lundgren, M., Westra, E. R., Slijkhuis, R. J., Snijders, A. P., Dickman, M. J., Makarova, K. S., Koonin, E. V., & van der Oost, J. (2008). Small CRISPR RNAs guide antiviral defense in prokaryotes. *Science, 321*(5891), 960-964. doi:10.1126/science.1159689

Brown, S., Teo, A., Pauklin, S., Hannan, N., Cho, C. H., Lim, B., Vardy, L., Dunn, N. R., Trotter, M., Pedersen, R., *et al.* (2011). Activin/Nodal signaling controls divergent transcriptional networks in human embryonic stem cells and in endoderm progenitors. *Stem Cells, 29*(8), 1176-1185. doi:10.1002/stem.666

Buganim, Y., Faddah, D. A., Cheng, A. W., Itskovich, E., Markoulaki, S., Ganz, K., Klemm, S. L., van Oudenaarden, A., & Jaenisch, R. (2012). Single-cell expression analyses during cellular reprogramming reveal an early stochastic and a late hierarchic phase. *Cell, 150*(6), 1209-1222. doi:10.1016/j.cell.2012.08.023

Buiting, K. (2010). Prader-Willi syndrome and Angelman syndrome. *Am J Med Genet C Semin Med Genet, 154C*(3), 365-376. doi:10.1002/ajmg.c.30273

Buiting, K., Clayton-Smith, J., Driscoll, D. J., Gillessen-Kaesbach, G., Kanber, D., Schwinger, E., Williams, C., & Horsthemke, B. (2015). Clinical utility gene card for: Angelman Syndrome. *Eur J Hum Genet, 23*(2). doi:10.1038/ejhg.2014.93

Buiting, K., Dittrich, B., Gross, S., Lich, C., Farber, C., Buchholz, T., Smith, E., Reis, A., Burger, J., Nothen, M. M., *et al.* (1998). Sporadic imprinting defects in Prader-Willi syndrome and Angelman syndrome: implications for imprint-switch models, genetic counseling, and prenatal diagnosis. *Am J Hum Genet, 63*(1), 170-180. doi:10.1086/301935

Buiting, K., Gross, S., Lich, C., Gillessen-Kaesbach, G., el-Maarri, O., & Horsthemke, B. (2003). Epimutations in Prader-Willi and Angelman syndromes: a molecular study of 136 patients with an imprinting defect. *Am J Hum Genet, 72*(3), 571-577. doi:10.1086/367926

Buiting, K., Lich, C., Cottrell, S., Barnicoat, A., & Horsthemke, B. (1999). A 5-kb imprinting center deletion in a family with Angelman syndrome reduces the shortest region of deletion overlap to 880 bp. *Hum Genet, 105*(6), 665-666.

Buzzard, J. J., Gough, N. M., Crook, J. M., & Colman, A. (2004). Karyotype of human ES cells during extended culture. *Nat Biotechnol, 22*(4), 381-382; author reply 382. doi:10.1038/nbt0404-381

Byrne, J. A., Pedersen, D. A., Clepper, L. L., Nelson, M., Sanger, W. G., Gokhale, S., Wolf, D. P., & Mitalipov, S. M. (2007). Producing primate embryonic stem cells by somatic cell nuclear transfer. *Nature, 450*(7169), 497-502. doi:10.1038/nature06357

Cedar, H., & Bergman, Y. (2009). Linking DNA methylation and histone modification: patterns and paradigms. *Nat Rev Genet, 10*(5), 295-304. doi:10.1038/nrg2540

Collas, P. (2009). Epigenetic states in stem cells. *Biochim Biophys Acta, 1790*(9), 900-905. doi:10.1016/j.bbagen.2008.10.006

Cong, L., Ran, F. A., Cox, D., Lin, S., Barretto, R., Habib, N., Hsu, P. D., Wu, X., Jiang, W., Marraffini, L. A., *et al.* (2013). Multiplex genome engineering using CRISPR/Cas systems. *Science, 339*(6121), 819-823. doi:10.1126/science.1231143

Cowan, C. A., Atienza, J., Melton, D. A., & Eggan, K. (2005). Nuclear reprogramming of somatic cells after fusion with human embryonic stem cells. *Science, 309*(5739), 1369-1373. doi:10.1126/science.1116447

Dagli, A., Buiting, K., & Williams, C. A. (2012). Molecular and Clinical Aspects of Angelman Syndrome. *Mol Syndromol, 2*(3-5), 100-112. doi:000328837

Dalton, S. (2013). Signaling networks in human pluripotent stem cells. *Curr Opin Cell Biol, 25*(2), 241-246. doi:10.1016/j.ceb.2012.09.005

Davidson, K. C., Adams, A. M., Goodson, J. M., McDonald, C. E., Potter, J. C., Berndt, J. D., Biechele, T. L., Taylor, R. J., & Moon, R. T. (2012). Wnt/beta-catenin signaling promotes differentiation, not self-renewal, of human embryonic stem cells and is repressed by Oct4. *Proc Natl Acad Sci U S A, 109*(12), 4485-4490. doi:10.1073/pnas.1118777109

Davis, R. P., Nemes, C., Varga, E., Freund, C., Kosmidis, G., Gkatzis, K., de Jong, D., Szuhai, K., Dinnyes, A., & Mummery, C. L. (2013). Generation of induced pluripotent stem cells from human foetal fibroblasts using the Sleeping Beauty transposon gene delivery system. *Differentiation, 86*(1-2), 30-37. doi:10.1016/j.diff.2013.06.002

Davis, T. L., Yang, G. J., McCarrey, J. R., & Bartolomei, M. S. (2000). The H19 methylation imprint is erased and re-established differentially on the parental alleles during male germ cell development. *Hum Mol Genet, 9*(19), 2885-2894.

Dean, W., Lucifero, D., & Santos, F. (2005). DNA methylation in mammalian development and disease. *Birth Defects Res C Embryo Today, 75*(2), 98-111. doi:10.1002/bdrc.20037

Dean, W., Santos, F., & Reik, W. (2003). Epigenetic reprogramming in early mammalian development and following somatic nuclear transfer. *Semin Cell Dev Biol, 14*(1), 93-100.

Deaton, A. M., & Bird, A. (2011). CpG islands and the regulation of transcription. *Genes Dev, 25*(10), 1010-1022. doi:10.1101/gad.2037511

DeBaun, M. R., & Tucker, M. A. (1998). Risk of cancer during the first four years of life in children from The Beckwith-Wiedemann Syndrome Registry. *J Pediatr, 132*(3 Pt 1), 398-400.

Deltcheva, E., Chylinski, K., Sharma, C. M., Gonzales, K., Chao, Y., Pirzada, Z. A., Eckert, M. R., Vogel, J., & Charpentier, E. (2011). CRISPR RNA maturation by trans-encoded small RNA and host factor RNase III. *Nature, 471*(7340), 602-607. doi:10.1038/nature09886

Deng, J., Shoemaker, R., Xie, B., Gore, A., LeProust, E. M., Antosiewicz-Bourget, J., Egli, D., Maherali, N., Park, I. H., Yu, J., *et al.* (2009). Targeted bisulfite sequencing reveals changes in DNA methylation associated with nuclear reprogramming. *Nat Biotechnol, 27*(4), 353-360. doi:10.1038/nbt.1530

Dindot, S. V., Person, R., Strivens, M., Garcia, R., & Beaudet, A. L. (2009). Epigenetic profiling at mouse imprinted gene clusters reveals novel epigenetic and genetic features at differentially methylated regions. *Genome Res, 19*(8), 1374-1383. doi:10.1101/gr.089185.108

Dittrich, B., Buiting, K., Korn, B., Rickard, S., Buxton, J., Saitoh, S., Nicholls, R. D., Poustka, A., Winterpacht, A., Zabel, B., *et al.* (1996). Imprint switching on human chromosome 15 may involve alternative transcripts of the SNRPN gene. *Nat Genet, 14*(2), 163-170. doi:10.1038/ng1096-163

Doetschman, T. C., Eistetter, H., Katz, M., Schmidt, W., & Kemler, R. (1985). The in vitro development of blastocyst-derived embryonic stem cell lines: formation of visceral yolk sac, blood islands and myocardium. *J Embryol Exp Morphol, 87*, 27-45.

Draper, J. S., Smith, K., Gokhale, P., Moore, H. D., Maltby, E., Johnson, J., Meisner, L., Zwaka, T. P., Thomson, J. A., & Andrews, P. W. (2004). Recurrent gain of chromosomes 17q and 12 in cultured human embryonic stem cells. *Nat Biotechnol, 22*(1), 53-54. doi:10.1038/nbt922

Eiges, R., Schuldiner, M., Drukker, M., Yanuka, O., Itskovitz-Eldor, J., & Benvenisty, N. (2001). Establishment of human embryonic stem cell-transfected clones carrying a marker for undifferentiated cells. *Curr Biol, 11*(7), 514-518.

Emperle, M., Rajavelu, A., Reinhardt, R., Jurkowska, R. Z., & Jeltsch, A. (2014). Cooperative DNA binding and protein/DNA fiber formation increases the activity of the Dnmt3a DNA methyltransferase. *J Biol Chem, 289*(43), 29602-29613. doi:10.1074/jbc.M114.572032

Esvelt, K. M., Mali, P., Braff, J. L., Moosburner, M., Yaung, S. J., & Church, G. M. (2013). Orthogonal Cas9 proteins for RNA-guided gene regulation and editing. *Nat Methods, 10*(11), 1116-1121. doi:10.1038/nmeth.2681

Fallahian, M., Sebire, N. J., Savage, P. M., Seckl, M. J., & Fisher, R. A. (2013). Mutations in NLRP7 and KHDC3L confer a complete hydatidiform mole phenotype on digynic triploid conceptions. *Hum Mutat, 34*(2), 301-308. doi:10.1002/humu.22228

Feil, R., & Berger, F. (2007). Convergent evolution of genomic imprinting in plants and mammals. *Trends Genet, 23*(4), 192-199. doi:10.1016/j.tig.2007.02.004

Feltus, F. A., Lee, E. K., Costello, J. F., Plass, C., & Vertino, P. M. (2003). Predicting aberrant CpG island methylation. *Proc Natl Acad Sci U S A, 100*(21), 12253-12258. doi:10.1073/pnas.2037852100

Fink, J. J., Robinson, T. M., Germain, N. D., Sirois, C. L., Bolduc, K. A., Ward, A. J., Rigo, F., Chamberlain, S. J., & Levine, E. S. (2017). Disrupted neuronal maturation in Angelman syndrome-derived induced pluripotent stem cells. *Nat Commun, 8*, 15038. doi:10.1038/ncomms15038

Fisher, C. L., & Fisher, A. G. (2011). Chromatin states in pluripotent, differentiated, and reprogrammed cells. *Curr Opin Genet Dev, 21*(2), 140-146. doi:10.1016/j.gde.2011.01.015

Fonfara, I., Le Rhun, A., Chylinski, K., Makarova, K. S., Lecrivain, A. L., Bzdrenga, J., Koonin, E. V., & Charpentier, E. (2014). Phylogeny of Cas9 determines functional exchangeability of dual-RNA and Cas9 among orthologous type II CRISPR-Cas systems. *Nucleic Acids Res, 42*(4), 2577-2590. doi:10.1093/nar/gkt1074

Fusaki, N., Ban, H., Nishiyama, A., Saeki, K., & Hasegawa, M. (2009). Efficient induction of transgene-free human pluripotent stem cells using a vector based on Sendai virus, an RNA virus that does not integrate into the host genome. *Proc Jpn Acad Ser B Phys Biol Sci, 85*(8), 348-362.

Gao, Y., Chen, J., Li, K., Wu, T., Huang, B., Liu, W., Kou, X., Zhang, Y., Huang, H., Jiang, Y., *et al.* (2013). Replacement of Oct4 by Tet1 during iPSC induction reveals an important role of DNA methylation and hydroxymethylation in reprogramming. *Cell Stem Cell, 12*(4), 453-469. doi:10.1016/j.stem.2013.02.005

Gardiner-Garden, M., & Frommer, M. (1987). CpG islands in vertebrate genomes. *J Mol Biol, 196*(2), 261-282.

Gasiunas, G., Barrangou, R., Horvath, P., & Siksnys, V. (2012). Cas9-crRNA ribonucleoprotein complex mediates specific DNA cleavage for adaptive immunity in bacteria. *Proc Natl Acad Sci U S A, 109*(39), E2579-2586. doi:10.1073/pnas.1208507109

Gasiunas, G., & Siksnys, V. (2013). RNA-dependent DNA endonuclease Cas9 of the CRISPR system: Holy Grail of genome editing? *Trends Microbiol, 21*(11), 562-567. doi:10.1016/j.tim.2013.09.001

Gaudet, F., Rideout, W. M., 3rd, Meissner, A., Dausman, J., Leonhardt, H., & Jaenisch, R. (2004). Dnmt1 expression in pre- and postimplantation embryogenesis and the maintenance of IAP silencing. *Mol Cell Biol, 24*(4), 1640-1648.

Gentile, J. K., Tan, W. H., Horowitz, L. T., Bacino, C. A., Skinner, S. A., Barbieri-Welge, R., Bauer-Carlin, A., Beaudet, A. L., Bichell, T. J., Lee, H. S., *et al.* (2010). A neurodevelopmental survey of Angelman syndrome with genotype-phenotype correlations. *J Dev Behav Pediatr, 31*(7), 592-601. doi:10.1097/DBP.0b013e3181ee408e

Gerrard, L., Zhao, D., Clark, A. J., & Cui, W. (2005). Stably transfected human embryonic stem cell clones express OCT4-specific green fluorescent protein and maintain self-renewal and pluripotency. *Stem Cells, 23*(1), 124-133. doi:10.1634/stemcells.2004-0102

Globisch, D., Munzel, M., Muller, M., Michalakis, S., Wagner, M., Koch, S., Bruckl, T., Biel, M., & Carell, T. (2010). Tissue distribution of 5-hydroxymethylcytosine and search for active demethylation intermediates. *PLoS One, 5*(12), e15367. doi:10.1371/journal.pone.0015367

Goll, M. G., & Bestor, T. H. (2005). Eukaryotic cytosine methyltransferases. *Annu Rev Biochem, 74*, 481-514. doi:10.1146/annurev.biochem.74.010904.153721

Gonzalez, F., Barragan Monasterio, M., Tiscornia, G., Montserrat Pulido, N., Vassena, R., Batlle Morera, L., Rodriguez Piza, I., & Izpisua Belmonte, J. C. (2009). Generation of mouse-induced pluripotent stem cells by transient expression of a single nonviral

polycistronic vector. *Proc Natl Acad Sci U S A, 106*(22), 8918-8922. doi:10.1073/pnas.0901471106

Greally, J. M., Gray, T. A., Gabriel, J. M., Song, L., Zemel, S., & Nicholls, R. D. (1999). Conserved characteristics of heterochromatin-forming DNA at the 15q11-q13 imprinting center. *Proc Natl Acad Sci U S A, 96*(25), 14430-14435.

Grieco, J. C., Ciarlone, S. L., Gieron-Korthals, M., Schoenberg, M. R., Smith, A. G., Philpot, R. M., Heussler, H. S., Banko, J. L., & Weeber, E. J. (2014). An open-label pilot trial of minocycline in children as a treatment for Angelman syndrome. *BMC Neurol, 14*, 232. doi:10.1186/s12883-014-0232-x

Grissa, I., Vergnaud, G., & Pourcel, C. (2007). The CRISPRdb database and tools to display CRISPRs and to generate dictionaries of spacers and repeats. *BMC Bioinformatics, 8*, 172. doi:10.1186/1471-2105-8-172

Grybek, V., Aubry, L., Maupetit-Mehouas, S., Le Stunff, C., Denis, C., Girard, M., Linglart, A., & Silve, C. (2014). Methylation and transcripts expression at the imprinted GNAS locus in human embryonic and induced pluripotent stem cells and their derivatives. *Stem Cell Reports, 3*(3), 432-443. doi:10.1016/j.stemcr.2014.07.002

Gurdon, J. B. (1962). The developmental capacity of nuclei taken from intestinal epithelium cells of feeding tadpoles. *J Embryol Exp Morphol, 10*, 622-640.

Hahn, M. A., Qiu, R., Wu, X., Li, A. X., Zhang, H., Wang, J., Jui, J., Jin, S. G., Jiang, Y., Pfeifer, G. P., *et al.* (2013). Dynamics of 5-hydroxymethylcytosine and chromatin marks in Mammalian neurogenesis. *Cell Rep, 3*(2), 291-300. doi:10.1016/j.celrep.2013.01.011

Haig, D. (1997). Parental antagonism, relatedness asymmetries, and genomic imprinting. *Proc Biol Sci, 264*(1388), 1657-1662. doi:10.1098/rspb.1997.0230

Hajkova, P., Erhardt, S., Lane, N., Haaf, T., El-Maarri, O., Reik, W., Walter, J., & Surani, M. A. (2002). Epigenetic reprogramming in mouse primordial germ cells. *Mech Dev, 117*(1-2), 15-23.

Hale, C. R., Majumdar, S., Elmore, J., Pfister, N., Compton, M., Olson, S., Resch, A. M., Glover, C. V., 3rd, Graveley, B. R., Terns, R. M., *et al.* (2012). Essential features and rational design of CRISPR RNAs that function with the Cas RAMP module complex to cleave RNAs. *Mol Cell, 45*(3), 292-302. doi:10.1016/j.molcel.2011.10.023

Hale, C. R., Zhao, P., Olson, S., Duff, M. O., Graveley, B. R., Wells, L., Terns, R. M., & Terns, M. P. (2009). RNA-guided RNA cleavage by a CRISPR RNA-Cas protein complex. *Cell, 139*(5), 945-956. doi:10.1016/j.cell.2009.07.040

Hall, J. G. (1990). Genomic imprinting: review and relevance to human diseases. *Am J Hum Genet, 46*(5), 857-873.

Hanna, C. W., & Kelsey, G. (2014). The specification of imprints in mammals. *Heredity (Edinb), 113*(2), 176-183. doi:10.1038/hdy.2014.54

Hanna, J., Wernig, M., Markoulaki, S., Sun, C. W., Meissner, A., Cassady, J. P., Beard, C., Brambrink, T., Wu, L. C., Townes, T. M., *et al.* (2007). Treatment of sickle cell anemia mouse model with iPS cells generated from autologous skin. *Science, 318*(5858), 1920-1923. doi:10.1126/science.1152092

Hark, A. T., Schoenherr, C. J., Katz, D. J., Ingram, R. S., Levorse, J. M., & Tilghman, S. M. (2000). CTCF mediates methylation-sensitive enhancer-blocking activity at the H19/Igf2 locus. *Nature, 405*(6785), 486-489. doi:10.1038/35013106

Hata, K., Okano, M., Lei, H., & Li, E. (2002). Dnmt3L cooperates with the Dnmt3 family of de novo DNA methyltransferases to establish maternal imprints in mice. *Development, 129*(8), 1983-1993.

Haurwitz, R. E., Jinek, M., Wiedenheft, B., Zhou, K., & Doudna, J. A. (2010). Sequence- and structure-specific RNA processing by a CRISPR endonuclease. *Science, 329*(5997), 1355-1358. doi:10.1126/science.1192272

Henckel, A., Chebli, K., Kota, S. K., Arnaud, P., & Feil, R. (2012). Transcription and histone methylation changes correlate with imprint acquisition in male germ cells. *EMBO J, 31*(3), 606-615. doi:10.1038/emboj.2011.425

Henderson, J. K., Draper, J. S., Baillie, H. S., Fishel, S., Thomson, J. A., Moore, H., & Andrews, P. W. (2002). Preimplantation human embryos and embryonic stem cells show comparable expression of stage-specific embryonic antigens. *Stem Cells, 20*(4), 329-337. doi:10.1634/stemcells.20-4-329

Hilton, I. B., D'Ippolito, A. M., Vockley, C. M., Thakore, P. I., Crawford, G. E., Reddy, T. E., & Gersbach, C. A. (2015). Epigenome editing by a CRISPR-Cas9-based acetyltransferase activates genes from promoters and enhancers. *Nat Biotechnol, 33*(5), 510-517. doi:10.1038/nbt.3199

Hoffman, A. R., & Hu, J. F. (2006). Directing DNA methylation to inhibit gene expression. *Cell Mol Neurobiol, 26*(4-6), 425-438. doi:10.1007/s10571-006-9057-5

Hohenstein, K. A., Pyle, A. D., Chern, J. Y., Lock, L. F., & Donovan, P. J. (2008). Nucleofection mediates high-efficiency stable gene knockdown and transgene expression in human embryonic stem cells. *Stem Cells, 26*(6), 1436-1443. doi:10.1634/stemcells.2007-0857

Hochedlinger, K., & Plath, K. (2009). Epigenetic reprogramming and induced pluripotency. *Development, 136*(4), 509-523. doi:10.1242/dev.020867

Horsthemke, B. (2010). Mechanisms of imprint dysregulation. *Am J Med Genet C Semin Med Genet, 154C*(3), 321-328. doi:10.1002/ajmg.c.30269

Horsthemke, B. (2014). In brief: genomic imprinting and imprinting diseases. *J Pathol, 232*(5), 485-487. doi:10.1002/path.4326

Horsthemke, B., & Wagstaff, J. (2008). Mechanisms of imprinting of the Prader-Willi/Angelman region. *Am J Med Genet A, 146A*(16), 2041-2052. doi:10.1002/ajmg.a.32364

Horsthemke, B., Wawrzik, M., Gross, S., Lich, C., Sauer, B., Rost, I., Krasemann, E., Kosyakova, N., Liehr, T., Weise, A., *et al.* (2011). Parental origin and functional relevance of a de novo UBE3A variant. *Eur J Med Genet, 54*(1), 19-24. doi:10.1016/j.ejmg.2010.09.005

Howell, C. Y., Bestor, T. H., Ding, F., Latham, K. E., Mertineit, C., Trasler, J. M., & Chaillet, J. R. (2001). Genomic imprinting disrupted by a maternal effect mutation in the Dnmt1 gene. *Cell, 104*(6), 829-838.

Hsiao, S. H., Lee, K. D., Hsu, C. C., Tseng, M. J., Jin, V. X., Sun, W. S., Hung, Y. C., Yeh, K. T., Yan, P. S., Lai, Y. Y., *et al.* (2010). DNA methylation of the Trip10 promoter accelerates mesenchymal stem cell lineage determination. *Biochem Biophys Res Commun, 400*(3), 305-312. doi:10.1016/j.bbrc.2010.08.048

Hsu, C. C., Leu, Y. W., Tseng, M. J., Lee, K. D., Kuo, T. Y., Yen, J. Y., Lai, Y. L., Hung, Y. C., Sun, W. S., Chen, C. M., *et al.* (2011). Functional characterization of Trip10 in cancer cell growth and survival. *J Biomed Sci, 18*, 12. doi:10.1186/1423-0127-18-12

Huangfu, D., Maehr, R., Guo, W., Eijkelenboom, A., Snitow, M., Chen, A. E., & Melton, D. A. (2008a). Induction of pluripotent stem cells by defined factors is greatly improved by small-molecule compounds. *Nat Biotechnol, 26*(7), 795-797. doi:10.1038/nbt1418

Huangfu, D., Osafune, K., Maehr, R., Guo, W., Eijkelenboom, A., Chen, S., Muhlestein, W., & Melton, D. A. (2008b). Induction of pluripotent stem cells from primary human

fibroblasts with only Oct4 and Sox2. *Nat Biotechnol, 26*(11), 1269-1275. doi:10.1038/nbt.1502

Chamberlain, S. J., & Brannan, C. I. (2001). The Prader-Willi syndrome imprinting center activates the paternally expressed murine Ube3a antisense transcript but represses paternal Ube3a. *Genomics, 73*(3), 316-322. doi:10.1006/geno.2001.6543

Chamberlain, S. J., Chen, P. F., Ng, K. Y., Bourgois-Rocha, F., Lemtiri-Chlieh, F., Levine, E. S., & Lalande, M. (2010). Induced pluripotent stem cell models of the genomic imprinting disorders Angelman and Prader-Willi syndromes. *Proc Natl Acad Sci U S A, 107*(41), 17668-17673. doi:10.1073/pnas.1004487107

Chamberlain, S. J., & Lalande, M. (2010). Angelman syndrome, a genomic imprinting disorder of the brain. *J Neurosci, 30*(30), 9958-9963. doi:10.1523/JNEUROSCI.1728-10.2010

Chambers, S. M., Fasano, C. A., Papapetrou, E. P., Tomishima, M., Sadelain, M., & Studer, L. (2009). Highly efficient neural conversion of human ES and iPS cells by dual inhibition of SMAD signaling. *Nat Biotechnol, 27*(3), 275-280. doi:10.1038/nbt.1529

Chan, E. M., Ratanasirintrawoot, S., Park, I. H., Manos, P. D., Loh, Y. H., Huo, H., Miller, J. D., Hartung, O., Rho, J., Ince, T. A., *et al.* (2009). Live cell imaging distinguishes bona fide human iPS cells from partially reprogrammed cells. *Nat Biotechnol, 27*(11), 1033-1037. doi:10.1038/nbt.1580

Chao, W., & D'Amore, P. A. (2008). IGF2: epigenetic regulation and role in development and disease. *Cytokine Growth Factor Rev, 19*(2), 111-120. doi:10.1016/j.cytogfr.2008.01.005

Chen, J., Liu, H., Liu, J., Qi, J., Wei, B., Yang, J., Liang, H., Chen, Y., Chen, J., Wu, Y., *et al.* (2013). H3K9 methylation is a barrier during somatic cell reprogramming into iPSCs. *Nat Genet, 45*(1), 34-42. doi:10.1038/ng.2491

Cheng, A. W., Wang, H., Yang, H., Shi, L., Katz, Y., Theunissen, T. W., Rangarajan, S., Shivalila, C. S., Dadon, D. B., & Jaenisch, R. (2013). Multiplexed activation of endogenous genes by CRISPR-on, an RNA-guided transcriptional activator system. *Cell Res, 23*(10), 1163-1171. doi:10.1038/cr.2013.122

Chesne, P., Adenot, P. G., Viglietta, C., Baratte, M., Boulanger, L., & Renard, J. P. (2002). Cloned rabbits produced by nuclear transfer from adult somatic cells. *Nat Biotechnol, 20*(4), 366-369. doi:10.1038/nbt0402-366

Chester, N., & Marshak, D. R. (1993). Dimethyl sulfoxide-mediated primer Tm reduction: a method for analyzing the role of renaturation temperature in the polymerase chain reaction. *Anal Biochem, 209*(2), 284-290. doi:10.1006/abio.1993.1121

Chotalia, M., Smallwood, S. A., Ruf, N., Dawson, C., Lucifero, D., Frontera, M., James, K., Dean, W., & Kelsey, G. (2009). Transcription is required for establishment of germline methylation marks at imprinted genes. *Genes Dev, 23*(1), 105-117. doi:10.1101/gad.495809

Ideraabdullah, F. Y., Vigneau, S., & Bartolomei, M. S. (2008). Genomic imprinting mechanisms in mammals. *Mutat Res, 647*(1-2), 77-85. doi:10.1016/j.mrfmmm.2008.08.008

International Stem Cell, I., Adewumi, O., Aflatoonian, B., Ahrlund-Richter, L., Amit, M., Andrews, P. W., Beighton, G., Bello, P. A., Benvenisty, N., Berry, L. S., *et al.* (2007). Characterization of human embryonic stem cell lines by the International Stem Cell Initiative. *Nat Biotechnol, 25*(7), 803-816. doi:10.1038/nbt1318

Itskovitz-Eldor, J., Schuldiner, M., Karsenti, D., Eden, A., Yanuka, O., Amit, M., Soreq, H., & Benvenisty, N. (2000). Differentiation of human embryonic stem cells into

embryoid bodies compromising the three embryonic germ layers. *Mol Med, 6*(2), 88-95.

Jaenisch, R., & Young, R. (2008). Stem cells, the molecular circuitry of pluripotency and nuclear reprogramming. *Cell, 132*(4), 567-582. doi:10.1016/j.cell.2008.01.015

Jansen, R., Embden, J. D., Gaastra, W., & Schouls, L. M. (2002). Identification of genes that are associated with DNA repeats in prokaryotes. *Mol Microbiol, 43*(6), 1565-1575.

Jia, F., Wilson, K. D., Sun, N., Gupta, D. M., Huang, M., Li, Z., Panetta, N. J., Chen, Z. Y., Robbins, R. C., Kay, M. A., *et al.* (2010). A nonviral minicircle vector for deriving human iPS cells. *Nat Methods, 7*(3), 197-199. doi:10.1038/nmeth.1426

Jinek, M., East, A., Cheng, A., Lin, S., Ma, E., & Doudna, J. (2013). RNA-programmed genome editing in human cells. *Elife, 2*, e00471. doi:10.7554/eLife.00471

Jinek, M., Chylinski, K., Fonfara, I., Hauer, M., Doudna, J. A., & Charpentier, E. (2012). A programmable dual-RNA-guided DNA endonuclease in adaptive bacterial immunity. *Science, 337*(6096), 816-821. doi:10.1126/science.1225829

Johannesson, B., Sagi, I., Gore, A., Paull, D., Yamada, M., Golan-Lev, T., Li, Z., LeDuc, C., Shen, Y., Stern, S., *et al.* (2014). Comparable frequencies of coding mutations and loss of imprinting in human pluripotent cells derived by nuclear transfer and defined factors. *Cell Stem Cell, 15*(5), 634-642. doi:10.1016/j.stem.2014.10.002

Judson, M. C., Sosa-Pagan, J. O., Del Cid, W. A., Han, J. E., & Philpot, B. D. (2014). Allelic specificity of Ube3a expression in the mouse brain during postnatal development. *J Comp Neurol, 522*(8), 1874-1896. doi:10.1002/cne.23507

Jurkowska, R. Z., Anspach, N., Urbanke, C., Jia, D., Reinhardt, R., Nellen, W., Cheng, X., & Jeltsch, A. (2008). Formation of nucleoprotein filaments by mammalian DNA methyltransferase Dnmt3a in complex with regulator Dnmt3L. *Nucleic Acids Res, 36*(21), 6656-6663. doi:10.1093/nar/gkn747

Kaji, K., Norrby, K., Paca, A., Mileikovsky, M., Mohseni, P., & Woltjen, K. (2009). Virus-free induction of pluripotency and subsequent excision of reprogramming factors. *Nature, 458*(7239), 771-775. doi:10.1038/nature07864

Kaneda, M., Okano, M., Hata, K., Sado, T., Tsujimoto, N., Li, E., & Sasaki, H. (2004). Essential role for de novo DNA methyltransferase Dnmt3a in paternal and maternal imprinting. *Nature, 429*(6994), 900-903. doi:10.1038/nature02633

Kearns, N. A., Pham, H., Tabak, B., Genga, R. M., Silverstein, N. J., Garber, M., & Maehr, R. (2015). Functional annotation of native enhancers with a Cas9-histone demethylase fusion. *Nat Methods, 12*(5), 401-403. doi:10.1038/nmeth.3325

Kelsey, G., & Feil, R. (2013). New insights into establishment and maintenance of DNA methylation imprints in mammals. *Philos Trans R Soc Lond B Biol Sci, 368*(1609), 20110336. doi:10.1098/rstb.2011.0336

Kim, D., Kim, C. H., Moon, J. I., Chung, Y. G., Chang, M. Y., Han, B. S., Ko, S., Yang, E., Cha, K. Y., Lanza, R., *et al.* (2009). Generation of human induced pluripotent stem cells by direct delivery of reprogramming proteins. *Cell Stem Cell, 4*(6), 472-476. doi:10.1016/j.stem.2009.05.005

Kim, J. S., Choi, H. W., Choi, S., Seo, H. G., Moon, S. H., Chung, H. M., & Do, J. T. (2014). Conversion of partially reprogrammed cells to fully pluripotent stem cells is associated with further activation of stem cell maintenance- and gamete generation-related genes. *Stem Cells Dev, 23*(21), 2637-2648. doi:10.1089/scd.2014.0020

Kim, K., Doi, A., Wen, B., Ng, K., Zhao, R., Cahan, P., Kim, J., Aryee, M. J., Ji, H., Ehrlich, L. I., *et al.* (2010). Epigenetic memory in induced pluripotent stem cells. *Nature, 467*(7313), 285-290. doi:10.1038/nature09342

Kishino, T., Lalande, M., & Wagstaff, J. (1997). UBE3A/E6-AP mutations cause Angelman syndrome. *Nat Genet, 15*(1), 70-73. doi:10.1038/ng0197-70

Kleinstiver, B. P., Pattanayak, V., Prew, M. S., Tsai, S. Q., Nguyen, N. T., Zheng, Z., & Joung, J. K. (2016). High-fidelity CRISPR-Cas9 nucleases with no detectable genome-wide off-target effects. *Nature, 529*(7587), 490-495. doi:10.1038/nature16526

Knoll, J. H., Nicholls, R. D., Magenis, R. E., Graham, J. M., Jr., Lalande, M., & Latt, S. A. (1989). Angelman and Prader-Willi syndromes share a common chromosome 15 deletion but differ in parental origin of the deletion. *Am J Med Genet, 32*(2), 285-290. doi:10.1002/ajmg.1320320235

Kobayashi, H., Sakurai, T., Imai, M., Takahashi, N., Fukuda, A., Yayoi, O., Sato, S., Nakabayashi, K., Hata, K., Sotomaru, Y., *et al.* (2012). Contribution of intragenic DNA methylation in mouse gametic DNA methylomes to establish oocyte-specific heritable marks. *PLoS Genet, 8*(1), e1002440. doi:10.1371/journal.pgen.1002440

Koch, P., Opitz, T., Steinbeck, J. A., Ladewig, J., & Brustle, O. (2009). A rosette-type, self-renewing human ES cell-derived neural stem cell with potential for in vitro instruction and synaptic integration. *Proc Natl Acad Sci U S A, 106*(9), 3225-3230. doi:10.1073/pnas.0808387106

Kriaucionis, S., & Heintz, N. (2009). The nuclear DNA base 5-hydroxymethylcytosine is present in Purkinje neurons and the brain. *Science, 324*(5929), 929-930. doi:10.1126/science.1169786

Kues, W. A., Herrmann, D., Barg-Kues, B., Haridoss, S., Nowak-Imialek, M., Buchholz, T., Streeck, M., Grebe, A., Grabundzija, I., Merkert, S., *et al.* (2013). Derivation and characterization of sleeping beauty transposon-mediated porcine induced pluripotent stem cells. *Stem Cells Dev, 22*(1), 124-135. doi:10.1089/scd.2012.0382

Kunin, V., Sorek, R., & Hugenholtz, P. (2007). Evolutionary conservation of sequence and secondary structures in CRISPR repeats. *Genome Biol, 8*(4), R61. doi:10.1186/gb-2007-8-4-r61

Kurihara, Y., Kawamura, Y., Uchijima, Y., Amamo, T., Kobayashi, H., Asano, T., & Kurihara, H. (2008). Maintenance of genomic methylation patterns during preimplantation development requires the somatic form of DNA methyltransferase 1. *Dev Biol, 313*(1), 335-346. doi:10.1016/j.ydbio.2007.10.033

Landers, M., Bancescu, D. L., Le Meur, E., Rougeulle, C., Glatt-Deeley, H., Brannan, C., Muscatelli, F., & Lalande, M. (2004). Regulation of the large (approximately 1000 kb) imprinted murine Ube3a antisense transcript by alternative exons upstream of Snurf/Snrpn. *Nucleic Acids Res, 32*(11), 3480-3492. doi:10.1093/nar/gkh670

Latos, P. A., Pauler, F. M., Koerner, M. V., Senergin, H. B., Hudson, Q. J., Stocsits, R. R., Allhoff, W., Stricker, S. H., Klement, R. M., Warczok, K. E., *et al.* (2012). Airn transcriptional overlap, but not its lncRNA products, induces imprinted Igf2r silencing. *Science, 338*(6113), 1469-1472. doi:10.1126/science.1228110

Lee, J., Inoue, K., Ono, R., Ogonuki, N., Kohda, T., Kaneko-Ishino, T., Ogura, A., & Ishino, F. (2002). Erasing genomic imprinting memory in mouse clone embryos produced from day 11.5 primordial germ cells. *Development, 129*(8), 1807-1817.

Leonhardt, H., Page, A. W., Weier, H. U., & Bestor, T. H. (1992). A targeting sequence directs DNA methyltransferase to sites of DNA replication in mammalian nuclei. *Cell, 71*(5), 865-873.

Lewis, M. W., Brant, J. O., Kramer, J. M., Moss, J. I., Yang, T. P., Hansen, P. J., Williams, R. S., & Resnick, J. L. (2015). Angelman syndrome imprinting center encodes a transcriptional promoter. *Proc Natl Acad Sci U S A, 112*(22), 6871-6875. doi:10.1073/pnas.1411261111

Li, E., Beard, C., & Jaenisch, R. (1993). Role for DNA methylation in genomic imprinting. *Nature, 366*(6453), 362-365. doi:10.1038/366362a0

Li, E., Bestor, T. H., & Jaenisch, R. (1992). Targeted mutation of the DNA methyltransferase gene results in embryonic lethality. *Cell, 69*(6), 915-926.

Li, F., Papworth, M., Minczuk, M., Rohde, C., Zhang, Y., Ragozin, S., & Jeltsch, A. (2007). Chimeric DNA methyltransferases target DNA methylation to specific DNA sequences and repress expression of target genes. *Nucleic Acids Res, 35*(1), 100-112. doi:10.1093/nar/gkl1035

Li, L., Zheng, P., & Dean, J. (2010). Maternal control of early mouse development. *Development, 137*(6), 859-870. doi:10.1242/dev.039487

Li, X., Ito, M., Zhou, F., Youngson, N., Zuo, X., Leder, P., & Ferguson-Smith, A. C. (2008). A maternal-zygotic effect gene, Zfp57, maintains both maternal and paternal imprints. *Dev Cell, 15*(4), 547-557. doi:10.1016/j.devcel.2008.08.014

Li, Y., McClintick, J., Zhong, L., Edenberg, H. J., Yoder, M. C., & Chan, R. J. (2005). Murine embryonic stem cell differentiation is promoted by SOCS-3 and inhibited by the zinc finger transcription factor Klf4. *Blood, 105*(2), 635-637. doi:10.1182/blood-2004-07-2681

Lillestol, R. K., Redder, P., Garrett, R. A., & Brugger, K. (2006). A putative viral defence mechanism in archaeal cells. *Archaea, 2*(1), 59-72.

Lintner, N. G., Kerou, M., Brumfield, S. K., Graham, S., Liu, H., Naismith, J. H., Sdano, M., Peng, N., She, Q., Copie, V., *et al.* (2011). Structural and functional characterization of an archaeal clustered regularly interspaced short palindromic repeat (CRISPR)-associated complex for antiviral defense (CASCADE). *J Biol Chem, 286*(24), 21643-21656. doi:10.1074/jbc.M111.238485

Lister, R., Mukamel, E. A., Nery, J. R., Urich, M., Puddifoot, C. A., Johnson, N. D., Lucero, J., Huang, Y., Dwork, A. J., Schultz, M. D., *et al.* (2013). Global epigenomic reconfiguration during mammalian brain development. *Science, 341*(6146), 1237905. doi:10.1126/science.1237905

Lister, R., Pelizzola, M., Dowen, R. H., Hawkins, R. D., Hon, G., Tonti-Filippini, J., Nery, J. R., Lee, L., Ye, Z., Ngo, Q. M., *et al.* (2009). Human DNA methylomes at base resolution show widespread epigenomic differences. *Nature, 462*(7271), 315-322. doi:10.1038/nature08514

Liu, Y. P., Dambaeva, S. V., Dovzhenko, O. V., Garthwaite, M. A., & Golos, T. G. (2005). Stable plasmid-based siRNA silencing of gene expression in human embryonic stem cells. *Stem Cells Dev, 14*(5), 487-492. doi:10.1089/scd.2005.14.487

Loh, Y. H., Wu, Q., Chew, J. L., Vega, V. B., Zhang, W., Chen, X., Bourque, G., George, J., Leong, B., Liu, J., *et al.* (2006). The Oct4 and Nanog transcription network regulates pluripotency in mouse embryonic stem cells. *Nat Genet, 38*(4), 431-440. doi:10.1038/ng1760

Lossie, A. C., Whitney, M. M., Amidon, D., Dong, H. J., Chen, P., Theriaque, D., Hutson, A., Nicholls, R. D., Zori, R. T., Williams, C. A., *et al.* (2001). Distinct phenotypes distinguish the molecular classes of Angelman syndrome. *J Med Genet, 38*(12), 834-845.

Lucifero, D., Mann, M. R., Bartolomei, M. S., & Trasler, J. M. (2004). Gene-specific timing and epigenetic memory in oocyte imprinting. *Hum Mol Genet, 13*(8), 839-849. doi:10.1093/hmg/ddh104

Lyko, F., Ramsahoye, B. H., Kashevsky, H., Tudor, M., Mastrangelo, M. A., Orr-Weaver, T. L., & Jaenisch, R. (1999). Mammalian (cytosine-5) methyltransferases cause genomic

DNA methylation and lethality in Drosophila. *Nat Genet, 23*(3), 363-366. doi:10.1038/15551

Ma, A. N., Huang, W. L., Wu, Z. N., Hu, J. F., Li, T., Zhou, X. J., & Wang, Y. X. (2010). Induced epigenetic modifications of the promoter chromatin silence survivin and inhibit tumor growth. *Biochem Biophys Res Commun, 393*(4), 592-597. doi:10.1016/j.bbrc.2010.02.020

Ma, A. N., Wang, H., Guo, R., Wang, Y. X., Li, W., Cui, J., Wang, G., Hoffman, A. R., & Hu, J. F. (2014a). Targeted gene suppression by inducing de novo DNA methylation in the gene promoter. *Epigenetics Chromatin, 7*, 20. doi:10.1186/1756-8935-7-20

Ma, H., Morey, R., O'Neil, R. C., He, Y., Daughtry, B., Schultz, M. D., Hariharan, M., Nery, J. R., Castanon, R., Sabatini, K., *et al.* (2014b). Abnormalities in human pluripotent cells due to reprogramming mechanisms. *Nature, 511*(7508), 177-183. doi:10.1038/nature13551

MacDonald, W. A., & Mann, M. R. (2014). Epigenetic regulation of genomic imprinting from germ line to preimplantation. *Mol Reprod Dev, 81*(2), 126-140. doi:10.1002/mrd.22220

Makarova, K. S., Haft, D. H., Barrangou, R., Brouns, S. J., Charpentier, E., Horvath, P., Moineau, S., Mojica, F. J., Wolf, Y. I., Yakunin, A. F., *et al.* (2011). Evolution and classification of the CRISPR-Cas systems. *Nat Rev Microbiol, 9*(6), 467-477. doi:10.1038/nrmicro2577

Malcolm, S., Clayton-Smith, J., Nichols, M., Robb, S., Webb, T., Armour, J. A., Jeffreys, A. J., & Pembrey, M. E. (1991). Uniparental paternal disomy in Angelman's syndrome. *Lancet, 337*(8743), 694-697.

Mali, P., Yang, L., Esvelt, K. M., Aach, J., Guell, M., DiCarlo, J. E., Norville, J. E., & Church, G. M. (2013). RNA-guided human genome engineering via Cas9. *Science, 339*(6121), 823-826. doi:10.1126/science.1232033

Margolis, S. S., Sell, G. L., Zbinden, M. A., & Bird, L. M. (2015). Angelman Syndrome. *Neurotherapeutics, 12*(3), 641-650. doi:10.1007/s13311-015-0361-y

Markman, M. (2005). Topotecan as second-line therapy for ovarian cancer: dosage versus toxicity. *Oncologist, 10*(9), 695-697. doi:10.1634/theoncologist.10-9-695

Martinez-Noel, G., Galligan, J. T., Sowa, M. E., Arndt, V., Overton, T. M., Harper, J. W., & Howley, P. M. (2012). Identification and proteomic analysis of distinct UBE3A/E6AP protein complexes. *Mol Cell Biol, 32*(15), 3095-3106. doi:10.1128/MCB.00201-12

Martins-Taylor, K., Hsiao, J. S., Chen, P. F., Glatt-Deeley, H., De Smith, A. J., Blakemore, A. I., Lalande, M., & Chamberlain, S. J. (2014). Imprinted expression of UBE3A in non-neuronal cells from a Prader-Willi syndrome patient with an atypical deletion. *Hum Mol Genet, 23*(9), 2364-2373. doi:10.1093/hmg/ddt628

Matsuura, T., Sutcliffe, J. S., Fang, P., Galjaard, R. J., Jiang, Y. H., Benton, C. S., Rommens, J. M., & Beaudet, A. L. (1997). De novo truncating mutations in E6-AP ubiquitin-protein ligase gene (UBE3A) in Angelman syndrome. *Nat Genet, 15*(1), 74-77. doi:10.1038/ng0197-74

Mauceri, L., Sorge, G., Incorpora, G., & Pavone, L. (2000). Pallister-Killian syndrome: case report with pineal tumor. *Am J Med Genet, 95*(1), 75-78.

Mayshar, Y., Ben-David, U., Lavon, N., Biancotti, J. C., Yakir, B., Clark, A. T., Plath, K., Lowry, W. E., & Benvenisty, N. (2010). Identification and classification of chromosomal aberrations in human induced pluripotent stem cells. *Cell Stem Cell, 7*(4), 521-531. doi:10.1016/j.stem.2010.07.017

McDonald, J. I., Celik, H., Rois, L. E., Fishberger, G., Fowler, T., Rees, R., Kramer, A., Martens, A., Edwards, J. R., & Challen, G. A. (2016). Reprogrammable

CRISPR/Cas9-based system for inducing site-specific DNA methylation. *Biol Open, 5*(6), 866-874. doi:10.1242/bio.019067

McGrath, J., & Solter, D. (1984). Completion of mouse embryogenesis requires both the maternal and paternal genomes. *Cell, 37*(1), 179-183.

McLean, A. B., D'Amour, K. A., Jones, K. L., Krishnamoorthy, M., Kulik, M. J., Reynolds, D. M., Sheppard, A. M., Liu, H., Xu, Y., Baetge, E. E., *et al.* (2007). Activin a efficiently specifies definitive endoderm from human embryonic stem cells only when phosphatidylinositol 3-kinase signaling is suppressed. *Stem Cells, 25*(1), 29-38. doi:10.1634/stemcells.2006-0219

Meng, L., Person, R. E., & Beaudet, A. L. (2012). Ube3a-ATS is an atypical RNA polymerase II transcript that represses the paternal expression of Ube3a. *Hum Mol Genet, 21*(13), 3001-3012. doi:10.1093/hmg/dds130

Meng, L., Person, R. E., Huang, W., Zhu, P. J., Costa-Mattioli, M., & Beaudet, A. L. (2013). Truncation of Ube3a-ATS unsilences paternal Ube3a and ameliorates behavioral defects in the Angelman syndrome mouse model. *PLoS Genet, 9*(12), e1004039. doi:10.1371/journal.pgen.1004039

Meng, L., Ward, A. J., Chun, S., Bennett, C. F., Beaudet, A. L., & Rigo, F. (2015). Towards a therapy for Angelman syndrome by targeting a long non-coding RNA. *Nature, 518*(7539), 409-412. doi:10.1038/nature13975

Mertz, L. G., Thaulov, P., Trillingsgaard, A., Christensen, R., Vogel, I., Hertz, J. M., & Ostergaard, J. R. (2014). Neurodevelopmental outcome in Angelman syndrome: genotype-phenotype correlations. *Res Dev Disabil, 35*(7), 1742-1747. doi:10.1016/j.ridd.2014.02.018

Messerschmidt, D. M. (2012). Should I stay or should I go: protection and maintenance of DNA methylation at imprinted genes. *Epigenetics, 7*(9), 969-975. doi:10.4161/epi.21337

Mikkelsen, T. S., Hanna, J., Zhang, X., Ku, M., Wernig, M., Schorderet, P., Bernstein, B. E., Jaenisch, R., Lander, E. S., & Meissner, A. (2008). Dissecting direct reprogramming through integrative genomic analysis. *Nature, 454*(7200), 49-55. doi:10.1038/nature07056

Mitalipova, M. M., Rao, R. R., Hoyer, D. M., Johnson, J. A., Meisner, L. F., Jones, K. L., Dalton, S., & Stice, S. L. (2005). Preserving the genetic integrity of human embryonic stem cells. *Nat Biotechnol, 23*(1), 19-20. doi:10.1038/nbt0105-19

Monk, M., Boubelik, M., & Lehnert, S. (1987). Temporal and regional changes in DNA methylation in the embryonic, extraembryonic and germ cell lineages during mouse embryo development. *Development, 99*(3), 371-382.

Montserrat, N., Garreta, E., Gonzalez, F., Gutierrez, J., Eguizabal, C., Ramos, V., Borros, S., & Izpisua Belmonte, J. C. (2011). Simple generation of human induced pluripotent stem cells using poly-beta-amino esters as the non-viral gene delivery system. *J Biol Chem, 286*(14), 12417-12428. doi:10.1074/jbc.M110.168013

Moore, T., & Haig, D. (1991). Genomic imprinting in mammalian development: a parental tug-of-war. *Trends Genet, 7*(2), 45-49. doi:10.1016/0168-9525(91)90230-N

Muenthaisong, S., Ujhelly, O., Polgar, Z., Varga, E., Ivics, Z., Pirity, M. K., & Dinnyes, A. (2012). Generation of mouse induced pluripotent stem cells from different genetic backgrounds using Sleeping beauty transposon mediated gene transfer. *Exp Cell Res, 318*(19), 2482-2489. doi:10.1016/j.yexcr.2012.07.014

Nakagawa, M., Koyanagi, M., Tanabe, K., Takahashi, K., Ichisaka, T., Aoi, T., Okita, K., Mochiduki, Y., Takizawa, N., & Yamanaka, S. (2008). Generation of induced

pluripotent stem cells without Myc from mouse and human fibroblasts. *Nat Biotechnol, 26*(1), 101-106. doi:10.1038/nbt1374

Nakamura, T., Arai, Y., Umehara, H., Masuhara, M., Kimura, T., Taniguchi, H., Sekimoto, T., Ikawa, M., Yoneda, Y., Okabe, M., *et al.* (2007). PGC7/Stella protects against DNA demethylation in early embryogenesis. *Nat Cell Biol, 9*(1), 64-71. doi:10.1038/ncb1519

Nazor, K. L., Altun, G., Lynch, C., Tran, H., Harness, J. V., Slavin, I., Garitaonandia, I., Muller, F. J., Wang, Y. C., Boscolo, F. S., *et al.* (2012). Recurrent variations in DNA methylation in human pluripotent stem cells and their differentiated derivatives. *Cell Stem Cell, 10*(5), 620-634. doi:10.1016/j.stem.2012.02.013

Nicholls, R. D., & Knepper, J. L. (2001). Genome organization, function, and imprinting in Prader-Willi and Angelman syndromes. *Annu Rev Genomics Hum Genet, 2*, 153-175. doi:10.1146/annurev.genom.2.1.153

Nishino, K., Toyoda, M., Yamazaki-Inoue, M., Fukawatase, Y., Chikazawa, E., Sakaguchi, H., Akutsu, H., & Umezawa, A. (2011). DNA methylation dynamics in human induced pluripotent stem cells over time. *PLoS Genet, 7*(5), e1002085. doi:10.1371/journal.pgen.1002085

Nordin, M., Bergman, D., Halje, M., Engstrom, W., & Ward, A. (2014). Epigenetic regulation of the Igf2/H19 gene cluster. *Cell Prolif, 47*(3), 189-199. doi:10.1111/cpr.12106

Numata, K., Kohama, C., Abe, K., & Kiyosawa, H. (2011). Highly parallel SNP genotyping reveals high-resolution landscape of mono-allelic Ube3a expression associated with locus-wide antisense transcription. *Nucleic Acids Res, 39*(7), 2649-2657. doi:10.1093/nar/gkq1201

Obata, Y., & Kono, T. (2002). Maternal primary imprinting is established at a specific time for each gene throughout oocyte growth. *J Biol Chem, 277*(7), 5285-5289. doi:10.1074/jbc.M108586200

Ohi, Y., Qin, H., Hong, C., Blouin, L., Polo, J. M., Guo, T., Qi, Z., Downey, S. L., Manos, P. D., Rossi, D. J., *et al.* (2011). Incomplete DNA methylation underlies a transcriptional memory of somatic cells in human iPS cells. *Nat Cell Biol, 13*(5), 541-549. doi:10.1038/ncb2239

Ohta, T., Buiting, K., Kokkonen, H., McCandless, S., Heeger, S., Leisti, H., Driscoll, D. J., Cassidy, S. B., Horsthemke, B., & Nicholls, R. D. (1999a). Molecular mechanism of angelman syndrome in two large families involves an imprinting mutation. *Am J Hum Genet, 64*(2), 385-396. doi:10.1086/302232

Ohta, T., Gray, T. A., Rogan, P. K., Buiting, K., Gabriel, J. M., Saitoh, S., Muralidhar, B., Bilienska, B., Krajewska-Walasek, M., Driscoll, D. J., *et al.* (1999b). Imprinting-mutation mechanisms in Prader-Willi syndrome. *Am J Hum Genet, 64*(2), 397-413. doi:10.1086/302233

Okamura, K., Ohno, M., & Tsutsui, T. (2011). Possible involvement of loss of imprinting in immortalization of human fibroblasts. *Int J Oncol, 38*(4), 903-910. doi:10.3892/ijo.2011.931

Okano, M., Bell, D. W., Haber, D. A., & Li, E. (1999). DNA methyltransferases Dnmt3a and Dnmt3b are essential for de novo methylation and mammalian development. *Cell, 99*(3), 247-257.

Okita, K., Ichisaka, T., & Yamanaka, S. (2007). Generation of germline-competent induced pluripotent stem cells. *Nature, 448*(7151), 313-317. doi:10.1038/nature05934

Onder, T. T., Kara, N., Cherry, A., Sinha, A. U., Zhu, N., Bernt, K. M., Cahan, P., Marcarci, B. O., Unternaehrer, J., Gupta, P. B., *et al.* (2012). Chromatin-modifying enzymes as modulators of reprogramming. *Nature, 483*(7391), 598-602. doi:10.1038/nature10953

Pastor, W. A., Pape, U. J., Huang, Y., Henderson, H. R., Lister, R., Ko, M., McLoughlin, E. M., Brudno, Y., Mahapatra, S., Kapranov, P., *et al.* (2011). Genome-wide mapping of 5-hydroxymethylcytosine in embryonic stem cells. *Nature, 473*(7347), 394-397. doi:10.1038/nature10102

Peat, J. R., Dean, W., Clark, S. J., Krueger, F., Smallwood, S. A., Ficz, G., Kim, J. K., Marioni, J. C., Hore, T. A., & Reik, W. (2014). Genome-wide bisulfite sequencing in zygotes identifies demethylation targets and maps the contribution of TET3 oxidation. *Cell Rep, 9*(6), 1990-2000. doi:10.1016/j.celrep.2014.11.034

Penson, R. T., & Seiden, M. V. (2005). Topotecan: weighing in when there are many options. *Oncologist, 10*(9), 698-700. doi:10.1634/theoncologist.10-9-698

Pera, M. F. (2004). Unnatural selection of cultured human ES cells? *Nat Biotechnol, 22*(1), 42-43. doi:10.1038/nbt0104-42

Peters, J. (2014). The role of genomic imprinting in biology and disease: an expanding view. *Nat Rev Genet, 15*(8), 517-530. doi:10.1038/nrg3766

Pick, M., Stelzer, Y., Bar-Nur, O., Mayshar, Y., Eden, A., & Benvenisty, N. (2009). Clone- and gene-specific aberrations of parental imprinting in human induced pluripotent stem cells. *Stem Cells, 27*(11), 2686-2690. doi:10.1002/stem.205

Polejaeva, I. A., Chen, S. H., Vaught, T. D., Page, R. L., Mullins, J., Ball, S., Dai, Y., Boone, J., Walker, S., Ayares, D. L., *et al.* (2000). Cloned pigs produced by nuclear transfer from adult somatic cells. *Nature, 407*(6800), 86-90. doi:10.1038/35024082

Prickett, A. R., & Oakey, R. J. (2012). A survey of tissue-specific genomic imprinting in mammals. *Mol Genet Genomics, 287*(8), 621-630. doi:10.1007/s00438-012-0708-6

Probst, A. V., & Almouzni, G. (2011). Heterochromatin establishment in the context of genome-wide epigenetic reprogramming. *Trends Genet, 27*(5), 177-185. doi:10.1016/j.tig.2011.02.002

Proudhon, C., Duffie, R., Ajjan, S., Cowley, M., Iranzo, J., Carbajosa, G., Saadeh, H., Holland, M. L., Oakey, R. J., Rakyan, V. K., *et al.* (2012). Protection against de novo methylation is instrumental in maintaining parent-of-origin methylation inherited from the gametes. *Mol Cell, 47*(6), 909-920. doi:10.1016/j.molcel.2012.07.010

Qi, L. S., Larson, M. H., Gilbert, L. A., Doudna, J. A., Weissman, J. S., Arkin, A. P., & Lim, W. A. (2013). Repurposing CRISPR as an RNA-guided platform for sequence-specific control of gene expression. *Cell, 152*(5), 1173-1183. doi:10.1016/j.cell.2013.02.022

Quenneville, S., Verde, G., Corsinotti, A., Kapopoulou, A., Jakobsson, J., Offner, S., Baglivo, I., Pedone, P. V., Grimaldi, G., Riccio, A., *et al.* (2011). In embryonic stem cells, ZFP57/KAP1 recognize a methylated hexanucleotide to affect chromatin and DNA methylation of imprinting control regions. *Mol Cell, 44*(3), 361-372. doi:10.1016/j.molcel.2011.08.032

Rahmann S., B. J., Kanber D., Martin M., Horsthemke B., Buiting K.. (2013). Amplikyzer: Automated methylation analysis of amplicons from bisulfite flowgram sequencing. . *PeerJ PrePrints, 1:e122v2*.

Rajavelu, A., Jurkowska, R. Z., Fritz, J., & Jeltsch, A. (2012). Function and disruption of DNA methyltransferase 3a cooperative DNA binding and nucleoprotein filament formation. *Nucleic Acids Res, 40*(2), 569-580. doi:10.1093/nar/gkr753

Ramos-Mejia, V., Montes, R., Bueno, C., Ayllon, V., Real, P. J., Rodriguez, R., & Menendez, P. (2012). Residual expression of the reprogramming factors prevents differentiation of iPSC generated from human fibroblasts and cord blood CD34+ progenitors. *PLoS One, 7*(4), e35824. doi:10.1371/journal.pone.0035824

Reik, W., & Walter, J. (2001). Evolution of imprinting mechanisms: the battle of the sexes begins in the zygote. *Nat Genet, 27*(3), 255-256. doi:10.1038/85804

Renfree, M. B., Suzuki, S., & Kaneko-Ishino, T. (2013). The origin and evolution of genomic imprinting and viviparity in mammals. *Philos Trans R Soc Lond B Biol Sci, 368*(1609), 20120151. doi:10.1098/rstb.2012.0151

Reubinoff, B. E., Pera, M. F., Fong, C. Y., Trounson, A., & Bongso, A. (2000). Embryonic stem cell lines from human blastocysts: somatic differentiation in vitro. *Nat Biotechnol, 18*(4), 399-404. doi:10.1038/74447

Rougeulle, C., Cardoso, C., Fontes, M., Colleaux, L., & Lalande, M. (1998). An imprinted antisense RNA overlaps UBE3A and a second maternally expressed transcript. *Nat Genet, 19*(1), 15-16. doi:10.1038/ng0598-15

Rougeulle, C., Glatt, H., & Lalande, M. (1997). The Angelman syndrome candidate gene, UBE3A/E6-AP, is imprinted in brain. *Nat Genet, 17*(1), 14-15. doi:10.1038/ng0997-14

Rousseau, C., Gonnet, M., Le Romancer, M., & Nicolas, J. (2009). CRISPI: a CRISPR interactive database. *Bioinformatics, 25*(24), 3317-3318. doi:10.1093/bioinformatics/btp586

Rugg-Gunn, P. J., Ferguson-Smith, A. C., & Pedersen, R. A. (2007). Status of genomic imprinting in human embryonic stem cells as revealed by a large cohort of independently derived and maintained lines. *Hum Mol Genet, 16 Spec No. 2*, R243-251. doi:10.1093/hmg/ddm245

Runte, M., Huttenhofer, A., Gross, S., Kiefmann, M., Horsthemke, B., & Buiting, K. (2001). The IC-SNURF-SNRPN transcript serves as a host for multiple small nucleolar RNA species and as an antisense RNA for UBE3A. *Hum Mol Genet, 10*(23), 2687-2700.

Runte, M., Kroisel, P. M., Gillessen-Kaesbach, G., Varon, R., Horn, D., Cohen, M. Y., Wagstaff, J., Horsthemke, B., & Buiting, K. (2004). SNURF-SNRPN and UBE3A transcript levels in patients with Angelman syndrome. *Hum Genet, 114*(6), 553-561. doi:10.1007/s00439-004-1104-z

Saferali, A., Grundberg, E., Berlivet, S., Beauchemin, H., Morcos, L., Polychronakos, C., Pastinen, T., Graham, J., McNeney, B., & Naumova, A. K. (2010). Cell culture-induced aberrant methylation of the imprinted IG DMR in human lymphoblastoid cell lines. *Epigenetics, 5*(1), 50-60.

Sahoo, T., Bacino, C. A., German, J. R., Shaw, C. A., Bird, L. M., Kimonis, V., Anselm, I., Waisbren, S., Beaudet, A. L., & Peters, S. U. (2007). Identification of novel deletions of 15q11q13 in Angelman syndrome by array-CGH: molecular characterization and genotype-phenotype correlations. *Eur J Hum Genet, 15*(9), 943-949. doi:10.1038/sj.ejhg.5201859

Sakatani, T., Kaneda, A., Iacobuzio-Donahue, C. A., Carter, M. G., de Boom Witzel, S., Okano, H., Ko, M. S., Ohlsson, R., Longo, D. L., & Feinberg, A. P. (2005). Loss of imprinting of Igf2 alters intestinal maturation and tumorigenesis in mice. *Science, 307*(5717), 1976-1978. doi:10.1126/science.1108080

Santos, F., Hendrich, B., Reik, W., & Dean, W. (2002). Dynamic reprogramming of DNA methylation in the early mouse embryo. *Dev Biol, 241*(1), 172-182. doi:10.1006/dbio.2001.0501

Sato, M., & Stryker, M. P. (2010). Genomic imprinting of experience-dependent cortical plasticity by the ubiquitin ligase gene Ube3a. *Proc Natl Acad Sci U S A, 107*(12), 5611-5616. doi:10.1073/pnas.1001281107

Scheffner, M., Huibregtse, J. M., Vierstra, R. D., & Howley, P. M. (1993). The HPV-16 E6 and E6-AP complex functions as a ubiquitin-protein ligase in the ubiquitination of p53. *Cell, 75*(3), 495-505.

Schultz, R. M. (2002). The molecular foundations of the maternal to zygotic transition in the preimplantation embryo. *Hum Reprod Update, 8*(4), 323-331.

Siddique, A. N., Nunna, S., Rajavelu, A., Zhang, Y., Jurkowska, R. Z., Reinhardt, R., Rots, M. G., Ragozin, S., Jurkowski, T. P., & Jeltsch, A. (2013). Targeted methylation and gene silencing of VEGF-A in human cells by using a designed Dnmt3a-Dnmt3L single-chain fusion protein with increased DNA methylation activity. *J Mol Biol, 425*(3), 479-491. doi:10.1016/j.jmb.2012.11.038

Siemen, H., Nolden, L., Terstegge, S., Koch, P., & Brustle, O. (2008). Nucleofection of human embryonic stem cells. *Methods Mol Biol, 423*, 131-138. doi:10.1007/978-1-59745-194-9_8

Silva, J., Barrandon, O., Nichols, J., Kawaguchi, J., Theunissen, T. W., & Smith, A. (2008). Promotion of reprogramming to ground state pluripotency by signal inhibition. *PLoS Biol, 6*(10), e253. doi:10.1371/journal.pbio.0060253

Singh, A. M., Bechard, M., Smith, K., & Dalton, S. (2012a). Reconciling the different roles of Gsk3beta in "naive" and "primed" pluripotent stem cells. *Cell Cycle, 11*(16), 2991-2996. doi:10.4161/cc.21110

Singh, A. M., Reynolds, D., Cliff, T., Ohtsuka, S., Mattheyses, A. L., Sun, Y., Menendez, L., Kulik, M., & Dalton, S. (2012b). Signaling network crosstalk in human pluripotent cells: a Smad2/3-regulated switch that controls the balance between self-renewal and differentiation. *Cell Stem Cell, 10*(3), 312-326. doi:10.1016/j.stem.2012.01.014

Slaymaker, I. M., Gao, L., Zetsche, B., Scott, D. A., Yan, W. X., & Zhang, F. (2016). Rationally engineered Cas9 nucleases with improved specificity. *Science, 351*(6268), 84-88. doi:10.1126/science.aad5227

Sleutels, F., Zwart, R., & Barlow, D. P. (2002). The non-coding Air RNA is required for silencing autosomal imprinted genes. *Nature, 415*(6873), 810-813. doi:10.1038/415810a

Smallwood, S. A., Lee, H. J., Angermueller, C., Krueger, F., Saadeh, H., Peat, J., Andrews, S. R., Stegle, O., Reik, W., & Kelsey, G. (2014). Single-cell genome-wide bisulfite sequencing for assessing epigenetic heterogeneity. *Nat Methods, 11*(8), 817-820. doi:10.1038/nmeth.3035

Sommer, C. A., Sommer, A. G., Longmire, T. A., Christodoulou, C., Thomas, D. D., Gostissa, M., Alt, F. W., Murphy, G. J., Kotton, D. N., & Mostoslavsky, G. (2010). Excision of reprogramming transgenes improves the differentiation potential of iPS cells generated with a single excisable vector. *Stem Cells, 28*(1), 64-74. doi:10.1002/stem.255

Stadtfeld, M., Apostolou, E., Ferrari, F., Choi, J., Walsh, R. M., Chen, T., Ooi, S. S., Kim, S. Y., Bestor, T. H., Shioda, T., *et al.* (2012). Ascorbic acid prevents loss of Dlk1-Dio3 imprinting and facilitates generation of all-iPS cell mice from terminally differentiated B cells. *Nat Genet, 44*(4), 398-405, S391-392. doi:10.1038/ng.1110

Stadtfeld, M., Nagaya, M., Utikal, J., Weir, G., & Hochedlinger, K. (2008). Induced pluripotent stem cells generated without viral integration. *Science, 322*(5903), 945-949. doi:10.1126/science.1162494

Stanurova, J., Neureiter, A., Hiber, M., de Oliveira Kessler, H., Stolp, K., Goetzke, R., Klein, D., Bankfalvi, A., Klump, H., & Steenpass, L. (2016). Angelman syndrome-derived neurons display late onset of paternal UBE3A silencing. *Sci Rep, 6*, 30792. doi:10.1038/srep30792

Stepper, P., Kungulovski, G., Jurkowska, R. Z., Chandra, T., Krueger, F., Reinhardt, R., Reik, W., Jeltsch, A., & Jurkowski, T. P. (2017). Efficient targeted DNA methylation with chimeric dCas9-Dnmt3a-Dnmt3L methyltransferase. *Nucleic Acids Res, 45*(4), 1703-1713. doi:10.1093/nar/gkw1112

Stolzenburg, S., Beltran, A. S., Swift-Scanlan, T., Rivenbark, A. G., Rashwan, R., & Blancafort, P. (2015). Stable oncogenic silencing in vivo by programmable and targeted de novo DNA methylation in breast cancer. *Oncogene, 34*(43), 5427-5435. doi:10.1038/onc.2014.470

Strickfaden, H., Zunhammer, A., van Koningsbruggen, S., Kohler, D., & Cremer, T. (2010). 4D chromatin dynamics in cycling cells: Theodor Boveri's hypotheses revisited. *Nucleus, 1*(3), 284-297. doi:10.4161/nucl.1.3.11969

Sumi, T., Tsuneyoshi, N., Nakatsuji, N., & Suemori, H. (2008). Defining early lineage specification of human embryonic stem cells by the orchestrated balance of canonical Wnt/beta-catenin, Activin/Nodal and BMP signaling. *Development, 135*(17), 2969-2979. doi:10.1242/dev.021121

Surani, M. A., Barton, S. C., & Norris, M. L. (1984). Development of reconstituted mouse eggs suggests imprinting of the genome during gametogenesis. *Nature, 308*(5959), 548-550.

Szwagierczak, A., Bultmann, S., Schmidt, C. S., Spada, F., & Leonhardt, H. (2010). Sensitive enzymatic quantification of 5-hydroxymethylcytosine in genomic DNA. *Nucleic Acids Res, 38*(19), e181. doi:10.1093/nar/gkq684

Tada, M., Takahama, Y., Abe, K., Nakatsuji, N., & Tada, T. (2001). Nuclear reprogramming of somatic cells by in vitro hybridization with ES cells. *Curr Biol, 11*(19), 1553-1558.

Tahiliani, M., Koh, K. P., Shen, Y., Pastor, W. A., Bandukwala, H., Brudno, Y., Agarwal, S., Iyer, L. M., Liu, D. R., Aravind, L., *et al.* (2009). Conversion of 5-methylcytosine to 5-hydroxymethylcytosine in mammalian DNA by MLL partner TET1. *Science, 324*(5929), 930-935. doi:10.1126/science.1170116

Takahashi, K., Tanabe, K., Ohnuki, M., Narita, M., Ichisaka, T., Tomoda, K., & Yamanaka, S. (2007). Induction of pluripotent stem cells from adult human fibroblasts by defined factors. *Cell, 131*(5), 861-872. doi:10.1016/j.cell.2007.11.019

Takahashi, K., & Yamanaka, S. (2006). Induction of pluripotent stem cells from mouse embryonic and adult fibroblast cultures by defined factors. *Cell, 126*(4), 663-676. doi:10.1016/j.cell.2006.07.024

Takahashi, Y., Wu, J., Suzuki, K., Martinez-Redondo, P., Li, M., Liao, H. K., Wu, M. Z., Hernandez-Benitez, R., Hishida, T., Shokhirev, M. N., *et al.* (2017). Integration of CpG-free DNA induces de novo methylation of CpG islands in pluripotent stem cells. *Science, 356*(6337), 503-508. doi:10.1126/science.aag3260

Takai, D., & Jones, P. A. (2002). Comprehensive analysis of CpG islands in human chromosomes 21 and 22. *Proc Natl Acad Sci U S A, 99*(6), 3740-3745. doi:10.1073/pnas.052410099

Tan, W. H., Bacino, C. A., Skinner, S. A., Anselm, I., Barbieri-Welge, R., Bauer-Carlin, A., Beaudet, A. L., Bichell, T. J., Gentile, J. K., Glaze, D. G., *et al.* (2011). Angelman syndrome: Mutations influence features in early childhood. *Am J Med Genet A, 155A*(1), 81-90. doi:10.1002/ajmg.a.33775

Teng, I. W., Hou, P. C., Lee, K. D., Chu, P. Y., Yeh, K. T., Jin, V. X., Tseng, M. J., Tsai, S. J., Chang, Y. S., Wu, C. S., *et al.* (2011). Targeted methylation of two tumor suppressor genes is sufficient to transform mesenchymal stem cells into cancer stem/initiating cells. *Cancer Res, 71*(13), 4653-4663. doi:10.1158/0008-5472.CAN-10-3418

Terada, N., Hamazaki, T., Oka, M., Hoki, M., Mastalerz, D. M., Nakano, Y., Meyer, E. M., Morel, L., Petersen, B. E., & Scott, E. W. (2002). Bone marrow cells adopt the phenotype of other cells by spontaneous cell fusion. *Nature, 416*(6880), 542-545. doi:10.1038/nature730

Terns, M. P., & Terns, R. M. (2011). CRISPR-based adaptive immune systems. *Curr Opin Microbiol, 14*(3), 321-327. doi:10.1016/j.mib.2011.03.005

Terns, R. M., & Terns, M. P. (2014). CRISPR-based technologies: prokaryotic defense weapons repurposed. *Trends Genet, 30*(3), 111-118. doi:10.1016/j.tig.2014.01.003

Tesarova, L., Simara, P., Stejskal, S., & Koutna, I. (2016). The Aberrant DNA Methylation Profile of Human Induced Pluripotent Stem Cells Is Connected to the Reprogramming Process and Is Normalized During In Vitro Culture. *PLoS One, 11*(6), e0157974. doi:10.1371/journal.pone.0157974

Thakore, P. I., D'Ippolito, A. M., Song, L., Safi, A., Shivakumar, N. K., Kabadi, A. M., Reddy, T. E., Crawford, G. E., & Gersbach, C. A. (2015). Highly specific epigenome editing by CRISPR-Cas9 repressors for silencing of distal regulatory elements. *Nat Methods, 12*(12), 1143-1149. doi:10.1038/nmeth.3630

Thomson, J. A., Itskovitz-Eldor, J., Shapiro, S. S., Waknitz, M. A., Swiergiel, J. J., Marshall, V. S., & Jones, J. M. (1998). Embryonic stem cell lines derived from human blastocysts. *Science, 282*(5391), 1145-1147.

Trivers, R., & Burt, A. (1999). Kinship and genomic imprinting. *Results Probl Cell Differ, 25*, 1-21.

Ueda, T., Abe, K., Miura, A., Yuzuriha, M., Zubair, M., Noguchi, M., Niwa, K., Kawase, Y., Kono, T., Matsuda, Y., *et al.* (2000). The paternal methylation imprint of the mouse H19 locus is acquired in the gonocyte stage during foetal testis development. *Genes Cells, 5*(8), 649-659.

Ulaner, G. A., Vu, T. H., Li, T., Hu, J. F., Yao, X. M., Yang, Y., Gorlick, R., Meyers, P., Healey, J., Ladanyi, M., *et al.* (2003). Loss of imprinting of IGF2 and H19 in osteosarcoma is accompanied by reciprocal methylation changes of a CTCF-binding site. *Hum Mol Genet, 12*(5), 535-549.

Varela, M. C., Kok, F., Otto, P. A., & Koiffmann, C. P. (2004). Phenotypic variability in Angelman syndrome: comparison among different deletion classes and between deletion and UPD subjects. *Eur J Hum Genet, 12*(12), 987-992. doi:10.1038/sj.ejhg.5201264

Veselovska, L., Smallwood, S. A., Saadeh, H., Stewart, K. R., Krueger, F., Maupetit-Mehouas, S., Arnaud, P., Tomizawa, S., Andrews, S., & Kelsey, G. (2015). Deep sequencing and de novo assembly of the mouse oocyte transcriptome define the contribution of transcription to the DNA methylation landscape. *Genome Biol, 16*, 209. doi:10.1186/s13059-015-0769-z

Voelkel, C., Galla, M., Maetzig, T., Warlich, E., Kuehle, J., Zychlinski, D., Bode, J., Cantz, T., Schambach, A., & Baum, C. (2010). Protein transduction from retroviral Gag precursors. *Proc Natl Acad Sci U S A, 107*(17), 7805-7810. doi:10.1073/pnas.0914517107

Vojta, A., Dobrinic, P., Tadic, V., Bockor, L., Korac, P., Julg, B., Klasic, M., & Zoldos, V. (2016). Repurposing the CRISPR-Cas9 system for targeted DNA methylation. *Nucleic Acids Res, 44*(12), 5615-5628. doi:10.1093/nar/gkw159

Vu, T. H., & Hoffman, A. R. (1997). Imprinting of the Angelman syndrome gene, UBE3A, is restricted to brain. *Nat Genet, 17*(1), 12-13. doi:10.1038/ng0997-12

Wakayama, T., Perry, A. C., Zuccotti, M., Johnson, K. R., & Yanagimachi, R. (1998). Full-term development of mice from enucleated oocytes injected with cumulus cell nuclei. *Nature, 394*(6691), 369-374. doi:10.1038/28615

Wang, J., Rao, S., Chu, J., Shen, X., Levasseur, D. N., Theunissen, T. W., & Orkin, S. H. (2006). A protein interaction network for pluripotency of embryonic stem cells. *Nature, 444*(7117), 364-368. doi:10.1038/nature05284

Wang, Q. T., Piotrowska, K., Ciemerych, M. A., Milenkovic, L., Scott, M. P., Davis, R. W., & Zernicka-Goetz, M. (2004). A genome-wide study of gene activity reveals developmental signaling pathways in the preimplantation mouse embryo. *Dev Cell, 6*(1), 133-144.

Wang, R., Preamplume, G., Terns, M. P., Terns, R. M., & Li, H. (2011). Interaction of the Cas6 riboendonuclease with CRISPR RNAs: recognition and cleavage. *Structure, 19*(2), 257-264. doi:10.1016/j.str.2010.11.014

Warren, L., Manos, P. D., Ahfeldt, T., Loh, Y. H., Li, H., Lau, F., Ebina, W., Mandal, P. K., Smith, Z. D., Meissner, A., *et al.* (2010). Highly efficient reprogramming to pluripotency and directed differentiation of human cells with synthetic modified mRNA. *Cell Stem Cell, 7*(5), 618-630. doi:10.1016/j.stem.2010.08.012

Wawrzik, M., Spiess, A. N., Herrmann, R., Buiting, K., & Horsthemke, B. (2009). Expression of SNURF-SNRPN upstream transcripts and epigenetic regulatory genes during human spermatogenesis. *Eur J Hum Genet, 17*(11), 1463-1470. doi:10.1038/ejhg.2009.83

Wernig, M., Lengner, C. J., Hanna, J., Lodato, M. A., Steine, E., Foreman, R., Staerk, J., Markoulaki, S., & Jaenisch, R. (2008). A drug-inducible transgenic system for direct reprogramming of multiple somatic cell types. *Nat Biotechnol, 26*(8), 916-924. doi:10.1038/nbt1483

Wiedenheft, B., Sternberg, S. H., & Doudna, J. A. (2012). RNA-guided genetic silencing systems in bacteria and archaea. *Nature, 482*(7385), 331-338. doi:10.1038/nature10886

Wilkins, J. F., & Haig, D. (2003). What good is genomic imprinting: the function of parent-specific gene expression. *Nat Rev Genet, 4*(5), 359-368. doi:10.1038/nrg1062

Williams, D., Hodgetts, V., & Gupta, J. (2010). Recurrent hydatidiform moles. *Eur J Obstet Gynecol Reprod Biol, 150*(1), 3-7. doi:10.1016/j.ejogrb.2010.01.003

Williamson, C. M., Ball, S. T., Dawson, C., Mehta, S., Beechey, C. V., Fray, M., Teboul, L., Dear, T. N., Kelsey, G., & Peters, J. (2011). Uncoupling antisense-mediated silencing and DNA methylation in the imprinted Gnas cluster. *PLoS Genet, 7*(3), e1001347. doi:10.1371/journal.pgen.1001347

Wilmut, I., Schnieke, A. E., McWhir, J., Kind, A. J., & Campbell, K. H. (1997). Viable offspring derived from fetal and adult mammalian cells. *Nature, 385*(6619), 810-813. doi:10.1038/385810a0

Witzgall, R., O'Leary, E., Leaf, A., Onaldi, D., & Bonventre, J. V. (1994). The Kruppel-associated box-A (KRAB-A) domain of zinc finger proteins mediates transcriptional repression. *Proc Natl Acad Sci U S A, 91*(10), 4514-4518.

Wobus, A. M., Holzhausen, H., Jakel, P., & Schoneich, J. (1984). Characterization of a pluripotent stem cell line derived from a mouse embryo. *Exp Cell Res, 152*(1), 212-219.

Woltjen, K., Michael, I. P., Mohseni, P., Desai, R., Mileikovsky, M., Hamalainen, R., Cowling, R., Wang, W., Liu, P., Gertsenstein, M., *et al.* (2009). piggyBac transposition reprograms fibroblasts to induced pluripotent stem cells. *Nature, 458*(7239), 766-770. doi:10.1038/nature07863

Woods, N. B., Muessig, A., Schmidt, M., Flygare, J., Olsson, K., Salmon, P., Trono, D., von Kalle, C., & Karlsson, S. (2003). Lentiviral vector transduction of NOD/SCID repopulating cells results in multiple vector integrations per transduced cell: risk of insertional mutagenesis. *Blood, 101*(4), 1284-1289. doi:10.1182/blood-2002-07-2238

Wu, H., D'Alessio, A. C., Ito, S., Xia, K., Wang, Z., Cui, K., Zhao, K., Sun, Y. E., & Zhang, Y. (2011). Dual functions of Tet1 in transcriptional regulation in mouse embryonic stem cells. *Nature, 473*(7347), 389-393. doi:10.1038/nature09934

Xiao, B., Wilson, J. R., & Gamblin, S. J. (2003). SET domains and histone methylation. *Curr Opin Struct Biol, 13*(6), 699-705.

Xie, W., Barr, C. L., Kim, A., Yue, F., Lee, A. Y., Eubanks, J., Dempster, E. L., & Ren, B. (2012). Base-resolution analyses of sequence and parent-of-origin dependent DNA methylation in the mouse genome. *Cell, 148*(4), 816-831. doi:10.1016/j.cell.2011.12.035

Xu, C., Inokuma, M. S., Denham, J., Golds, K., Kundu, P., Gold, J. D., & Carpenter, M. K. (2001). Feeder-free growth of undifferentiated human embryonic stem cells. *Nat Biotechnol, 19*(10), 971-974. doi:10.1038/nbt1001-971

Xu, R. H., Sampsell-Barron, T. L., Gu, F., Root, S., Peck, R. M., Pan, G., Yu, J., Antosiewicz-Bourget, J., Tian, S., Stewart, R., *et al.* (2008). NANOG is a direct target of TGFbeta/activin-mediated SMAD signaling in human ESCs. *Cell Stem Cell, 3*(2), 196-206. doi:10.1016/j.stem.2008.07.001

Xu, X., Smorag, L., Nakamura, T., Kimura, T., Dressel, R., Fitzner, A., Tan, X., Linke, M., Zechner, U., Engel, W., *et al.* (2015). Dppa3 expression is critical for generation of fully reprogrammed iPS cells and maintenance of Dlk1-Dio3 imprinting. *Nat Commun, 6*, 6008. doi:10.1038/ncomms7008

Yamamoto, Y., Huibregtse, J. M., & Howley, P. M. (1997). The human E6-AP gene (UBE3A) encodes three potential protein isoforms generated by differential splicing. *Genomics, 41*(2), 263-266. doi:10.1006/geno.1997.4617

Yao, X., Hu, J. F., Daniels, M., Shiran, H., Zhou, X., Yan, H., Lu, H., Zeng, Z., Wang, Q., Li, T., *et al.* (2003). A methylated oligonucleotide inhibits IGF2 expression and enhances survival in a model of hepatocellular carcinoma. *J Clin Invest, 111*(2), 265-273. doi:10.1172/JCI15109

Yen, R. W., Vertino, P. M., Nelkin, B. D., Yu, J. J., el-Deiry, W., Cumaraswamy, A., Lennon, G. G., Trask, B. J., Celano, P., & Baylin, S. B. (1992). Isolation and characterization of the cDNA encoding human DNA methyltransferase. *Nucleic Acids Res, 20*(9), 2287-2291.

Ying, Q. L., Nichols, J., Evans, E. P., & Smith, A. G. (2002). Changing potency by spontaneous fusion. *Nature, 416*(6880), 545-548. doi:10.1038/nature729

Yoder, J. A., Soman, N. S., Verdine, G. L., & Bestor, T. H. (1997). DNA (cytosine-5)-methyltransferases in mouse cells and tissues. Studies with a mechanism-based probe. *J Mol Biol, 270*(3), 385-395. doi:10.1006/jmbi.1997.1125

Yu, J., Vodyanik, M. A., He, P., Slukvin, II, & Thomson, J. A. (2006). Human embryonic stem cells reprogram myeloid precursors following cell-cell fusion. *Stem Cells, 24*(1), 168-176. doi:10.1634/stemcells.2005-0292

Yu, J., Vodyanik, M. A., Smuga-Otto, K., Antosiewicz-Bourget, J., Frane, J. L., Tian, S., Nie, J., Jonsdottir, G. A., Ruotti, V., Stewart, R., *et al.* (2007). Induced pluripotent stem cell lines derived from human somatic cells. *Science, 318*(5858), 1917-1920. doi:10.1126/science.1151526

Yu, P., Pan, G., Yu, J., & Thomson, J. A. (2011). FGF2 sustains NANOG and switches the outcome of BMP4-induced human embryonic stem cell differentiation. *Cell Stem Cell, 8*(3), 326-334. doi:10.1016/j.stem.2011.01.001

Yusa, K., Rad, R., Takeda, J., & Bradley, A. (2009). Generation of transgene-free induced pluripotent mouse stem cells by the piggyBac transposon. *Nat Methods, 6*(5), 363-369. doi:10.1038/nmeth.1323

Zhang, R. R., Cui, Q. Y., Murai, K., Lim, Y. C., Smith, Z. D., Jin, S., Ye, P., Rosa, L., Lee, Y. K., Wu, H. P., *et al.* (2013). Tet1 regulates adult hippocampal neurogenesis and cognition. *Cell Stem Cell, 13*(2), 237-245. doi:10.1016/j.stem.2013.05.006

Zhou, H., Wu, S., Joo, J. Y., Zhu, S., Han, D. W., Lin, T., Trauger, S., Bien, G., Yao, S., Zhu, Y., *et al.* (2009a). Generation of induced pluripotent stem cells using recombinant proteins. *Cell Stem Cell, 4*(5), 381-384. doi:10.1016/j.stem.2009.04.005

Zhou, J., Su, P., Wang, L., Chen, J., Zimmermann, M., Genbacev, O., Afonja, O., Horne, M. C., Tanaka, T., Duan, E., *et al.* (2009b). mTOR supports long-term self-renewal and suppresses mesoderm and endoderm activities of human embryonic stem cells. *Proc Natl Acad Sci U S A, 106*(19), 7840-7845. doi:10.1073/pnas.0901854106

Zhou, Q., Chipperfield, H., Melton, D. A., & Wong, W. H. (2007). A gene regulatory network in mouse embryonic stem cells. *Proc Natl Acad Sci U S A, 104*(42), 16438-16443. doi:10.1073/pnas.0701014104

Zhou, W., & Freed, C. R. (2009). Adenoviral gene delivery can reprogram human fibroblasts to induced pluripotent stem cells. *Stem Cells, 27*(11), 2667-2674. doi:10.1002/stem.201

Zhu, X., Leav, I., Leung, Y. K., Wu, M., Liu, Q., Gao, Y., McNeal, J. E., & Ho, S. M. (2004). Dynamic regulation of estrogen receptor-beta expression by DNA methylation during prostate cancer development and metastasis. *Am J Pathol, 164*(6), 2003-2012.

Zuo, X., Sheng, J., Lau, H. T., McDonald, C. M., Andrade, M., Cullen, D. E., Bell, F. T., Iacovino, M., Kyba, M., Xu, G., *et al.* (2012). Zinc finger protein ZFP57 requires its co-factor to recruit DNA methyltransferases and maintains DNA methylation imprint in embryonic stem cells via its transcriptional repression domain. *J Biol Chem, 287*(3), 2107-2118. doi:10.1074/jbc.M111.322644

8. Appendix

8.1 PCR Programmes

Table 1. qRT-PCR programme for all qRT-PCR applications including quantitative allele distinction.

95 °C	1 min	
95 °C	15 s	40x
60 °C	30 s	
95 °C	1 min	
55 °C	30 s	
95 °C	by 0.5 °C	
4 °C	∞	

Table 2. PCR programme for Sanger sequencing.

96 °C	1 min	
96 °C	10 s	
50-56 °C	5 s	25x
60 °C	4 min	
4 °C	∞	

Table 3. PCR programme for cloning the 280 bp *UBE3A* fragment from patient-specific cDNA.

95 °C	15 min	
95 °C	30 sec	
50-60 °C	30 sec	35x
72 °C	30 sec	
72 °C	7 min	
4 °C	∞	

Table 4. PCR programme for amplifying bisulphite-converted DNA.

95 °C	15 min	
95 °C	30 sec	35x
50-60 °C	30 sec	

72 °C	30 sec	
72 °C	7 min	
4 °C	∞	

Table 5. Primer annealing temperatures for amplifying bisulphite-converted DNA.

PWS-SRO	56 °C
ICR1	59 °C
ICR2	56 °C
NESPAS	54 °C
CpG85	54 °C
IG-DMR	55 °C

Table 6. PCR programme for Re-PCR with MID primers preceding next-generation bisulphite sequencing.

95 °C	15 min	
95 °C	30 sec	35x
72 °C	1 min	
72 °C	5 min	
4 °C	∞	

Table 7. PCR programme for amplifying the 1413 bp fragment encompassing CpG77.

98 °C	30 sec	
98 °C	10 sec	
52 °C	30 sec	35x
72 °C	70 sec	
72 °C	7 min	
4 °C	∞	

Table 8. PCR programme for amplifying DNA for T7 assay.

98 °C	30 sec	
98 °C	10 sec	
60 °C	30 sec	35x
72 °C	30 sec	
72 °C	7 min	
4 °C	∞	

Table 9. Annealing programme for T7 assay.

95 °C	10 min
95 °C => 85 °C	by 2 °C/s
85 °C => 25 °C	by 0.1 °C/s
4 °C	∞

8.2 Oligonucleotides

Table 10. Primer sequences, probes, methylated oligonucleotides and gRNAs.

Name	Sequence 5’ => 3’	Product size (bp)
Sequencing *UBE3A*		
UBE3A_100bp_fw	CCTGCAGACTTGAAGAAGCA	100
UBE3A_100bp_r	CCTCCACAACCAGCTGAAA	
Pluripotency		
RPL13A_F	CCATCGTGGCTAAACAGGAGT	112
RPL13A_R	AGGAAAGCCAGGTACTTCAACTT	
GAPDH_F	TGCACCACCAACTGCTTAGC	87
GAPDH_R	GGCATGGAGTGTGGTCATGAG	
OCT4_F	GAAGGTGAAGTTCAATGATGCTG	139
OCT4_R	ATTCCCATCCCTACCTCAGTAAC	
SOX2_F	AGTATCAGGAGTTGTCAAGGCAG	79
SOX2_R	TCCTAGTCTTAAAGAGGCAGCAA	
KLF4_F	CTAAATGATGGTGCTTGGTGAGT	124
KLF4_R	GGTCATAAATGTTGATCGGAAGAC	
MYC_F	TCCTGAGCAATCACCTATGAACT	110
MYC_R	TTGAGGCAGTTTACATTATGGC	
NANOG_F	ACCTCAGCTACAAACAGGTGAAG	156
NANOG_R	ATCCCTGGTGGTAGGAAGAGTAA	
LIN28A_F	TTGAGGAGCAGGCAGAGTGG	162
LIN28A_R	TGCATTTGGACAGAGCATGG	
DNMT3B_F	GGATGTTTGAGAATGTTGTAGCC	72
DNMT3B_R	GATTACACTCCAGGAACCGTGA	
ZFP42_F	AGCTGAAACAAATGTACTGAGGCT	127
ZFP42_R	CTCCAGGCAGTAGTGATCTGAGTA	
EB differentiation		
b_ACTIN_F	CTGGAACGGTGAAGGTGACA	139

b_ACTIN_R	AAGGGACTTCCTGTAACAATGCA	
OCT4_F	TGGGCTCGAGAAGGATGTG	78
OCT4_R	GCATAGTCGCTGCTTGATCG	
PAX6_F	AACAGACACAGCCCTCACAAACA	275
PAX6_R	CGGGAACTTGAACTGGAACTGAC	
BRACHYURY_F	TGCTTCCCTGAGACCCAGTT	121
BRACHYURY_R	GATCACTTCTTTCCTTTGCATCAAG	
SOX17_F	GAACGCTTTCATGGTGTGGG	151
SOX17_R	CTCTGCCTCCTCCACGAAGG	
Neuronal differentiation		
OCT4_F	GAAGGTGAAGTTCAATGATGCTG	139
OCT4_R	ATTCCCATCCCTACCTCAGTAAC	
NESTIN_F	GGAAGAGAACCTGGGAAAGG	122
NESTIN_R	CTTGGTCCTTCTCCACCGTA	
PAX6_F	AATAACCTGCCTATGCAACCC	275
PAX6_R	AACTTGAACTGGAACTGACACAC	
SOX1_F	CAATGCGGGGAGGAGAAGTC	95
SOX1_R	CTCGAAACATTTTGGGTGGGG	
PLZF_F	CCTGGATAGTTTGCGGCTGA	144
PLZF_R	GCCATGTCAGTGCCAGTATG	
NR2F1_F	ACAGGAACTGTCCCATCGAC	194
NR2F1_R	GATGTAGCCGGACAGGTAGC	
FOXG1_F	TGCCAAGTTTTACGACGGGA	79
FOXG1_R	GGGTTGGAAGAAGACCCCTG	
NURR1_F	TTCTCCTTTAAGCAATCGCCC	332
NURR1_R	AAGCCTTTGCAGCCCTCACAG	
TH_F	GAGTACACCGCCGAGGAGATTG	279
TH_R	GCGGATATACTGGGTGCACTGG	
PAX2_F	CAGGCATCAGAGCACATC	165
PAX2_R	GTCACGACCAGTCACAAC	
β-III TUBULIN_F	CTCAGGGGCCTTTGGACATC	160
β-III TUBULIN_R	CAGGCAGTCGCAGTTTTCAC	
UBE3A_F	CTCTTCTTGCAGTTTACAACGG	152
UBE3A_R	CTTGAGTATTCCGGAAGTAAAAGC	
SNHG14__RT17_F	GGCACTGAAAATGTGGCATCCAGTC	120
SNHG14__RT17_R	GGTGTGTCAGCTGTGCTGGTGTCAA	
Bisulphite sequencing		
SNRPN_Ftag	CTTGCTTCCTGGCACGAGGGAGGGAGTTGGGATTTTTGTATTG	275
SNRPN_RM13	CAGGAAACAGCTATGACCCCCAAACTATCTCTTAAAAAAAACCACC	
H19-in-Ftag	CTTGCTTCCTGGCACGAGGGTAYGGAATTGGTTGTAGTTGTGG	204
CTCF-RM13_R_CTCF6	CAGGAAACAGCTATGACATATCCTATTCCCAAATAACCCC	

LIT1-Not1-F-tag	CTTGCTTCCTGGCACGAGTTTATAGGTTTTTATATYGAGGGTTTATAGTAG	156
LIT1-Not1-R-M13	CAGGAAACAGCTATGACAAATAAACYRAAAACACRAACCAATTCTCTAC	
NESPAS_F_neu_Bis	CTTGCTTCCTGGCACGAGGTAGTAGTTTTTGGATGGAGATTTT	272
NESPAS_R_neu_Bis	CAGGAAACAGCTATGACAAAAAAATACTTTTCCTCCCTCC	
RB1_CpG85_Ftag_1	CTTGCTTCCTGGCACGAGTTTGGATGGTTTTTTTAG	221
RB1_CpG85_RM13_1	CAGGAAACAGCTATGACAACAAAAAAACAAAAACAACC	
IG-DMR-Ftag	CTTGCTTCCTGGCACGAGGTTTATTGGGTTGGGTTTTGTTAG	302
IG-DMR-RM13	CAGGAAACAGCTATGACACCAATTACAATACCACAAAATTAC	
Bis_hOCT4_R2a_Ftag	CTTGCTTCCTGGCACGAGGGGGTTAGAGGTTAAGGTTAGTG	267
Bis_hOCT4_R2a_RM13	CAGGAAACAGCTATGACATTCCTAACCCTCCAAAAAAAC	
NANOG_R1_F_Stricker	CTTGCTTCCTGGCACGAGATGTTGGTTAGGTTGGTTTTAAATT	242
NANOG_R1_R_Stricker	CAGGAAACAGCTATGACCCCAACAACAAATACTTCTAAATTCACCAC	
AutMID1 (example)	CGTATCGCCTCCCTCGCGCCATCAGACGAGTGCGTCTTGCTTCCTGGCACGAG	Amplicon size +35
ButMID1 (example)	CTATGCGCCTTGCCAGCCCGCTCAGACGAGTGCGTCAGGAAACAGCTATGAC	
UBE3A cDNA cloning		
UBE3A_cDNA_fwd	CAGCAGTTGAATCCATATTTGAG	280
UBE3A_cDNA_rev	CCTCAGTTTCAAAAGAAGATGG	
UBE3A allele distinction		
UBE3A _mat_MGB	AATTTGAAGAACAAGGAGT	
UBE3A _pat_MGB	TTTGAAGGAGAACAAGGA	
Methylated oligos		
MON1	AAGCACGCCTGCGCGGCCGCAG	
MON2	CTGGCGCGCATGCTCAGGCGGGG	
MON3	GGCGCAGAGTGGAGCGGCCGCCGGA	
MON4	AGCGGTCAGTGACGCGATGGAGCGG	
CON1	GCCATTGTGCGTGACGACAGCA	
CON2	GCGTCGGGTACTGACGCGGCGAC	
CON3	GCTCCGTGACGCGGGGCGGAGGGGC	
CON4	AAAGCAGCAGCCCTCGAGCGCCCAT	
Methylated fragment		
T7_Promoter	AATACGACTCACTATAGGG	1413
M13_rev	CAGGAAACAGCTATGAC	
gRNAs for CRISPR/Cas9		
gRNA1	CCCCCAGGTCATTCCGGTGA	
gRNA2	GGCAAACAAGCACGCCTGCG	
gRNA3	TGTCTCTTGAGAGAAGCCAC	
gRNA4	GCTCCTCAGACAGATGCGTC	

T7 assay		
SNRPN_short1_Seq_F2	aggtagacatgtccattgat	520
SNRPN_CpG77_R1	gagcggacaggataccatcg	
Epi-Pluri-Score analysis		
ANKRD46_for	BIOTIN-AGGGGAGGGGTTAGATAGGGGTAG	173
ANKRD46_rev	CCACAATTTTAATACTTTCCCTAATTCAAAAC	
ANRD46_seq	CACAATTTTAATACTTTCCC	
C14ORF115_for	BIOTIN-GATTTTTTGGGGGGAGTGGTTTAAGT	182
C14ORF115_rev	CCACCTTCCAACCTAAAACATTTAAATCACC	
C14ORF115_seq	CCAAAACCAATTTCATATC	
POU5F1_for	GATTTTTGGTATTGTGTTTTTAGGGGTTAGTTA	416
POU5F1_rev	BIOTIN-TAAAACCCAATCAATCCAAAATCTAATCCC	
POU5F1_seq	TAGTTTTTTAAATTTATTGAATG	

8.3. Next-Generation Bisulphite Sequencing

Table 11. Chromosomal regions according to UCSC browser, build hg19.

ICR	Locus / gene	CpG sites	Chromosomal region
SNRPN	Prader-Willi / Angelman locus	21	chr15:25200011 -25200250
ICR1	*IGF2 / H19*	14	chr11:2021080-2021248
ICR2	*KCNQ1OT1*	7	chr11: 2721560- 2721680
NESPAS	*GNAS*	17	chr20:57429210- 57429446
CpG85	*RB1*	11	chr13:48,893,505-48,893,690
IG-DMR	*DLK1 / MEG3*	15	chr14: 101277219-101277485
POU5F1	*POU5F1*	10	chr6:31,138,276-31,138,507
NANOG	*NANOG*	6	chr12:7,941,603-7,941,810

Table 12. Methylation and read numbers at analysed loci in assayed cell lines corresponding with Figure 20 and Figure 21.

	SNRPN	ICR1	ICR2	NESPAS	CpG85	IG-DMR	POU5F1	NANOG
CpG sites	**21**	**14**	**7**	**17**	**11**	**15**	**10**	**6**
hESCs H1								
Methylation %	30.4	54.0	48.2	42.2	94.9	93.6	9.0	15.2
Reads	1549	1826	2371	1285	269	1245	756	971

hESCs H9								
Methylation %	37.1	37.1	47.5	36.0	95.1	95.3	20.6	25.9
Reads	643	753	658	2659	9678	2740	3369	1070
Control fibroblasts								
Methylation %	39.0	41.7	50.3	40.3	59.1	62.7	49.3	34.9
Reads	885	2879	3580	2347	232	7298	858	628
Control 42								
Methylation %	36.0	39.4	53.7	1.6	92.0	91.9	1.6	5.7
Reads	374	1292	1328	918	2827	1298	753	1489
Control 645								
Methylation %	41.7	46.8	53.9	6.0	91.3	92.0	1.0	2.3
Reads	699	1343	2463	1453	2485	1289	698	4390
Patient fibroblasts								
Methylation %	42.8	44.7	56.5	46.5	94.0	3.2	80.5	45.1
Reads	776	1837	1212	1855	3222	1311	748	374
Patient B1								
Methylation %	38.4	0.9	57.7	3.1	95.8	61.9	8.9	14.0
Reads	616	3201	2843	1910	154	1635	524	967
Patient D								
Methylation %	39.8	44.8	56.0	43.7	95.4	60.1	8.0	16.4
Reads	691	2299	1777	2526	459	1544	1059	900
Patient H								
Methylation %	37.6	39.7	54.3	63.6	96.1	65.8	12.4	27.8
Reads	2336	1875	5296	1075	576	2308	1160	571
Patient P								
Methylation %	36.4	43.4	2.0	4.1	94.8	53.9	21.8	42.1
Reads	1161	2566	1198	1764	405	3304	1241	2824
hESCs H9								
Methylation %	38.1	91.7	49.9	41.3	95.9	96.5	18.5	43.5
Reads	2886	390	581	8425	8438	458	2916	1538
AGI-0								
Methylation %	0.9	75.4	49.3	45.4	91.6	93.8	12.0	30.1
Reads	1151	1387	2072	1316	608	1632	680	1350
MCH2-10								
Methylation %	28.8	68.9	55.7	3.3	95.2	89.0	16.9	33.5
Reads	1214	1021	1576	1155	694	1558	610	1134

Control fibroblasts 2		
Methylation %	55.6	58.6
Reads	2591	1025
Control fibroblasts 3		
Methylation %	79.3	64.9
Reads	2593	1020
Patient blood		
Methylation %	63.1	61.6
Reads	475	1290

Table 13. Methylation and read numbers at analysed loci after methylation induction with a modified CRISPR/Cas9 system corresponding with Figure 28.

	No gRNA	gRNA1 + gRNA3	gRNA2 + gRNA4
D0			
Methylation %	1.5	22.8	3.1
Reads	278	863	665
D7			
Methylation %	1.0	15.7	5.6
Reads	894	1641	772
D14			
Methylation %	0.7	30.0	11.8
Reads	1804	750	765

8.4 Plasmid Maps

8.4.1 TOPO Vector with Inserted 280 bp Fragment from Patient-Specific cDNA

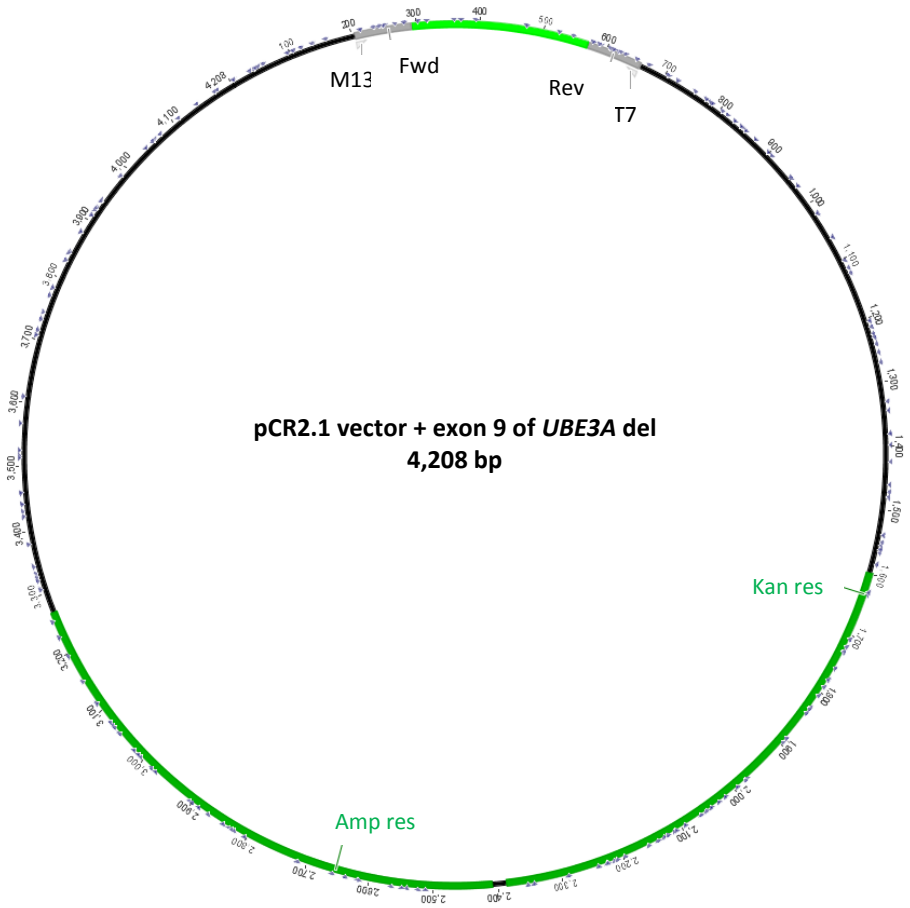

8.4.2 Cas9-DNMT3A-DNMT3L Construct

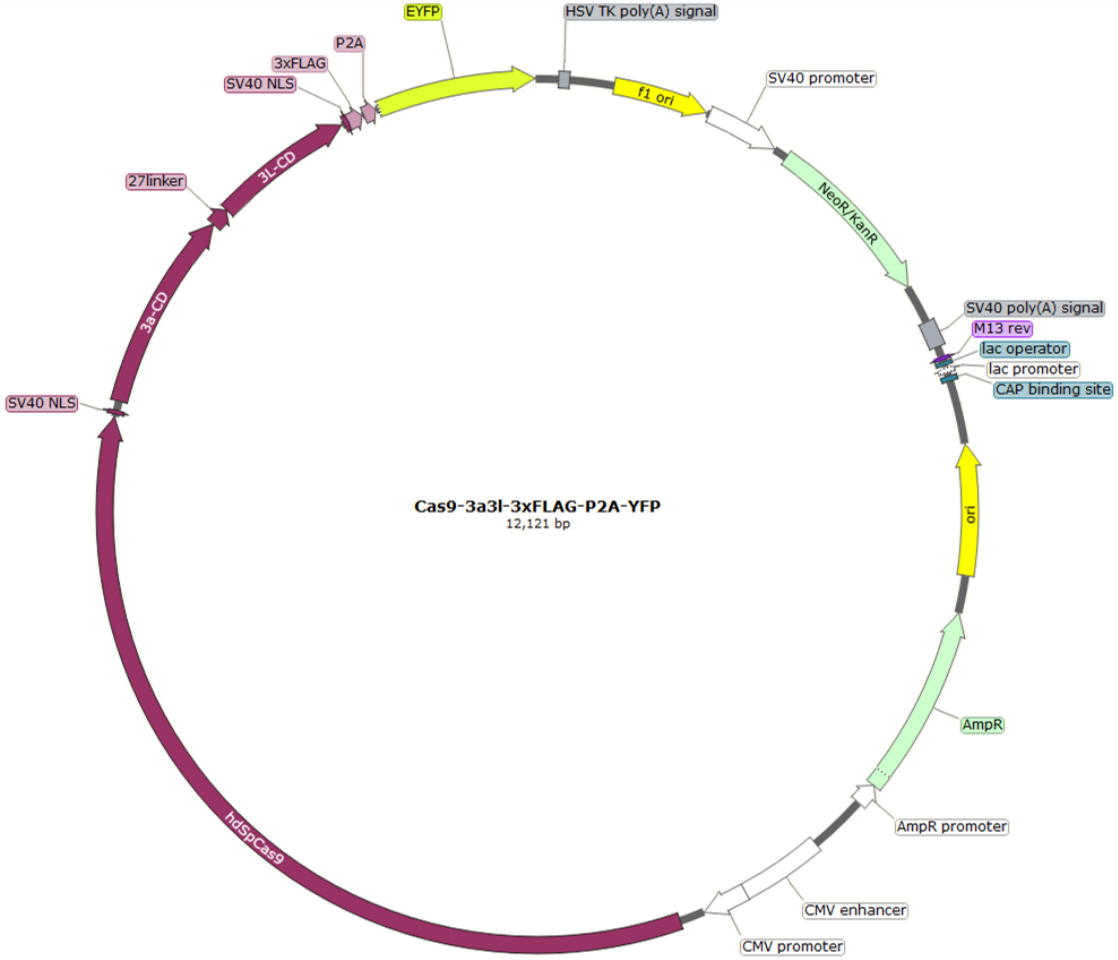

8.4.3 Plasmid containing gRNA1

8.5 List of Figures

8.6 List of Tables

9. Acknowledgements

This project was supported by the IFORES Sonderforschungprogramm of the Medical Faculty at the University Duisburg-Essen.

I would like to thank Prof. Dr. Bernhard Horsthemke for giving me the opportunity to carry out my project at the Institute of Human Genetics and for his valuable positive feedback.

My special thanks belong to Dr. Laura Steenpass for her excellent supervision and guidance throughout the whole project, her creative ideas whenever I would encounter difficulties and for always taking the time when I would need to discuss anything. I very much appreciate her insight, knowledge and support that helped me a lot on the way. Also, I am grateful for the opportunity to travel to many conferences.

I thank Michaela Hiber for her support especially in the cell culture and for her help with things around the lab.

For their help, friendship and support, I would like to acknowledge the current as well as the former members of the Institute of Human Genetics. Especially Helena Heinz was always a great support. She helped me cope with bad days and made it easier to get over little daily tragedies that do happen during a doctorate. Helena together with Jasmin Beygo made my time in Essen much more fun and I really appreciate them being there for me. I wish to thank Elsa Leitão and Christian Grosser for their kind words and understanding they offered. I also want to thank Jasmin and Christian for carefully reading my thesis and giving me valuable tips. Also, I am grateful for working with my (ex-) colleagues Nadja, Deniz, Tea, Hannah, Nicki, Alex, Katrin, Theresa, Yasaman, Julia and Gesa.

My cooperation partner Anika Neureiter and her colleague Hannah de Oliveira Kessler, I thank for their help and time. Our joint supervisor Dr. Hannes Klump, I wish to thank for his support, especially concerning the revision of our paper.

I thank my dear friends for being there for me. Although we are far apart, knowing that I can come around anytime gives me confidence. I wish to thank Mihai for believing in me at difficult times.

My special thanks belong to my brother Jan for being the best brother in the world. I am very grateful for him making me smile, for him listening, for discussions I could only lead with him, for his love, friendship and care. I am so glad to be your sisty.

For his patience, care, understanding and love, I wish to thank Stefan. His support, motivation and at times much needed distraction helped me get through moments of doubt. I cannot really express how grateful I am for having you by my side.

Finally, I want to thank my mum and dad for everything. I truly appreciate them letting me go my own way and supporting me all the way through. Their listening, encouragement, advice and love were always a source of strength and peace for me. Without you, my way would have been much more difficult. I will always remain grateful for having you.

10. Curriculum Vitae

Der Lebenslauf ist in der Online-Version aus Gründen des Datenschutzes nicht enthalten.

11. Eidesstattliche Erklärung

Erklärung

Hiermit erkläre ich, gem. § 6 Abs. 2, g der Promotionsordnung der Fakultät für Biologie zur Erlangung des Dr. rer. nat., dass ich das Arbeitsgebiet, dem das Thema „Induction of site-specific methylation induced pluripotent stem cells of a patient with Angelman syndrome“ zuzuordnen ist, in Forschung und Lehre vertrete und den Antrag von Jana Staňurová befürworte.

Essen, den _____ _____ _____

Name des wissenschaftl. Betreuers/Mitglied der Universität Duisburg-Essen	Unterschrift des wissenschaftl. Betreuers/Mitglied der Universität Duisburg-Essen

Erklärung

Hiermit erkläre ich, gem. § 7 Abs. 2, d und f der Promotionsordnung der Fakultät für Biologie zur Erlangung des Dr. rer. nat., dass ich die vorliegende Dissertation selbständig verfasst und mich keiner anderen als der angegebenen Hilfsmittel bedient habe und alle wörtlich oder inhaltlich übernommenen Stellen als solche gekennzeichnet habe.

Essen, den _____ _____
Unterschrift des/r Doktoranden/in

Erklärung

Hiermit erkläre ich, gem. § 7 Abs. 2, e und g der Promotionsordnung der Fakultät für Biologie zur Erlangung des Dr. rer. nat., dass ich keine anderen Promotionen bzw. Promotionsversuche in der Vergangenheit durchgeführt habe und dass diese Arbeit von keiner anderen Fakultät/Fachbereich abgelehnt worden ist.

Essen, den _____ _____
Unterschrift des/r Doktoranden/in